

Die approbierte Originalversion dieser Dissertation ist an der Hauptbibliothek der Technischen Universität Wien aufgestellt (<http://www.ub.tuwien.ac.at>).

The approved original version of this thesis is available at the main library of the Vienna University of Technology (<http://www.ub.tuwien.ac.at/englweb/>).



TECHNISCHE
UNIVERSITÄT
WIEN
Vienna University of Technology

DISSERTATION

Oxides on Plasma-Exposed Beryllium Surfaces

ausgeführt zum Zwecke der Erlangung des akademischen Grades eines
DOKTORS DER TECHNISCHEN WISSENSCHAFTEN
unter der Leitung von

Ao. Univ.-Prof. Dr. phil. **Herbert Störi**
E134 - Institut für Angewandte Physik

eingereicht an der Technischen Universität Wien
Fakultät für Physik

von

Dipl.-Ing. **Christian Tomastik**
Matrikelnummer: 8925476
Wehlstrasse 45/1/4, 1200 Wien

Wien, November 2012



TECHNISCHE
UNIVERSITÄT
WIEN
Vienna University of Technology

DISSERTATION

Oxides on Plasma-Exposed Beryllium Surfaces

submitted in partial fulfilment of the requirements for the degree of
DOCTOR OF TECHNICAL SCIENCES
under the supervision of

Ao. Univ.-Prof. Dr. phil. **Herbert Störi**
E 134 – Institute of Applied Physics

at the Vienna University of Technology
Faculty of Physics

by

Dipl.-Ing. **Christian Tomastik**
Matriculation No.: 8925476
Wehlstrasse 45/1/4, 1200 Wien

Vienna, November 2012

Danksagung

Diese Arbeit entstand im Zuge meiner Tätigkeiten als wissenschaftlicher Mitarbeiter am Institut für Allgemeine Physik (inzwischen Institut für Angewandte Physik) der Technischen Universität Wien. Die der Dissertation zugrunde liegende Forschungsarbeit wurde durch die Österreichische Akademie der Wissenschaften im Rahmen der Assoziation EURATOM-ÖAW in den Projekten KKKÖ-2/2001 ("Diffusion von Sauerstoff in Beryllium") und Vessel-in-Vessel UT6 ("Transport of Impurities in Beryllium") finanziell gefördert.

Mein Dank gilt zuallererst Herrn Prof. Dr. Herbert Störi, der mir diese Arbeit ermöglicht hat. Unter seiner Anleitung konnte ich sowohl von seinem reichen Schatz an Wissen und Erfahrung auf den verschiedensten wissenschaftlichen Gebieten als auch von seinem großen experimentellen Geschick profitieren, und mir hoffentlich einiges davon aneignen. Weiters möchte ich meinen Kollegen am IAP danken, die mich in vielfältigster Weise unterstützt und während dieser schönen Zeit begleitet haben. Insbesondere möchte ich drei Personen nennen:

Prof. Dr. Rudolf Dobrozemsky legte mit seinen Arbeiten die Grundlage zur Erforschung von Beryllium am IAP, und war bei Bedarf immer mit einem guten Ratschlag zur Hand.

Prof. Dr. Johann Laimer stand mir sowohl mit Rat und Tat im Labor als auch als Inspiration in meinen kreativen Pausen zur Seite.

Prof. Dr. Wolfgang Werner stellte mir nicht nur sein umfangreiches Wissen über Elektronenspektroskopie zur Verfügung, sondern sorgte mit seinem unvergleichlichen Elan auch immer wieder zur rechten Zeit dafür, daß meine Arbeit frischen Schwung bekam.

Ein großer Dank geht auch an Herrn Prof. Dr. Herbert Danningner für die kritische Durchsicht der Arbeit, die wesentlich zu ihrer Qualität beigetragen hat.

Zuletzt möchte ich mich bei meiner Familie bedanken: bei meinen Eltern, die mich auf diesen Weg gebracht haben, und mich auch dann immer unterstützt haben, als der Weg sehr viel länger als geplant wurde; und bei Ulli, die immer für mich da war.

Abstract

In nuclear fusion for energy generation the materials used for the reactor vessels are exposed to severely erosive conditions during operation. A promising material for the inner vessel surface, the so-called first wall, is beryllium, due to its low atomic mass and overall good mechanical and thermal properties.

An important aspect of material properties under fusion plasma conditions is oxidation behaviour, since oxygen and water vapour are major residual gases in the vessel. As much of the knowledge concerning beryllium oxidation has been acquired in the mid 20th century, the aim of this work is to revise these currently used data by applying modern surface analytical methods. In a second step, the same methods and the obtained data are applied to plasma exposure experiments of beryllium.

For this purpose, a tubular furnace with attached electrodes for plasma excitation and a supply for hydrogen and water vapour was set up. The oxidation experiments were carried out in air at temperatures between 390 and 600 °C and for durations up to 43 h. Plasma exposure experiments were done in the same temperature range with dry hydrogen and admixed water vapour fractions in hydrogen of up to 1%. After the experiments in the furnace, the beryllium samples were investigated with Auger electron spectroscopy (AES) sputter depth profiling and scanning electron microscopy (SEM).

For heating durations decreasing with higher temperatures (down to 1 h at 600 °C), diffusion-controlled parabolic oxidation was found to occur, and the activation energy for the rate-controlling diffusion of beryllium through the oxide layer could be determined. At 500 °C and above, grain boundary oxidation of the beryllium bulk occurred for longer heating durations, which indicates the onset of non-protective (catastrophic) oxidation.

Under dry hydrogen plasma exposure, native oxide layers were further oxidised, whereas thicker oxide layers on pre-oxidised surfaces were reduced, both ending up in a thickness range of 15-35 nm. The formation of this quasi-equilibrium oxide layer was attributed to the competition of oxidation by residual water vapour and reduction by atomic hydrogen. Further admixture of water vapour resulted in a dramatic increase in the thickness of the overlayer, combined with a very rough and jagged appearance of the surface. This striking difference was explained with the formation of beryllium hydroxide instead of oxide at higher water vapour fractions.

In the context of fusion research, the results demonstrate the critical role of the concentration of residual oxygen-containing gases in the plasma vessel.

Kurzfassung

Bei der Kernfusion zur Energiegewinnung sind die in den Reaktoren verwendeten Materialien extremen Bedingungen ausgesetzt. Ein vielversprechender Kandidat für die innere Reaktoroberfläche ist Beryllium, da es eine niedrige Atommasse sowie generell gute mechanische und thermische Eigenschaften hat.

Ein wichtiger Aspekt der Materialeigenschaften in einer Fusionsplasmaumgebung ist das Oxidationsverhalten, da Sauerstoff und Wasserdampf einen Hauptanteil des Restgases im Reaktor darstellen. Nachdem ein Großteil des Wissens über die Oxidation von Beryllium aus der Mitte des zwanzigsten Jahrhunderts stammt, hat sich die vorliegende Arbeit zum Ziel gesetzt, diese Daten mittels moderner oberflächenanalytischer Methoden zu überarbeiten. In einem zweiten Schritt werden diese Methoden, zusammen mit den erarbeiteten Daten, in Experimenten zur Wechselwirkung von Beryllium mit Wasserstoffplasma angewandt.

Für die Experimente wurde ein Rohrofen mit externen Elektroden zur Plasmaanregung und einer Gasversorgung für Wasserstoff und Wasserdampf verwendet. Die Oxidationsversuche wurden an Luft bei Temperaturen zwischen 390 und 600°C bei Heizzeiten bis 43 h durchgeführt. Bei den Plasmaversuchen wurde - im gleichen Temperaturbereich - sowohl trockener Wasserstoff als auch Mischungen mit einem Anteil von bis zu 1% Wasserdampf verwendet. Nach diesen Experimenten wurden die Berylliumproben mittels Augerelektronenspektroskopie-Sputtertiefenprofilen und Rasterelektronenmikroskopie untersucht.

Bei mit der Temperatur kürzer werdenden Heizdauern (bis zu 1 h bei 600°C) wurde diffusionsbestimmte parabolische Oxidation festgestellt. Die Aktivierungsenergie für die ratenbestimmende Diffusion von Beryllium durch die Oxidschicht konnte bestimmt werden. Über 500°C fand bei längeren Heizdauern Korngrenzenoxidation statt, ein Anzeichen für beginnende katastrophale Oxidation.

Im trockenen Wasserstoffplasma wurden natürliche Oxidschichten weiter oxidiert, während dickere voroxidierte Schichten reduziert wurden, wobei die Schichtdicke nach den Versuchen in allen Fällen in einem Bereich von 15-35 nm lag. Die Bildung dieses Quasi-Gleichgewichts mit zugehöriger Oxiddicke wurde der Konkurrenz von Oxidation durch Wasserdampf im Restgas und Reduktion durch atomaren Wasserstoff zugeschrieben. Weitere Beimischung von Wasserdampf verursachte eine starke Erhöhung des Schichtwachstums, zusammen mit einem sehr rauen und zerklüfteten Erscheinungsbild der Oberfläche. Dieser erhebliche Unterschied zur Wechselwirkung mit trockenem Plasma wurde durch die überwiegende Bildung von Berylliumhydroxid bei höherem Wasserdampfanteil erklärt.

Im Rahmen der Kernfusionsforschung zeigen die dargestellten Ergebnisse die entscheidende Rolle der Konzentration von sauerstoffhaltigen Restgasen im Plasmareaktor auf.

List of Symbols and Abbreviations

A ... atomic mass

AES ... Auger electron spectroscopy

AFM ... atomic force microscopy

A_{vial} ... cross section of sample heating vial

C ... concentration of diffusing particles

CAE ... constant analyzer energy

CBD ... chronic beryllium disease

C_d ... concentration of water vapour produced by furnace impurities

CFC ... carbon fibre composite

CRR ... constant retard ratio

c_w ... concentration of water vapour in the furnace

$C_{w,p}$... total concentration of water vapour in the plasma

$C_{w,0}$... concentration of oxygen impurities in the pure hydrogen flow

$C_{w,1}$... concentration of water vapour in hydrogen in the distilled water chamber

$C_{w,2}$... concentration of water vapour in the gas entering the furnace

D ... diffusion coefficient

D_{ox} ... diffusion coefficient of oxygen in air

E_A ... activation energy for particle transport

ΔG ... free energy of reaction

J ... current of uncharged particles in the direction of oxide growth

k ... oxidation rate constant

k_B ... Boltzmann constant

l ... length of mineral wool plug for sample heating vial

L ... oxide thickness

LEED ... low energy electron diffraction

LTE ... local thermodynamic equilibrium

MFC ... mass flow controller

P_w ... vapour pressure of water

p_0 ... pressure in the furnace

P_1 ... total pressure in the distilled water chamber

Q_d ... influx of water vapour from impurities in the furnace

QMA ... quadrupole mass analyser

Q_0 ... flow of pure hydrogen

Q_1 ... flow of hydrogen with water vapour admixture
RBS ... Rutherford backscattering
SEM ... scanning electron microscopy
SIMS ... secondary ion mass spectrometry
 t ... time
 T ... temperature [°C]
 τ ... time for exchange of oxygen in the sample heating vial
TEM ... transmission electron microscopy
 t_f ... freezing time
 T_1 ... temperature in the distilled water chamber
 V ... volume of oxide per particle
 V_{dial} ... volume of sample heating vial
VHP ... vacuum hot pressing
 x ... direction of oxide growth
XRD ... X-ray diffraction
 Z ... atomic number

Table of Contents

1. Introduction	1
1.1 Beryllium	1
1.2 Oxidation of Beryllium	1
1.3 Nuclear Fusion	2
1.4 Plasma-wall interactions in nuclear fusion reactors	2
1.5 This Work	4
2. Literature Review	5
2.1 Oxidation of Beryllium	5
2.2 Fusion Research	7
3. Theory of Diffusion-Controlled Oxidation	10
4. Experimental	13
4.1. Sample Preparation and Safety	13
4.1.1 Samples	13
4.1.2 Sample Preparation	14
4.2. Oxidation Experiments	15
4.2.1 Furnace Setup	15
4.2.2 Oxidation Experiments	16
4.3. Plasma Exposure Experiments	17
4.3.1 Furnace Setup for Plasma Exposure	17
4.3.2 Control of the Atmosphere inside the Furnace	18
4.3.3 Heating and Plasma Exposure Experiments in Hydrogen	20
4.3.4 Measurement of Impurities in the Furnace: Optical Spectrometry	21
4.3.5 Measurement of Impurities in the Furnace: Mass Spectrometry	21
4.4. Auger Electron Spectroscopy	23
4.4.1 Auger Effect	23
4.4.2 Application for Surface Analysis	23
4.4.3 Instrument	24
4.4.4 Experiment and Analysis Sequence	25
4.4.5 Evaluation of Sputter Depth Profiles	26

5. Results and Discussion	29
5.1. Oxidation in Air	29
5.1.1 Parabolic Oxidation Kinetics	29
5.1.2 Catastrophic Oxidation	35
5.2. Interaction of Beryllium Oxide with Hydrogen Plasma	45
5.2.1 Heating and Plasma Exposure in Dry Hydrogen	45
5.2.2 Plasma Exposure in Wet Hydrogen	51
6. Summary and Conclusion	62
References	65
Appendix: Compilation of AES Depth Profiles	75
List of Figures	88
List of Tables	90
Curriculum Vitae	91
List of Publications	92

1. Introduction

1.1 Beryllium

Beryllium is an outstanding material. Its combination of low density and high mechanical strength and stiffness (see table 1) makes it highly interesting for various fields of technology. Furthermore, it is a valuable material for applications dealing with nuclear reactions because of its low atomic mass (atomic number $Z = 4$, atomic mass $A = 9$ amu) and its neutron scattering properties (neutron moderator and multiplier) [1,2]. The main disadvantage of beryllium in pure form is its toxicity: inhaled dust particles or vapour can cause chronic beryllium disease (CBD), an incurable disease of the lung [3,4]. However, beryllium can also be applied as component metal for alloys, which is widely used to improve the mechanical properties of aluminium and copper parts [2].

1.2 Oxidation of Beryllium

In ambient atmosphere beryllium forms a native oxide layer of some nanometers [5,6]. The commonly accepted mechanism for further oxide growth at low temperatures (room temperature to several 100 °C) is diffusion of beryllium ions through the existing oxide layer and subsequent oxide formation at the surface. The resulting oxide growth rate is parabolic with time [6-8]. At higher temperatures the oxide layer forms cracks and eventually falls off in flakes, turning the oxidation catastrophic. The transition temperature between these two modes was initially estimated at a value around 700 °C, but may be as low as 500 °C [9].

	Be (grade I220H)	Be (grade S65C)	steels
density [g/cm³]	1,85	1,85	~ 8
Young's modulus [GPa]	303	303	~ 200
ultimate tensile strength [MPa]	448	289	~ 100 to >3000
yield strength [MPa]	345	206	~ 50 to >2000

Table 1: Mechanical properties of beryllium (hot isostatic pressed grade I220H and vacuum hot pressed grade S65C) and the respective ranges for various steels for comparison

1.3 Nuclear Fusion

The fusion of light atoms is an energy-generating process. Fusion of hydrogen atoms takes place in the core plasmas of stars and the sun and is the source of their energy. The reaction rates of fusion reactions increase strongly with high temperature and density, which are sufficiently given in stars. For fusion to work on earth as an energy producing technology, a fusion device has to provide confinement of a plasma of fusion partners with high confinement time, plasma density and ion temperature.

In the 1960's the first experimental plasma fusion reactors were developed, based on magnetic confinement of a plasma of reactants on a large scale (reactor dimensions in the order of meters, confinement times in the order of seconds). The chosen particle species for these experiments were deuterium and tritium, due to the comparatively large reaction rate of the D/T fusion reaction [10-12]. This reaction produces an alpha-particle and a neutron. While the energy of the alpha-particle can be used to maintain the temperature of the energy-producing fusion plasma, the neutron escapes the plasma and must be converted to thermal energy in a surrounding blanket system. By the late 80's, the tokamak, a reactor type with toroidal plasma shape, had shown the best fusion-plasma performance of all studied devices [10].

1.4 Plasma-wall interactions in nuclear fusion reactors

With the growing dimensions of the experimental fusion reactors, the interaction between the edge of the plasma and the wall material next to the plasma (first wall material, plasma facing material) became more and more important [10,13]. The most significant issue in this respect is the deterioration of plasma performance due to impurities produced by the interactions (sputtering of wall material). They lead to radiation losses in the plasma, limiting the achievable plasma temperature [10,14-16], and dilute the plasma, reducing the density of the D/T fuel [10,17]. But also the stability and life time of the wall itself is an important aspect [1,18,19].

Since the impurity radiation losses increase strongly with the atomic number Z of the impurities, the efforts to reduce them led to the application of low Z wall materials. As a first step, in the 1970's reactor walls were fitted with carbon first wall components [10,20], mostly in the form of graphite tiles. Apart from its low atomic number ($Z = 6$), graphite has the advantage of a high melting point and the ability to withstand high thermal loads. Its

biggest disadvantage is its sensitivity to chemical erosion in the D/T-plasma, which leads to a high dilution of the plasma and makes long term plasma density control difficult to achieve. [10,21-23]. Nowadays most reactor walls are still fitted with C components, by now in the form of carbon fibre composites (CFCs), at the points of highest thermal impact (limiters, divertors) [18,19,24-26].

But by the early 80's, it was clear that efforts to increase the plasma pulse length were severely impeded by the poor long term plasma density control of full carbon wall reactors, and first experiments with beryllium wall components were carried out [10,27-30]. Beryllium has a lower atomic number and consequently the radiation losses are reduced. Furthermore it is less susceptible to chemical erosion by hydrogen, which together with its low physical sputter yield results in a significantly lower dilution of the plasma, compared to carbon [1,31]. Experiments with beryllium components in the fusion reactors soon demonstrated an additional advantage of beryllium as wall material: its ability to getter oxygen and thereby reduce the impurity concentration in the plasma [1,18].

The main disadvantages of beryllium for fusion applications are its low melting temperature (1285°C), with the consequently reduced ability to withstand thermal loads [1,18], and its toxicity. Operation of the fusion experiments was - and still is - difficult since beryllium divertors suffered from severe melting, which often raised the impurity concentrations to levels too high for feasible operation.

Since the mid 80's concepts have been developed for a next step experimental fusion reactor, to be built by the international fusion community, called ITER (International Thermonuclear Experimental Reactor). In 2007 construction works for ITER started in Cadarache (France). ITER will extend the dimensions of current reactors (in size and confinement time) and bring fusion research one step closer to a nuclear fusion power plant. According to the current plans, its first wall (except divertors) will be fabricated fully from beryllium [24]. The interaction of beryllium with hydrogen isotopes and oxygen therefore remains a subject of tremendous importance. Apart from the behaviour of beryllium components during normal operation, the unprecedented extent of beryllium surface in a reaction chamber has raised the necessity to anticipate new potential accident scenarios (inflow of coolant or air into the reaction chamber), which adds a further dimension to the need for knowledge about beryllium.

1.5 This work

Much research has been done concerning interaction of beryllium with hydrogen, as well as carbon and tungsten as possible material for additional first wall components [1,6,10,18,19,24,32,33,37-47], but only few recent investigations deal with the interaction of beryllium with oxygen [48-51]. The results of the more extensive research on the oxidation of beryllium from the 1960's still serve as the major data-base on the topic [7-9, 52-55].

This work addresses the need to re-examine the oxidation behaviour of beryllium with modern surface analytical instruments and methods, and to apply the results to the present questions of fusion research.

The first part of the investigation deals with the oxidation of beryllium in air. The temperature range for these experiments was 390 °C to 600 °C, which is at or slightly above the temperatures relevant for fusion applications [24], and can be handled on a small laboratory scale. After oxidation, the beryllium surfaces were analysed with Auger electron spectroscopy (AES) and AES sputter depth profiling. These measurements yielded information about thickness and composition as well as inhomogenities and lateral distribution (e.g. grain boundary effects) of the surface oxide layers. By carrying out experiments with varying heating durations and fitting the results with a simple function for diffusion-controlled oxide growth (parabolic oxidation), the oxidation kinetics of beryllium could be determined. In the upper temperature range, catastrophic oxidation could be observed within the range of heating durations applied.

Prepared with the oxidation data, in the second part of this work the interaction of beryllium and beryllium oxide with hydrogen plasma was investigated. In a pure hydrogen plasma, without contamination, a reduction of the oxide layer thickness may be expected, as hydrogen would tend to bind and remove the oxygen. However, oxygen and water vapour are major impurities in modern fusion plasmas [29,45], and present a source for oxidation processes at the first wall. This situation was replicated in a laboratory scale plasma flow reactor with defined additions of water vapour to the hydrogen. After the experiments, the beryllium samples were again analysed with AES depth profiling. The results showed that the variation of the concentration of water vapour in the hydrogen plasma caused differences in the thickness of the oxide layer as well as in its structure.

2. Literature Review

2.1 Oxidation of Beryllium

Beryllium and its oxidation was studied already in the 1930's [56], followed by several works up to the 1950's [e.g. 7,57-59].

In 1943 Terem [57] could observe oxidation of beryllium only at temperatures above 500°C. From these data an Arrhenius law with an activation energy between 1 and 2,8 eV followed.

In 1950 Gulbransen *et al.* [7] did oxidation experiments with beryllium between 350 and 950°C. They determined that the oxidation follows a parabolic rate law over the whole temperature range, but with two different activation energies for low temperatures (0,37 eV between 350 and 700°C) and high temperatures (2,2 eV between 750 and 950°C).

Interest increased in the 60's due to the increasing possibilities of applying beryllium in nuclear and aerospace industries, and the importance of surface properties and interactions (at that point mainly in the form of oxidation behaviour) was already recognized.

In the early 60's Aylmore *et al.* [9,52] investigated the oxidation of beryllium in dry and moist oxygen and in water vapour at temperatures between 500 and 750°C by applying weight gain analysis. Based on their results they proposed a model for the oxidation kinetics, based on existing models for metal oxidation. Furthermore they could separate the oxide growth curves into two categories, a protective oxide growth mode at lower temperatures and a non-protective mode resulting in a breakaway behaviour of the oxidation at higher temperatures. They determined the transition temperature between these two regimes at approx. 700°C for dry oxygen. Water vapour or moisture content in oxygen accelerated the breakaway behaviour and lowered the transition temperature to approx. 650°C. By investigation of the oxidised samples with light microscopy they found blisters and cracks on the oxide surface and, for the experiments with water vapour and moist oxygen, strong evidence for intergranular oxidation.

In 1963 Jepson *et al.* [53,54] published investigations of oxidised beryllium with scanning electron microscopy (SEM). Their results led them to a qualitative description of beryllium oxidation as the combination of outer oxidation at the oxide surface and inner oxidation at the oxide-metal interface and metal grain boundaries, the latter made possible by cracks in the oxide layer. Additionally, beryllium carbide inclusions at the grain boundaries are more susceptible to water vapour and moisture than bulk beryllium and are oxidised

preferentially. The transition to breakaway behaviour observed in earlier publications is explained as the point where the rate of inner oxidation exceeds the rate of outer oxidation.

In 1964 Ervin *et al.* [55] again approached the oxidation of beryllium with the weight gain method and optical microscopy, carrying out experiments in dry oxygen at temperatures from 500 to 900 °C. In contrast to previous authors, they did not separate the oxidation into protective and catastrophic regimes below and above a certain transition temperature, but determined a protective part followed by a catastrophic part of the weight gain curve at all temperatures, with the duration of the initial protective part decreasing with increasing temperature. Consequently they proposed a model for the oxidation kinetics depending only on one rate determining process, the diffusion of beryllium ions through the oxide layer. Furthermore they found indications for grain boundary oxidation at all temperatures: optical microscopy of polished cross sections showed voids at the surface already for the initial oxidation phase, and oxide particles from the surface containing unoxidised metal indicated that during catastrophic oxidation not only the oxide layer disintegrates, but also the metal beneath fragments.

Literature up to 1968 is summarized in a review paper by Adams *et al.* [8]. Apart from the work mentioned above, articles about the physical properties of beryllium (structure, vapour pressure, etc.), preparation and characterisation of thin beryllium films, and oxidation in dry and moist gases including air, oxygen, CO₂ and CO, at temperatures from 350 to 1300 °C, are discussed.

In the 80's the investigation of beryllium was extended to the very early stages of oxidation with the help of Auger electron spectroscopy (AES) and low energy electron diffraction (LEED).

An important means to advance these studies was the distinction of metallic and oxidised beryllium in the Auger electron spectrum, consisting of a shift of the beryllium peak by approx. 10 eV. Several authors reported investigations of this feature already in the 70's and early 80's [60,61].

A series of investigations on early oxidation processes was performed on a beryllium (0001) single crystal surface at oxygen pressures between $4 \cdot 10^{-8}$ and $2,6 \cdot 10^{-4}$ mbar and temperatures between room temperature and 500 °C [62-64]. Two low-pressure oxidation modes were found, which are distinct from the two modes observed at atmospheric pressures. The first is the chemisorption of oxygen on a clean beryllium surface, the second the logarithmic growth of very thin oxide films, limited by electron tunnelling.

2.2 Fusion Research

From the late 70's, the growing field of fusion research started to show interest in beryllium because of its potential as material for the first wall of fusion reactors (plasma facing material), and the research effort focussing on beryllium and its relevant properties has kept increasing ever since.

One of the earliest works in this context was published by Langley in 1979 [65]. In this work, the interaction of beryllium with highly energetic deuterium and helium particles is examined with regard to its influence on oxidation. The experiments are carried out with a dedicated ion beam facility. The results show that the impact of the ions enhances oxidation of the beryllium surface by increasing the diffusion of beryllium ions through the oxide layer.

A similar work was presented by Bastasz in 1984 [66], who investigated the effect of hydrogen ions on beryllium oxide layers. For this purpose beryllium bulk samples with native oxide layers were bombarded with 1 keV hydrogen ions and the emerging secondary ions monitored with a mass detector. The results showed that both desorption of oxygen from the surface and oxide growth were enhanced by the irradiation. Depending on the hydrogen ion current and the oxygen (partial) pressure, the steady state that finally developed on the sample surface from these two counteracting processes could be either clean beryllium or a stable oxide layer.

In 1987 a comparison of the erosion of carbon and beryllium under fusion plasma like conditions was presented by Roth [31]. In this article the different mechanisms that lead to the respective erosion phenomena (chemical erosion, sputtering, sublimation, ...) are discussed, and particular attention is given to the influence of oxide layers on the overall material wear.

Experiments with small beryllium wall components in fusion test reactors started in the late 80's [30], at the Impurity Study Experiment B (ISX-B) in Oak Ridge (USA) [27,28,67], UNITOR in Düsseldorf (D) [28,68-73], and at the Joint European Torus (JET) in Culham (GB) [29,74,75]. The experience gained in these experiments indicated that beryllium wall components contributed significantly to the reduction of heavy impurities ($Z > 5$) in the plasma (and thereby decrease of radiation losses) by gettering (mainly of oxygen), but also increased fuel dilution by introducing sputtered beryllium into the plasma.

Since these early experiments, much research has been performed on beryllium as potential fusion plasma facing material.

Fundamental research on beryllium has been continued, concentrating on interactions of

single crystal surfaces with air and water vapour [4,33,49,51,76-78].

For the production of beryllium reactor components, sintering and various similar pressing methods have been pursued for bulk parts [1,79,80], and evaporation and plasma spraying for the fabrication of beryllium coatings and for repair purposes [81-86].

The most important question concerning beryllium as first wall material has been if and how long beryllium can withstand the extreme thermal conditions at the edge of a nuclear fusion plasma. Research in this regard has been conducted by investigating the physical properties of beryllium and using them for model calculations [19,87-89], testing beryllium samples in dedicated facilities simulating the plasma conditions [10,19,46,81,84,86,90], and by installing beryllium components in experimental fusion reactors [10,19,70,80,91,92].

Apart from thermal loads, all plasma facing surfaces are exposed to intense irradiation by neutrons, which makes the influence of neutron irradiation on the properties of beryllium a continuing topic of investigations [39,65,93].

Besides the problem of erosion, most research has dealt with the interaction of beryllium with hydrogen isotopes [1,6,10,18,19,24,32,33,37-47]. The main reason for the importance of this aspect is the trapping of tritium in the first wall during operation of a reactor. The resulting tritium inventory is strictly limited for safety reasons, and an excessive accumulation of tritium in the first wall can therefore severely interfere with regular operation.

It became obvious early in the work on materials for plasma facing components that beryllium is a viable choice for the first wall, but an insufficient material for more highly loaded components, like divertors. Consequently, assemblies of plasma facing components of different materials are scenarios that have been investigated extensively. The most important materials in this context are carbon and tungsten. In these cases, erosion and transport of particles will cause mixing of the materials on the inner surfaces of a reactor. Therefore interactions of beryllium with carbon and tungsten are the subject of much research [6,19,26,32,43,45,46,94].

Efforts to improve the performance of beryllium components have led to developments in the geometry and design of the various parts [80,89] as well as to attempts to reinforce them with other materials (carbon fibres, titanium alloys) [1,95-97].

The most extensive experience with the operation of a fusion reactor with beryllium components has been acquired at the Joint European Torus (JET) in Culham (GB) [3,10,29,32,74,75,80,91,92,98]. Handling of beryllium components started with the first tiles and evaporators installed in 1989 and culminated in the so-called ITER-like-wall (see

below) campaign with the first wall lined completely with beryllium. Today the experiments are still ongoing, yielding necessary and valuable data on all aspects of fusion reactor operation.

The next big step in fusion research is the construction of the International Thermonuclear Experimental Reactor ITER, surpassing previous experiments in size, confinement time and power output, and providing the necessary means to test fusion reactor operation at conditions closer to foreseen fusion power plants. The preliminary research and design effort is immense, and since ITER will have a full beryllium first wall, much of this work concerns the probable behaviour of beryllium at the planned fusion plasma power level [1,10,18,31,99-101].

The planned magnitude of ITER and the amount of beryllium involved entails new safety concerns that have to be addressed thoroughly. One is the generation of beryllium dust on a large scale by erosion. Beryllium can cause chronic beryllium disease (CBD), an incurable disease of the lung, if inhaled [3,4]. The regularly accumulating dust therefore has to be handled and disposed of properly and with great care [3,18,19,101-106].

A second safety issue is the possibility of a leak occurring between the plasma chamber and the cooling system or atmosphere. The inflowing steam or water vapour would react with the hot beryllium, resulting in large quantities of hydrogen gas combined with a rise in temperature caused by the released reaction energy, and therefore presenting a considerable safety hazard. Consequently, concerted investigations deal with the beryllium-water reaction under various conditions and with the design of measures to mitigate the dangers of these accident scenarios [19,39,48,103,106-109].

The ITER design also brought about a new application of beryllium in reactor operation as neutron multiplier in the tritium breeder blanket [1,48,96,110]. Apart from the somewhat different operating conditions, the considerations and concerns for beryllium in this application are the same as those for beryllium as plasma facing material.

3. Theory of Diffusion-Controlled Oxidation

In most cases, exposure of a clean metal surface to air or other oxygen-containing gases leads to adsorption of oxygen on the surface and subsequent oxidation of the metal. Once a closed oxide layer has formed, further growth of the oxide proceeds by diffusion of ions through the oxide layer and oxidation at an interface - either the diffusion of oxygen ions and oxidation at the oxide-metal interface, or the diffusion of metal ions and oxidation at the surface. [111]. If the supply with oxygen (i.e. the partial pressure of oxygen or other suitable gases, like air, water vapour or carbon dioxide) is sufficiently high, this diffusion is the process determining the rate of oxidation.

A simple model of diffusion-controlled oxidation was developed in the early 20th century by Tammann [112] and Pilling and Bedworth [113], based on the observation that oxide growth is proportional to the square root of time for many metals. For this model, the following assumptions are made:

- The charge of diffusing particles is neglected (atomic/molecular diffusion).
- The diffusion coefficient D is independent of the concentration C of the diffusing particles.
- The concentrations of the diffusing particles at the interface metal-oxide $C(0)$ and at the oxide surface $C(L)$ are independent of the oxide thickness L .
- Oxide growth is considered a steady state process.

The basic equations for this model are Fick's first law for the current J of uncharged particles in the direction of oxide growth x

$$J = -D \frac{\partial C}{\partial x} \quad (1)$$

and Fick's second law

$$\frac{\partial J}{\partial x} = - \frac{\partial C}{\partial t} \quad (2)$$

The assumption of a steady state means

$$\frac{\partial C}{\partial t} = 0 \quad (3)$$

and therefore

$$\frac{\partial J}{\partial x} = 0. \quad (4)$$

This means that J is independent of the position in the oxide, and eq. (1) can be written as

$$\frac{\partial C(x)}{\partial x} = -\frac{J}{D} = \text{const}. \quad (5)$$

Integration over the oxide thickness yields

$$C(L) - C(0) = -\frac{LJ}{D} \quad (6)$$

or

$$J = \frac{D[C(0) - C(L)]}{L}. \quad (7)$$

The particle flux J is connected to the oxide growth $dL(t)/dt$ by the volume of oxide V formed from each diffusing particle

$$J = \frac{1}{V} \frac{dL(t)}{dt}. \quad (8)$$

From eqs. (7) and (8) we get for the oxide growth

$$\frac{dL(t)}{dt} = \frac{k}{L} \quad (9)$$

or

$$L(t)^2 - L(0)^2 = 2kt \quad (10)$$

with the rate constant k

$$k = VD[C(0) - C(L)] \quad (11)$$

for parabolic oxide growth.

The diffusion of particles determining the rate of oxidation via the diffusion coefficient D can often be described as a thermally activated hopping of the particles between suitable lattice sites [114]. In the most simple case this takes the form of an Arrhenius-type equation for the diffusion coefficient [114]

$$D(T) = Ae^{\left(\frac{-E_A}{k_B T}\right)} \quad (12)$$

where E_A is the activation energy for particle transport, T the temperature, k_B the Boltzmann constant, and A a constant for the specific system of metal and gas.

4. Experimental

4.1. Sample Preparation and Safety

4.1.1 Samples

The beryllium samples that were used for this study were procured from a previous series of hydrogen outgassing experiments at the Institut für Allgemeine Physik (Vienna University of Technology) [115,116].

There were two different sets of samples: one was S65C grade vacuum hot pressed (VHP) beryllium from Brush Wellman, Inc. (USA). The other set consisted of plasma-sprayed samples that were prepared at the Los Alamos National Laboratory (USA) [85]. The composition for these two types of samples are given in table 2.

Both types of samples were approximately $5 \times 5 \times 2 \text{ mm}^3$ in size and had a weight of approximately 130 mg. All experiments were performed using at least one sample of each type, to detect any differences in behaviour. As no difference was detected for any of the experiments, the results apply to both types of samples.

impurity	S65C VHP	plasma sprayed
BeO	max 1 wt%	0,36 wt%
C	max 0,1 wt%	0,09 wt%
Fe	max 0,08 wt%	985 ppm
Al	max 0,06 wt%	600 ppm
Si	max 0,06 wt%	420 ppm
Mg	max 0,06 wt%	130 ppm
other	max 0,04 wt% each	< 200 ppm each

Table 2: Composition of the two sets of beryllium samples: S65C grade vacuum hot pressed from Brush Wellman (values provided by the manufacturer) and plasma-sprayed from Los Alamos National Laboratory [85]

4.1.2 Sample Preparation

Preliminary experiments with the as-received, unprepared samples showed that the surface of the samples was too rough to make sputter depth profiling analysis with an Auger electron spectrometer feasible. The samples needed to be polished before the experiments, which necessitated additional safety measures. For this purpose a glove box with integrated grinding machine was set up (see fig. 1). It consists of a main chamber with a closed filtered air circulation system (filter pore size 300 nm) that also keeps the pressure in the chamber slightly below atmospheric pressure, as well as an entry lock chamber. The grinding machine is suited for SiC abrasive paper and equipped with a closed water circuit for cooling and flushing, driven by an external peristaltic pump.

After entering a sample into the glove box by way of the entry lock, it was polished manually on the grinding machine under running water. For this purpose, four cycles with polishing paper of increasingly fine SiC grit (200 to 4400) were carried out. Afterwards, residual polishing dust particles were rinsed off the sample under running water and the sample was dried with lint-free tissue in order to avoid water stains. Subsequently a period of approximately one hour was allowed for airborne dust to settle or get filtered, after which the sample was removed from the glove box.

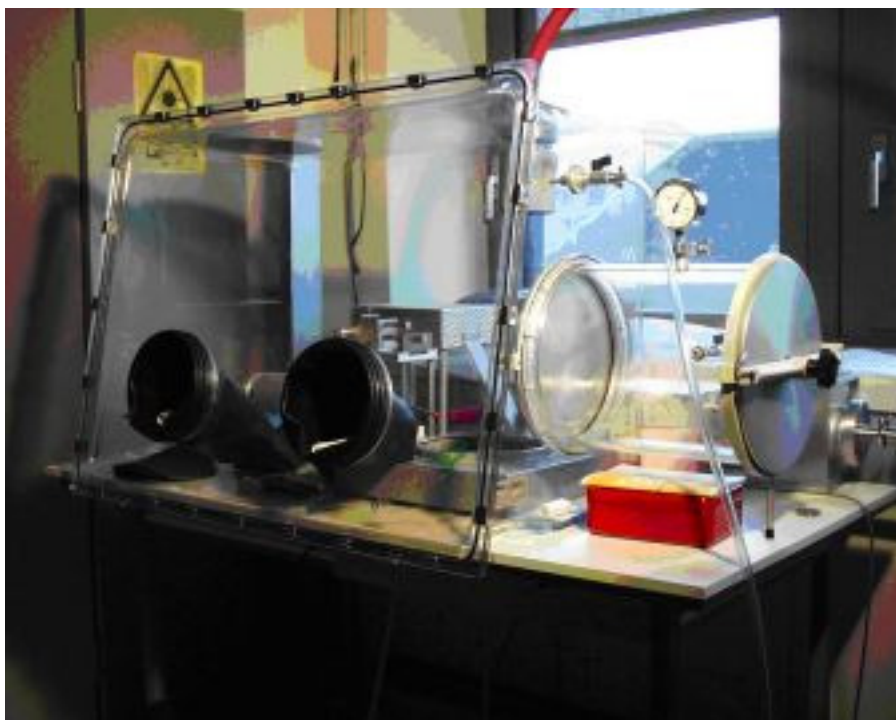


Fig. 1: Glove box for sample polishing

In order to monitor the beryllium dust contamination level in the laboratories, three times during the duration of this work a series of wipe samples was taken from various spots in the respective work areas. For the appropriate wipe testing procedure, a surface area of approximately 1000 cm² on the chosen spot is wiped with lint-free tissue that has been wetted with distilled water. These samples are then analysed with atomic absorption spectrometry.

The contamination of freely accessible surfaces was below the legal limits at all times, but showed a slight increase in the course of this work.

In order to obtain information about the structure of the samples and surface oxide layers, polished cross sections of selected samples were prepared with the grinding machine in the glove box. Additionally, a ball cratering device was installed in the glove box and ball craters of various sizes (5 - 20 mm ball diameter) were prepared. Both preparation methods proved to be qualitatively insufficient to provide metallographic information.

4.2. Oxidation Experiments

4.2.1 Furnace Setup

The heating and plasma exposure experiments were performed in an AHT tubular furnace adapted for use with various atmospheres under pressures from low vacuum to atmospheric pressure.

Fig. 2 shows a schematic setup of the furnace. It consists of insulation elements made of ceramic fibres with embedded Kanthal heating coils. Inside, an aluminium oxide tube equipped with three platinum/platinum-rhodium thermocouples is installed. In the aluminium oxide tube a fused silica tube with 25 mm internal diameter is installed, which can be evacuated to approximately 10⁻² mbar. Temperatures up to 1200 °C in air and up to 1100 °C in vacuum can be reached, and the temperature is precise and stable to within 1 to 3 °C. The whole setup is divided into three independently controlled heating zones, which permits a fairly even temperature distribution in the inner tube. Stability and temperature distribution were verified before the experiments with a trailing thermocouple.

4.2.2 Oxidation Experiments

The temperatures that were chosen for these experiments were 390 °C, 500 °C and 600 °C. 390 °C was chosen because at this temperature the vapour pressure of beryllium is well below 10^{-12} mbar. Below this value, it is safe to handle and heat beryllium without additional safety measures, and especially without a closed sample holder.

For heating above this temperature, the samples were put into fused silica vials, which were plugged with mineral wool. This reduced the distribution of beryllium vapour, but permitted access of air to the sample so that a depletion of oxygen in the vial would be replenished. A characteristic time for this exchange was estimated as $\tau \sim (V_{\text{vial}} \cdot l) / (A_{\text{vial}} \cdot D_{\text{ox}})$,

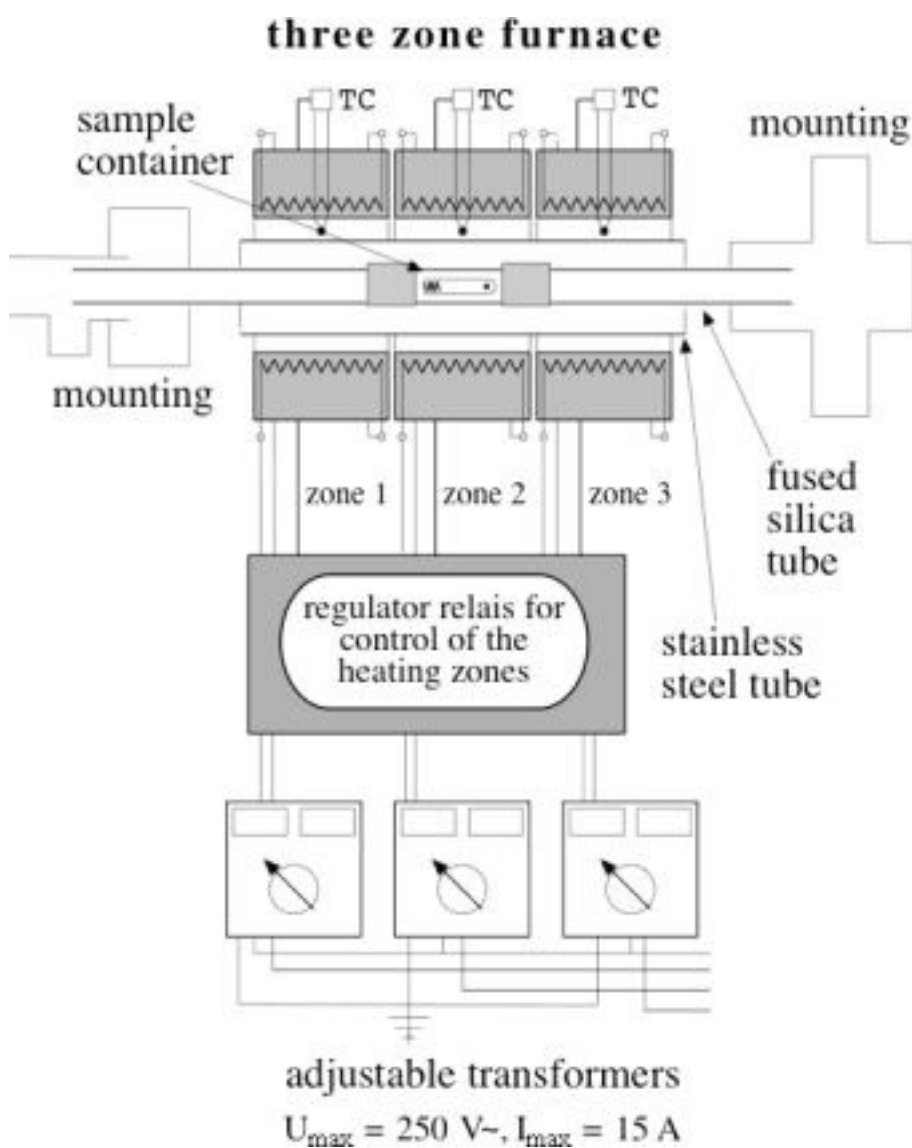


Fig. 2: Tubular furnace setup

with a vial volume of $V_{vial} \sim 100 \text{ cm}^3$, a diffusion length of $l \sim 1 \text{ cm}$, a cross section of $A_{vial} \sim 3 \text{ cm}^2$, and a diffusion coefficient of oxygen in air of $D_{ox} \sim 0,2 \text{ cm}^2/\text{s}$, which amounts to $\tau \sim 1 \text{ min}$.

Above 600°C , it is not safe to heat beryllium with the simple vials described. 500°C was chosen as an intermediate value.

Heating durations between 1 h and 43 h (the longest time for 390°C) were used. 1 h is near the shortest useful time considering the error introduced by the additional heating and cooling time. At 43 h and 390°C saturation of the thickness of the oxide layer had already set in. At the higher temperatures, saturation set in much earlier.

After polishing in the glove box, the beryllium samples were put into the mid heating section of the fused silica furnace tube, which was left open on both ends for heating in air. Heating of the furnace was started after the samples had been inserted, and after the oxidation experiment the samples were left in the furnace during the cooling period. This added the time of heating up and cooling down of the furnace to the nominal heating duration. In the cases where a vial was used, the whole vial was put into the glove box after heating, the sample removed and the mineral wool plug disposed of in the box. The sample was subsequently mounted on a sample holder for Auger electron spectroscopy and inserted into the spectrometer.

4.3. Plasma Exposure Experiments

4.3.1 Furnace Setup for Plasma Exposure

External electrodes are attached along a length of 20 cm to the mid section of the fused silica furnace tube in order to enable the excitation of a capacitively coupled r.f. plasma inside the furnace, provided the pressure in the tube is within the mbar range. The plasma volume is roughly 100 cm^3 and r.f. powers up to 1100 W are available. The typical powers for this series of experiments were around 100 W. Interaction of the hydrogen plasma with fused silica would introduce trace amounts of water vapour into the plasma. To avoid the interaction of the hydrogen plasma with the fused silica tube, an AlN tube was used as the innermost furnace tube. It fitted into the fused silica tube and could be inserted and removed as necessary.

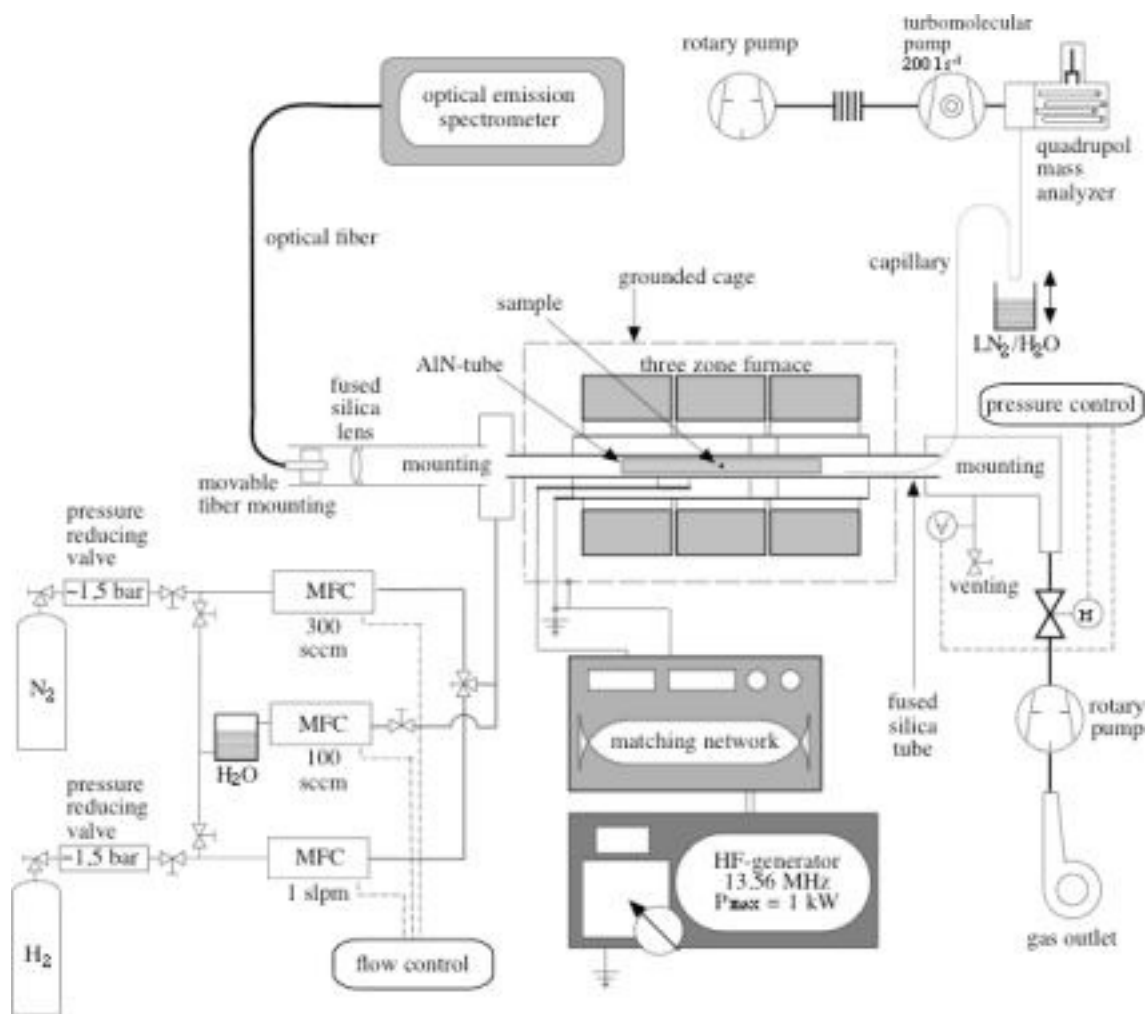


Fig. 3: Furnace setup for plasma exposure

Fig. 3 shows the schematics for this plasma exposure setup, with further components like roughing pump, pressure control valve, nitrogen and hydrogen gas supply system, water vapour supply and gas mixing system, optical and mass spectrometer (see below), as well as the approximate size and position of the sample inside the furnace tube.

4.3.2 Control of the Atmosphere inside the Furnace

A rotary roughing pump and a regulation valve are attached to the furnace for evacuation and pressure control. High purity (99,999%) hydrogen and nitrogen supplies are attached via pressure regulators and mass flow controllers (MFC). Nitrogen is used for flushing the gas supply system and the furnace prior to and after experiments in hydrogen atmosphere in order to avoid the formation of explosive gas mixtures.

The furnace volume (between the MFCs and the regulation valve) is kept at a pressure of approx. 5-10 mbar during the plasma exposure experiments. The pressure between the pressure regulators and the MFCs is kept at 1,5 bar. A value above atmospheric pressure is necessary in this stage of the gas supply to prevent the influx of impurities from air into the supply system if the system would be leaking. Furthermore, the mass flow controllers need a minimum pressure drop for proper operation. Higher pressures would present an increased risk of accumulation of a dangerous amount of hydrogen.

A water cooled chamber containing distilled water is attached to the gas supply system in order to supply minute amounts of water vapour. The temperature, controlled by the cold water bath, is kept at 11 ± 1 °C and gives a water vapour pressure of 13 ± 1 mbar. Hydrogen fed through the chamber at 1,5 bar is saturated with water vapour, resulting in a concentration of water vapour $C_{w,1} = 0,87 \pm 0,05$ %. The mixture can then be dynamically diluted in a second mixing stage using the MFCs for pure and water vapour saturated hydrogen: a flow Q_1 of water vapour saturated hydrogen is mixed with a much larger flow Q_0 of pure hydrogen, containing water vapour and possibly oxygen impurities with an unknown concentration $C_{w,0}$. The concentration of water vapour in the gas entering the furnace is then

$$C_{w,2} = \frac{C_{w,1}(T_1)Q_1 + C_{w,0}Q_0}{Q_0 + Q_1} \quad (13)$$

In the furnace tube, further addition of impurities has to be taken into account. Possible sources include desorption of oxygen and water vapour from the walls of the plasma vessel and backdiffusion from the vacuum pump. These contributions can be summarised as a single additional influx of water vapour Q_d . The total concentration of water vapour in the plasma is therefore

$$C_{w,p} = \frac{C_{w,1}(T_1)Q_1 + C_{w,0}Q_0 + Q_d}{Q_0 + Q_1} \quad (14)$$

$C_{w,0}$ is expected to be less than 10 ppm, as 99,999 % pure hydrogen is used at a sufficiently high flow rate. Measurement of the residual water vapour impurity concentration C_d produced by the flow Q_d has been attempted by means of optical spectrometry and mass spectrometry (see below) and was found to be less than 3 ppm.

4.3.3 Heating and Plasma Exposure Experiments in Hydrogen

The beryllium samples were first placed in the mid section of the furnace tube. A continuous flow of hydrogen was led through the furnace. By adjusting the valve between the downstream end of the furnace tube and the vacuum pump the pressure was stabilized at the pressure needed for the experiment (between 1 and 10 mbar). Heating was then carried out analogous to the oxidation experiments in air (see section Oxidation Experiments).

For heating in pure hydrogen a quartz vial was used as sample holder. For plasma exposure experiments an open sample holder was used to enable contact between the sample surface and the plasma. Once the hydrogen flow and pressure was established and the nominal temperature of the experiment was reached, the r.f. plasma was ignited. After the exposure experiment, heating and plasma supply were turned off at the same time.

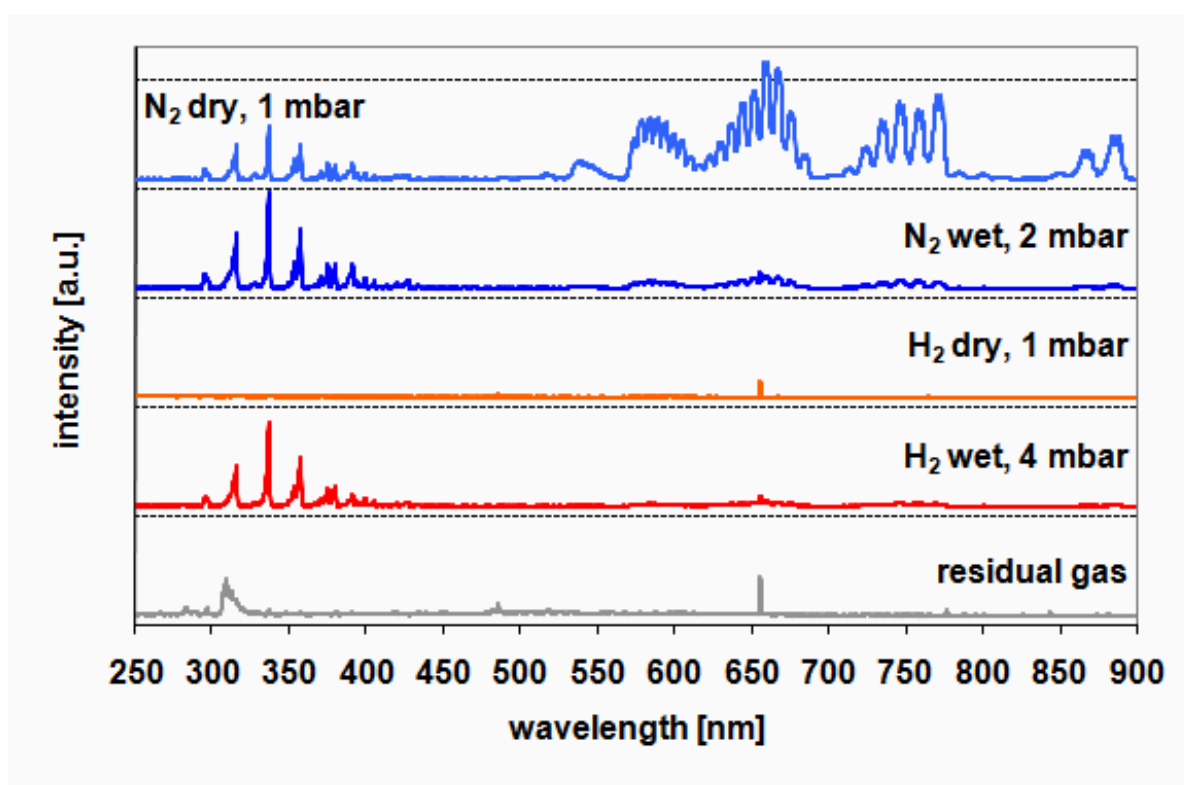


Fig. 4: Optical emission spectra in the furnace for various plasma compositions

4.3.4 Measurement of Impurities in the Furnace: Optical Spectrometry

In order to measure the concentration of oxygen-containing impurities in the plasma, an Ocean Optics HR-4000 high resolution UV-VIS-NIR spectrometer was attached to the furnace. It was mounted near the downstream end in the extension of the furnace tube and connected via a glass lens and fibre optics that were adjustable in their distance to each other so that the focus could be optimised. The molecule that was monitored with this setup was OH with its emission band near 308 nm, giving a general measure for oxygen-containing impurities in the hydrogen plasma. The method can be calibrated absolutely, using the gas mixing setup and comparing the intensity of the OH band with a spectroscopic feature of molecular hydrogen, e.g. the dissociation continuum with a maximum near 280 nm. Fig. 4 shows examples of spectra for various plasma compositions. However, the sensitivity of the method with respect to the OH-band is greatly reduced in hydrogen and nitrogen in comparison to noble gas atmospheres, where the OH-band is a common indicator for water vapour. Furthermore, the signal decreased rapidly above a pressure of 1 mbar, which is slightly too low for the purpose of these experiments.

4.3.5 Measurement of Impurities in the Furnace: Mass Spectrometry

A Balzers QMG 420 quadrupole mass spectrometer (quadrupole mass analyser, QMA) was connected to the furnace tube with a 0,8 mm diameter steel capillary (see fig. 3). The QMA chamber is pumped by three turbomolecular pumps to a pressure of approximately 10^{-6} mbar, resulting in a parabolic pressure gradient in the capillary emerging from the furnace tube (pressure range 1 to 10 mbar). Set to mass 18, the mass spectrometer gives a rough feedback of the water vapour content in the furnace tube, superimposed on a background signal from residual water vapour in the QMA chamber.

More refined results were obtained by freezing part of the capillary with liquid nitrogen for a certain time and then rapidly heating it with water at room temperature. Freezing and thawing the water vapour in the capillary periodically in this way permits to separate the water vapour transferred from the furnace from the background in the mass spectrometer. Furthermore, extended freezing periods accumulate water in the capillary and thus increase sensitivity. Thawing then results in a peak in the QMA-signal for mass 18 with a delay of approximately 30 s. The area of this peak is a measure for the amount of water

vapour accumulated during the freezing period. If this amount is assumed to be proportional to $p_0 \cdot t_f \cdot c_w$, where p_0 is the pressure in the furnace, t_f the freezing time and c_w the concentration of water vapour in the furnace, then the concentration c_w can be measured after calibration of the mass spectrometer with respect to the current conditions. The mass spectrometer was calibrated by measurements at defined pressures p_0 and concentrations c_w set by the flow controllers, and for different freezing times t_f (see fig. 5). These experimental data were fit with a second order polynomial, which was then extrapolated to lower amounts of water vapour. Inserting the results for measurements with dry hydrogen allows to estimate the fraction of water vapour impurities in the furnace to be below $3 \cdot 10^{-6}$ mbar or, with $p_0 = 1$ to 10 mbar, $c_w = 3 \cdot 10^{-6}$ to $3 \cdot 10^{-7}$.

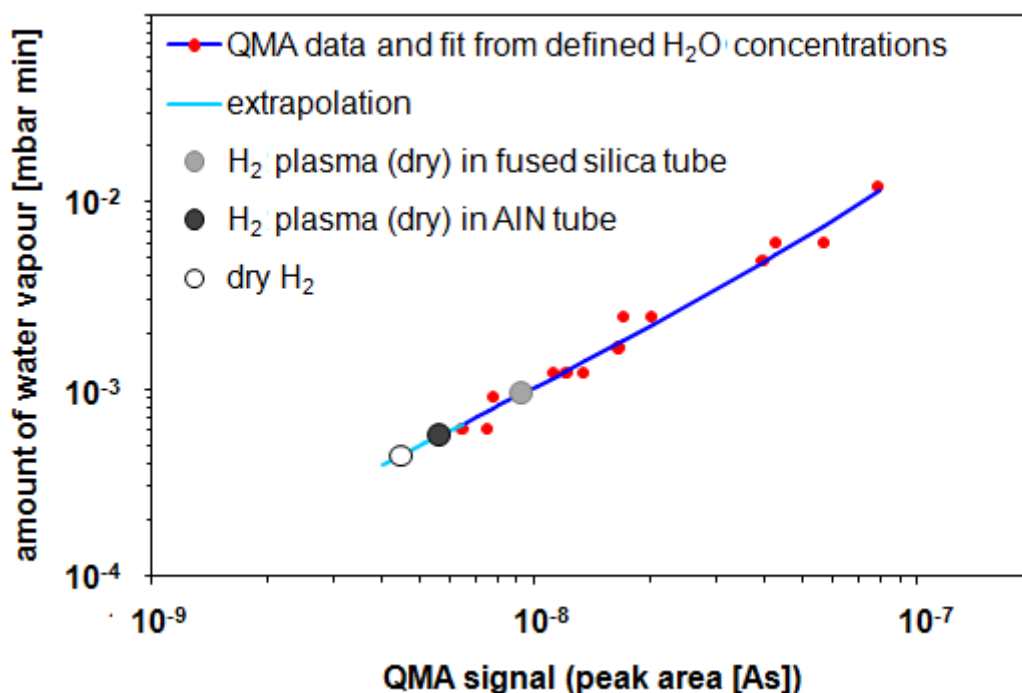


Fig. 5: Calibration of the quadrupole mass analyser by fitting a second order polynomial to the results for known concentrations and extrapolation to lower amounts of water vapour.

The y-axis gives the partial pressure in the oven multiplied with the freezing time.

4.4. Auger Electron Spectroscopy

4.4.1 Auger Effect

Auger electron spectroscopy is a surface analysis method based on the Auger effect, which was discovered by Lise Meitner [117] and Pierre Auger [118]. When an electron in an atomic shell is hit by an external particle or electromagnetic radiation with sufficient energy to remove it from its shell (lifting it up into a higher shell or removing it from the atom), a hole in the original shell is left behind. This hole is filled up by a second electron from a higher shell. The difference in potential energy between these two shells can either be released as electromagnetic radiation (characteristic x-ray radiation) or transferred to a third electron in this atom. If this energy is sufficiently high, the third electron is excited and ejected from the atom with a kinetic energy, which is characteristic for the atom and the combination of shells that were involved in the process, and it is then called an Auger electron.

4.4.2 Application for Surface Analysis

In Auger electron spectroscopy, a medium to high energy (typically 10 keV) electron probe beam is used to excite Auger electrons in the sample. These electrons can then be separated by their energy and appear as element characteristic peaks in the electron energy spectrum. The energy range of Auger electrons used for analysis is usually approx. between 100 eV and 3000 eV. Since electrons in this energy range travel only a short distance in a solid body before being scattered inelastically, the detected Auger electrons originate from a depth of only a few nm, making Auger electron spectroscopy a very surface sensitive analysis method. Depth profiling can be done by alternately recording a spectrum and ion etching the sample (sputtering).

Imaging is possible by scanning the electron beam, similar to scanning electron microscopy (SEM). The lateral resolution for imaging can be as low as 5 nm, the resolution for analysis is about 50 nm due to the extent of the area around the electron beam where Auger electrons are excited.

The detection limit for qualitative analysis is about 1 at%. For quantitative analysis, the areas of the Auger peaks are evaluated and related to each other. Auger electron spectroscopy is usually not sensitive to the chemical state of the detected elements.

However, some low energy Auger peaks, especially those of light metals, show a slight shift of their position on the energy scale when the element is oxidized.

4.4.3 Instrument

The instrument used for the analysis of the beryllium samples was a commercial Auger electron spectrometer, model VG Microlab 310 F. The apparatus is shown schematically in fig. 6.

The analysis chamber consists of a stainless steel vessel under ultra high vacuum conditions and is pumped by two ion pumps. Base pressure is $7 \cdot 10^{-10}$ mbar. The samples are inserted by way of a fast entry airlock which is pumped by a turbomolecular pump to a pressure of 10^{-7} mbar.

The electron beam is generated and focussed in the electron optical column arranged along the vertical axis. The source of the electron beam is a field emission gun. In the following sections of the column the electrons are accelerated to their final energy (primary beam energy, usually 10 keV) and focused by electrostatic and magnetic lenses. The final section is a deflection unit for scanning the electron beam across the sample, synchronized with a frame grabber for image generation.

Measurement of the electrons leaving the sample is accomplished by a hemispherical analyser. The electrons are focussed onto the entrance slit by means of a retarding lens. In the analyser they are separated with respect to their energy by applying an electrical field between the inner and outer hemispheres, and only electrons corresponding to the set pass energy reach the exit slit. There are two modes of adjusting the retarding field and the analysing field during spectrum acquisition: constant analyser energy (CAE) and constant retard ratio (CRR). For CAE, the analysing field, i.e. the voltage between the hemispheres, is set to a fixed value, and only the retarding field is adjusted to sequentially measure electrons of all energies. During CRR, both fields are adjusted while keeping the ratio between them constant.

The electron detector at the exit of the analyser consists of a linear array of five channel electron multipliers (channeltrons). The signal of the channeltrons is processed by a preamplifier and a discriminator and finally sent to a computer for counting and evaluation. The spectrometer is equipped with an EX05 ion gun system. It generates a 3 keV Ar ion beam for *in situ* sputter cleaning and depth profiling of the samples. The ion current is in

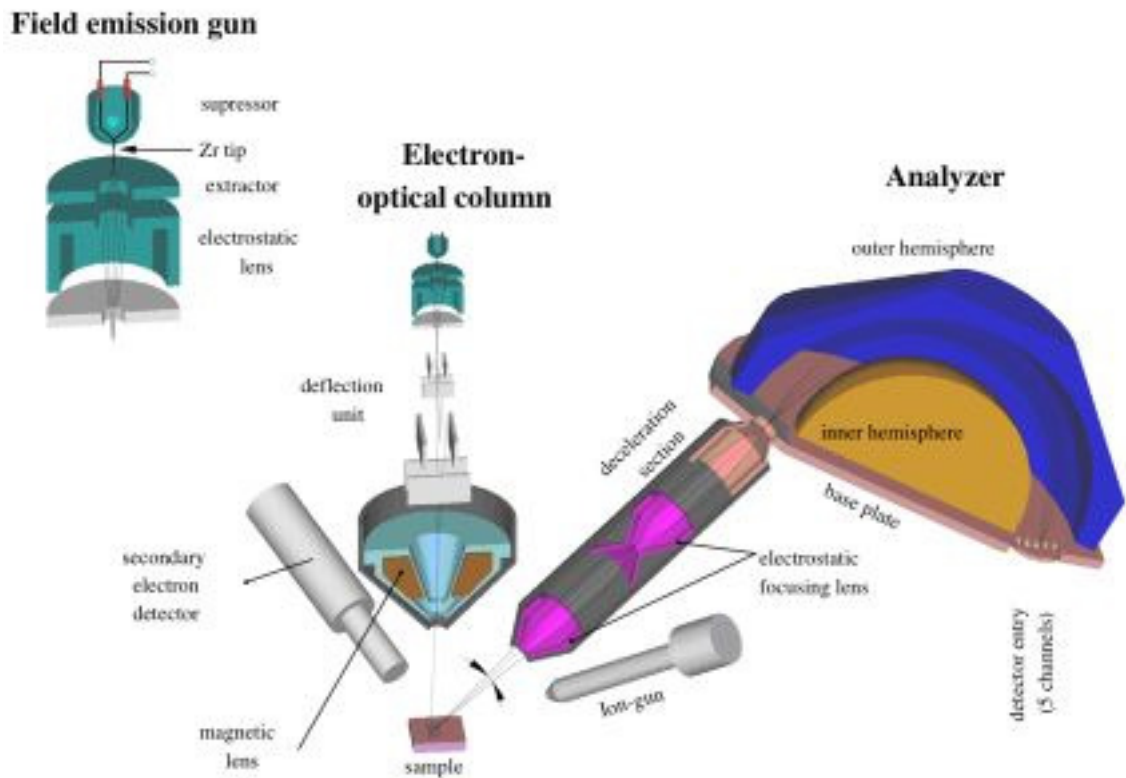


Fig. 6: Schematics of the Auger electron spectrometer

the range of approx. 0,1 to 1 μA . The beam can be focused on an area of approx. $0,5 \times 0,5 \text{ mm}^2$ coinciding with the analysis spot.

Mounted on a special sample holder, samples can be heated *in situ* inside the analysis chamber. Temperatures up to 600°C are possible, provided the pressure during heating remains below 10^{-7} mbar. Temperature measurement is performed with a thermocouple installed on a holder, which can be moved from outside the vacuum system (wobble stick). The temperature can be set with an error of $\pm 10^\circ$.

A quadrupole mass spectrometer is attached to the analysis chamber for residual gas analysis.

4.4.4 Experiment and Analysis Sequence

After the heating or plasma exposure experiments, the samples were examined with sputter depth profiling in the Auger electron spectrometer in order to determine the thickness of the oxide layer on the surface. The method consists of alternately taking an

Auger spectrum and removing a layer from the sample surface by sputtering it with argon ions. For this purpose a pressure of 10^{-6} mbar argon was established in the ion gun, corresponding to a pressure of 10^{-8} mbar in the analysis chamber. The energy of the primary electrons was 10 keV, the energy of the argon ions was 3 keV. Typical argon ion sputtering currents for this pressure were in the range of 100 to 500 nA. The ion image (ion beam scan area) magnification chosen for sputtering was usually 300x, corresponding to a sputtered area of approx. 0,5 x 0,5 mm. Within this sputtering area several spots with a diameter of approx. 100 nm were chosen for analysis. Fig. 7 shows an example of a secondary electron image of a sputter depth profiling area with marked analysis spots on a beryllium sample. On each sample 2 to 5 sputter depth profiles were taken. The retard ratio of the analyser was set to CRR=4 for all spectra.

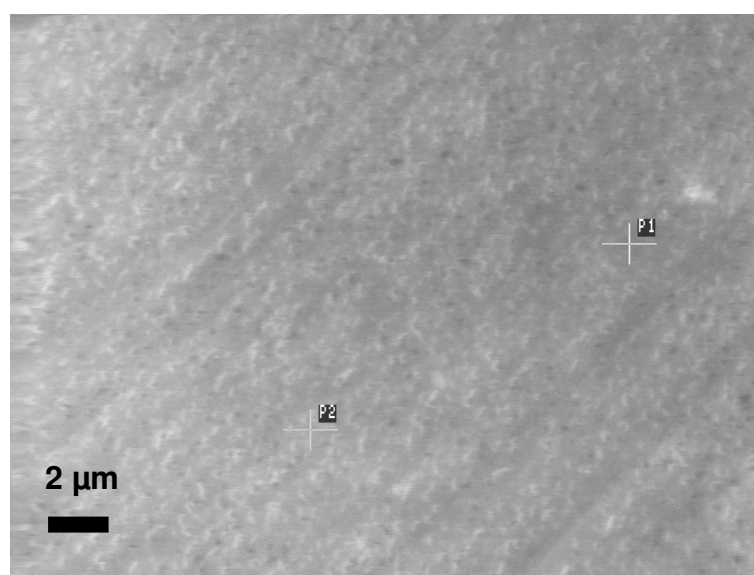


*Fig. 7: SEM image of sputter depth profiling area with marked analysis spots;
image size 24 x 18 μm*

4.4.5 Evaluation of Sputter Depth Profiles

The analysis data obtained from a sputter depth profile consists of a series of Auger spectra with corresponding sputtering times. Fig. 8 shows Auger spectra of beryllium surfaces in various states of oxidation. The peaks that were evaluated for the profiles were carbon (284 eV), oxygen (528 eV) and beryllium. The beryllium peak shows a shift of 9 eV between metallic state (104 eV) and oxidised state (95 eV) as has been established before

[60,61,119], which makes them well distinguishable. Further elements were not detected, the impurities listed in chapter 4.1.1 are below the detection limit of the Auger electron spectrometer.

From the spectra, the elemental concentrations are derived by evaluation of the Auger peaks. Each element peak is defined by setting its limits on the electron energy scale manually and by subtracting a background provided by the evaluation software (usually with a Shirley algorithm [120]). The peak area above this background and between its limits is calculated by the software and taken as a measure for the peak intensity. The element concentrations (in atomic percent) are calculated from these peak areas by using empirical peak sensitivity factors as well as the transmission function of the instrument.

The sputtering time is transformed to depth scale by calibration with tantalum oxide (Ta_2O_5) films, which can be produced electrochemically with a very accurately defined thickness. The resulting scale factor is further modified by taking the ion current and the ion image magnification into account.

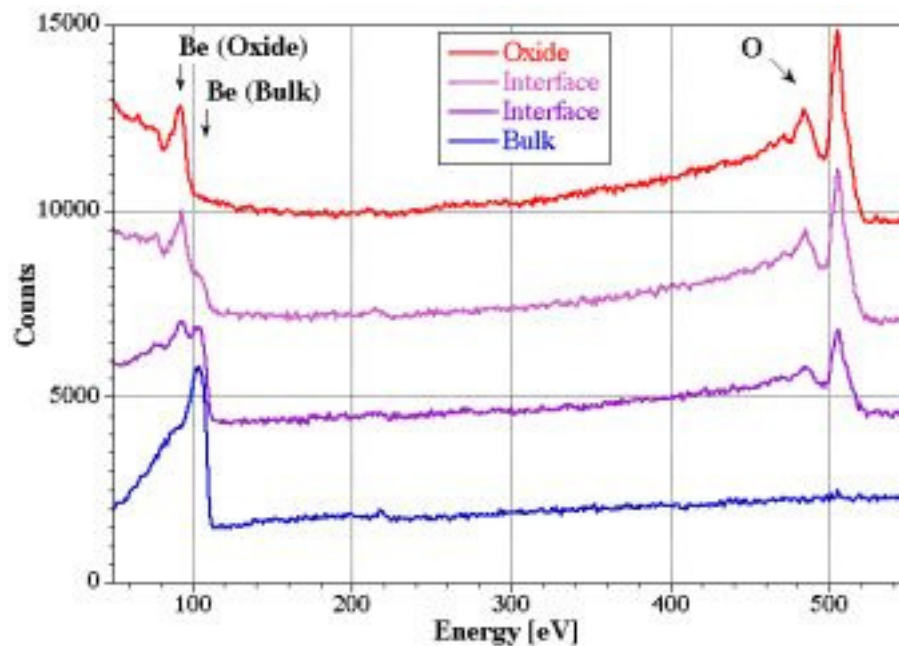


Fig. 8: Auger spectra of beryllium in various states of oxidation, from fully oxidised (top) to pure metal (bottom)

Since sputtering rates depend on the sputtered material, the scale determined by Ta_2O_5 calibration could only be considered an initial estimation. Possibly necessary corrections of it were estimated by comparison with literature values for beryllium oxide layer thicknesses. According to Adams and Hurd [8], the native oxide thickness is 10 nm, while

according to the depth scale in the present experiments, it is 1 nm, suggesting a depth error of a factor of 10 for these measurements. The value of Adams and Hurd is however based on an even older publication, and it is not clear whether this value is actually based on a measurement or is simply an estimate. Weight gain measurements published by Aylmore *et al.* [9] point to the formation of a protective oxide at 500-600 °C in oxygen at a weight gain of 30 $\mu\text{g}/\text{cm}^2$. The thickness in this case can be calculated to be 150 nm. In the present analysis, the according oxide layer thickness is 30-40 nm, pointing to a more plausible depth error of a factor of 3-4. The error could be even less if grain boundary oxidation also occurred in the experiments of Aylmore *et al.*, contributing to weight gain, but not to oxide thickness. Roth *et al.* [6] performed heating experiments of beryllium samples in oxygen at temperatures up to 600 °C which are comparable to the present heating experiments in air [7]. The resulting oxide thicknesses, measured by Rutherford backscattering (RBS), lie within about 20% of the present values for similar conditions, indicating that this is probably the magnitude of the error in the depth scale used here.

Fig. 9 exemplarily shows sputter depth profiles of a native oxide layer and of an oxide layer after heating for 43 h at 390 °C in air.

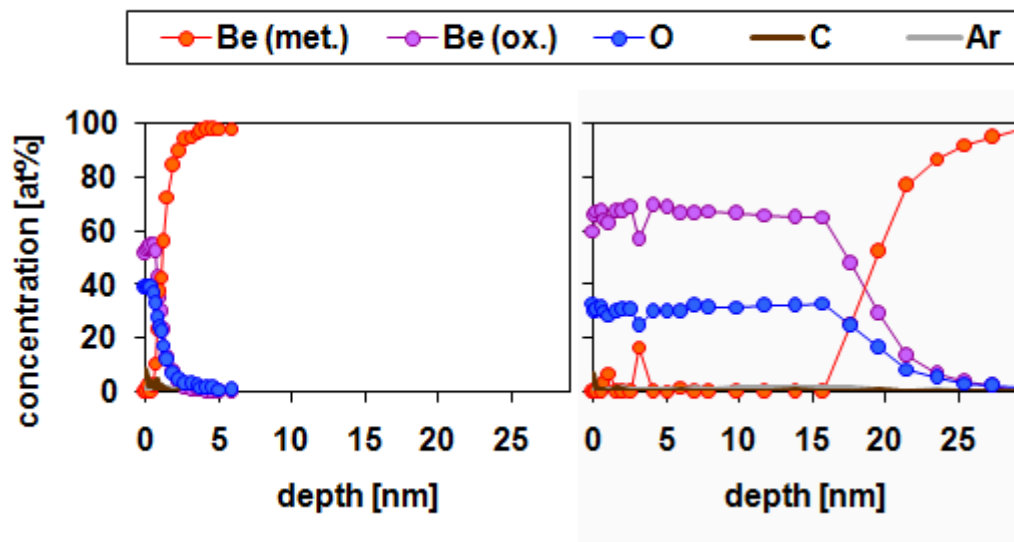


Fig. 9: Sputter depth profiles of native oxide (left) and after heating for 43 h at 390 °C in air (right)

5. Results and discussion

5.1 Oxidation in Air

5.1.1 Parabolic Oxidation Kinetics

The beryllium oxide thicknesses (averages of the measured values for each temperature and heating duration) are summarized in table 3. The complete thickness measurement results are compiled in the appendix. With these values the oxidation kinetics of beryllium in air were investigated.

For the conditions of the experiments presented here, i.e. oxidation at atmosphere and temperatures between 390 °C and 600 °C, diffusion controlled oxidation was assumed. The corresponding parabolic oxidation behaviour is common for many metals and has been reported for beryllium by several authors [6,7,48,54,55,57,101,106,108]. The associated mechanism is the diffusion of beryllium ions from the metal-oxide interface through the oxide layer to the surface and subsequent oxidation. With a sufficient supply of oxygen or oxidising compounds at the surface this diffusion is the rate-controlling step for the oxide growth. The fact that beryllium is the diffusing ion species would be expected since beryllium ions are smaller than oxygen ions, and can also be established on the basis of the weak dependence of the oxide growth rate on the pressure of the oxidising atmosphere [6,55]. Beryllium as the diffusing ion species has been verified by oxidation experiments with ^{18}O [6].

A simple model for parabolic oxidation is described in section 3.1. Applying this model to the measurement results, the oxide thicknesses can be fitted with eq. 10, with the oxidation rate constant as free fitting parameter. Using a standard linear least squares fitting procedure yields the oxidation curves that are shown in fig. 10 together with the measured values.

	1 h	4,5 h	17 h	20 h	41 h	43 h
390 °C	4,3 ± 1	8,0 ± 4	13,5 ± 2	-	-	15,6 ± 4
500 °C	11,5 ± 2		41,5 ± 4	-	-	42,0 ± 18
600 °C	40,0 ± 8	-	-	74,8 ± 36	62,3 ± 22	-

Table 3: Oxide thicknesses [nm] after heating at various temperatures for different durations

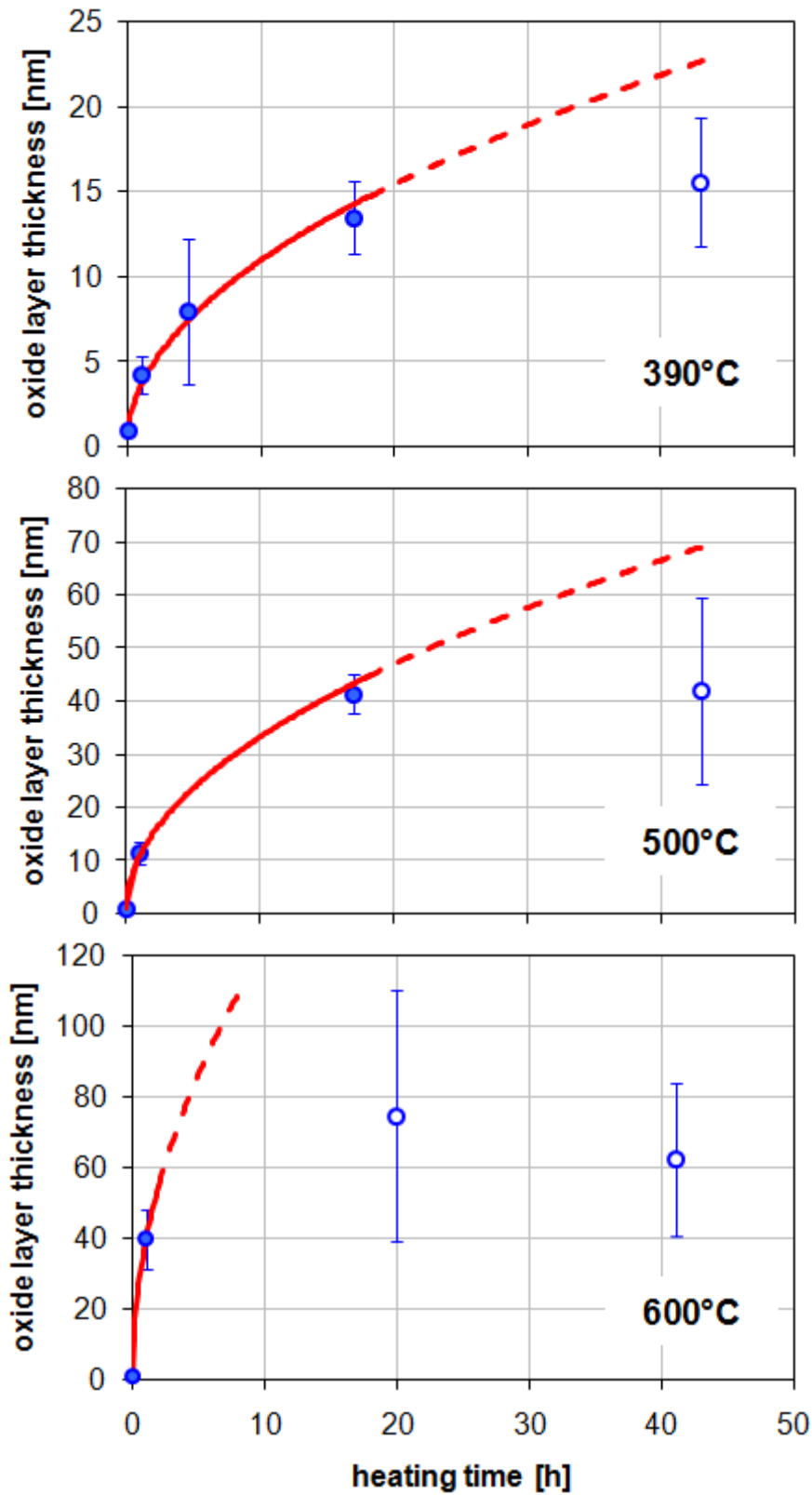


Fig. 10: Growth of the oxide thickness over time for heating at 390 °C, 500 °C and 600 °C. The curves are fits of parabolic oxidation (eq. 10) to the full symbols.

For 390°C and 500°C the data up to a heating duration of 17 h were used for the fit. The values above that duration show a much higher scatter and are lower than would be expected from the parabolic growth behaviour determined from the lower values. For 600°C this duration limit is even lower - data up to 1 h were used for fitting. However, it cannot be determined with certainty that the data at 600°C and 1 h are valid for this evaluation since there are only two data points (0 h and 1 h) used for the parabolic fit. Indications that the oxidation at 1 h is still parabolic are the lower oxide thickness and the much lower data scatter compared to the higher durations.

The deviation to lower than parabolic growth rates has been observed before [9,48,52]. As a possible explanation for this phenomenon the diffusion of impurities from the beryllium bulk into the oxide layer during the heating period has been put forward, which would change the composition of the oxide layer and therefore the diffusivity of the beryllium ions in the oxide (see discussion further below). In the present work no impurity elements were detected by AES during the depth profile analyses. However, since the detection limit for AES is approx. 1 at%, this would still allow for impurities below that level.

Another cause for the alteration in oxidation rate, for the experiments at 600°C, is the onset of catastrophic oxidation with loosening of oxide particles from the surface, which would also explain the high scatter of the oxide thickness values and their decrease from 20 to 41 h. This was verified with the help of SEM images for the experiments with durations higher than 1 h (see discussion of catastrophic oxidation below).

The temperature dependence of the diffusion can be described by an Arrhenius type equation (eq. 12) and displayed in an Arrhenius plot (see fig. 11). This is a graph of the logarithm of the diffusion coefficient or the oxidation rate constant vs. the inverse temperature. As can be seen from eq. 12, the slope of a linear fit through the data points gives the activation energy for the rate controlling diffusion process. For this determination of the activation energy, the oxidation rate constants can be used instead of the diffusion coefficients, since they differ only by a constant factor (eq. 11) that does not influence the slope of the linear fit. The result for the activation energy for these measurements is $1,16 \pm 0,2$ eV.

The oxidation rate constant at 600°C is determined only from data at one duration (1 h), which moreover cannot be identified as parabolic with certainty. For the case that saturation has already set in at 1 h heating, the oxidation rate constant for 600°C could be much higher and not be determined from these experimental data. For the activation energy, if evaluated with the same method, this would mean a value in the range of 1,5 to 2 eV. This would indicate a fundamental change in oxidation kinetics between 500°C and

600 °C, corresponding to a bend in the Arrhenius graph (as has been observed before [7,48,108]). In this case, the activation energy for the low temperature parabolic regime would have to be determined from the data at 390 °C and 500 °C only, which would result in a value of 0,93 eV.

Fig. 11 also includes the Arrhenius data of previous works. Gulbransen *et al.* [7] investigated the oxidation of beryllium in oxygen between 350 °C and 700 °C with weight gain analysis. They observed parabolic oxidation behaviour with an activation energy of 0,37 eV. Roth *et al.* [6] carried out oxidation experiments between 350 °C and 700 °C in 660 mbar oxygen and analysed the oxidised samples with Rutherford backscattering (RBS). They found the activation energy for diffusion controlled oxidation to be 0,73 eV.

Activation energies for diffusion-controlled beryllium oxidation were published by various authors. The respective experimental conditions and values for the activation energies are summarized in table 4, together with the data for the present work.

The values for activation energy in table 4 show a large spread, which can be attributed to several influencing factors.

Several authors noted that impurities in the beryllium bulk have a high influence on the

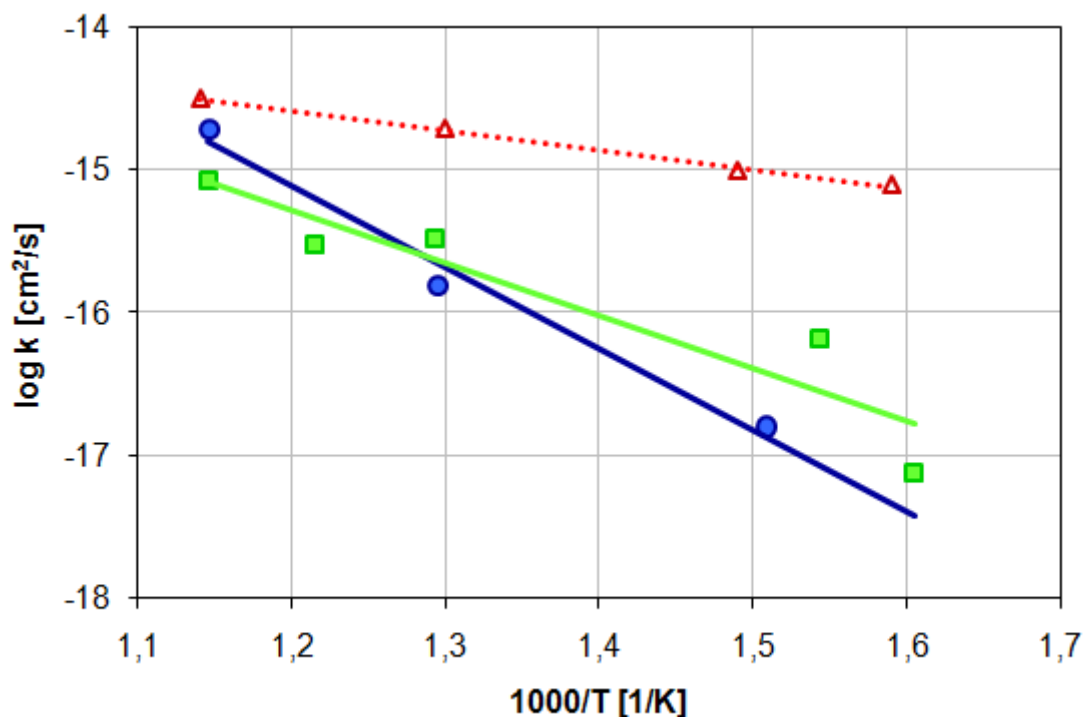


Fig. 11: Arrhenius plot of the oxidation rate constants obtained from the parabolic oxidation fits (dark blue circles), compared with similar studies (light green squares [6], empty red triangles [7]).

Reference	Samples	Oxidation conditions	Analysis	Activation energy [eV]
this work	S65C (VHP) and plasma sprayed	air 390-600 °C	AES	1,16 ± 0,2
[57]	fine powder	air > 500 °C	weight gain	1-2,8
[7]		oxygen 350-900 °C	weight gain	0,37
[55]	• polished • powdered	oxygen 500-900 °C	weight gain	• 1,33 • 1,25
[121]	dense and porous (SP200F)	steam 600-900 °C	reaction gas monitoring	2,23
[6]	S65C (VHP) and plasma sprayed	oxygen 350-600 °C	RBS	0,73 ± 0,14
[108]	• dense • plasma-sprayed	steam 400-900 °C	weight gain	• 0,51 • 0,75
[48]	pebbles	air 400-900 °C	weight gain	0,4 ± 0,2
[101]	dust	steam 500-900 °C	reaction gas monitoring	1,47 ± 0,05

Table 4: Experimental parameters and activation energies for diffusion-controlled oxidation from this work and various references

oxidation kinetics, most often in the form of irreproducible variations of the measurement results [9,57]. Impurities and other lattice defects at the metal surface influence the generation of beryllium ions at the metal-oxide interface as well as the growth of lattice defects in the oxide. As mentioned before, impurities could also be responsible for a deviation from parabolic oxidation if they get increasingly incorporated in the oxide layer with the progression of the heating experiment [9,48].

Although no data about specific impurities and their interactions in beryllium oxide are available, investigations on other metals and their oxidation have identified several possible effects of impurity elements on oxidation rate.

The main channel for diffusion in the oxide are the grain boundaries. Consequently, impurity elements that segregate to the grain boundaries can have a strong effect on diffusion within the oxide and thereby on the oxidation rate. Moreover, by segregation even

small amounts of impurities in the bulk can accumulate to form areas of increased concentration at the grain boundaries. A review of this effect can be found in [122], together with extensive experimental data for the impurity elements Ti, Fe, Ni, La, Y and others in Al_2O_3 and Cr_2O_3 . The main parameters determining the effect are ion size and oxygen affinity of the impurity. The effect on oxidation rate is mostly decreasing, although some cases with accelerated oxidation are reported.

In the oxide lattice itself, defects are necessary for diffusion to occur. Impurities migrating into the oxide lattice change its defect structure and thereby influence the oxidation rate. An example for this kind of effect is given in [123] for Si, Mg and Fe impurities in Al_2O_3 . The interaction depends on the one hand on the size of the impurity ion, on the other hand on its chemical properties in comparison to the base lattice (like possible oxidation states). The effect on oxidation rate can be increasing or decreasing and can vary strongly in magnitude.

A further factor promoting the uncertainty in beryllium oxidation kinetics lies in the method of analysis. Roth *et al.* [6] pointed out that earlier weight gain measurements might have been less sensitive to the processes occurring at low temperatures. A key issue for weight gain measurements is furthermore the knowledge of the specific surface area. This is necessary for calculating oxide growth from the weight gain data, and differences in grain size, porosity and surface roughness can cause large variations of this value [48,55,101,108,121]. Moreover, weight gain analysis and reaction gas monitoring include the alterations by grain boundary oxidation in the total results, whereas surface analysis methods like AES and RBS evaluate only the oxide layer at the surface.

The oxidising atmosphere influences mainly the oxidation rates. A weak pressure dependence exists in oxygen [7,55], and humidity strongly increases oxidation [52,57], however, the activation energies are not significantly altered by changes in pressure or water vapour content in the gas.

Several works have tried to take into account and quantify one or more factors influencing the oxidation kinetics. Ervin *et al.* [55] and Petti *et al.* [108] used a variety of sample materials and conditions for their weight gain measurements and could thereby discern that the highest influence was made by the difference between geometric area and true surface area of solid beryllium samples.

Authors who compared oxidising atmospheres with different humidities [52,57] could only quantify their influence on catastrophic oxidation, as will be discussed below, not on the kinetics of the protective oxidation regime.

Overall, the low repeatability and high data scatter at each given set of conditions

generally prevented the quantification of the influence of single parameter variations, which was uniformly attributed to impurities in the beryllium samples [6,48,52,55,57].

In the present work two kinds of beryllium metal (S65C grade vacuum hot pressed, plasma-sprayed) with comparable impurity concentrations were used to investigate the influence of these material types on oxidation kinetics, but again no differences greater than the overall uncertainty were discernable.

Analytical data about the crystal structure or impurity content of the oxide layers might have provided further insight concerning the factors that influence oxidation kinetics. However, X-ray diffraction (XRD) measurements were not attempted since the signal from a thin layer containing mainly beryllium and oxygen was expected to be too low for feasible evaluation, and transmission electron microscopy (TEM) and secondary ion mass spectrometry (SIMS) were not available while at the same time ensuring laboratory safety and avoiding contamination.

In view of these considerations, it can be concluded that the general precision of measurement (which improved over the years), the different systematic errors inherent in various analysis methods, and uncertainties in the used sample materials caused a large spread of the results for beryllium oxidation kinetics, as can be seen from the activation energy values for beryllium diffusion through the oxide. However, these data still indicate a range where the oxidation kinetics can be established.

The present measurements on the one hand confirm the validity of the previous measurements as a whole. On the other hand they contribute a set of data to narrow down this range, especially below 500 °C, where grain boundary oxidation can be neglected. Significantly, the resulting activation energy is close to the value determined by the only other work using a surface analytical method [6].

It also has to be suggested that if particularly relevant and reliable oxidation data for a specific application are needed, measurements taking into account the respective materials and conditions should be carried out.

5.1.2 Catastrophic Oxidation

After completion of the sputter depth profiles, electron micrographs of the surface were taken. The samples oxidised at 390 °C, as well as the samples heated at 500 °C up to 17 h, do not show any remarkable surface features (see fig. 7). In contrast to that, fig. 12 to 16 show SEM images of samples oxidised at 500 °C for 43 h and 600 °C.

On the samples heated at 500°C for 43 h (fig. 12) and 600°C for 1 h (fig. 13 to 15) oxidation along grain boundaries can be recognized, since the oxide appears brighter than beryllium metal in the SEM images due to its higher secondary electron yield [124]. Furthermore, some small pits at isolated spots scattered along the grain boundaries can be seen (intergranular voids).

The samples heated at 600°C for 20 h (fig. 16) clearly show pits where whole grains were loosened. Oxide along these grain boundaries is still recognizable.

In addition to SEM images, AES maps were acquired of selected exemplary areas on the samples oxidised at 600°C for 20 h (fig 17 and 18). The maps show the distribution of beryllium and oxygen in and around pits in the surface. The enrichment of oxygen along grain boundaries confirms the grain boundary oxidation seen in the SEM images.

It is well known that at high temperatures ($> 700^\circ\text{C}$) the oxidation of beryllium is no longer parabolic and protective, but changes to a regime that has been termed non-protective or catastrophic [9,48,52,54,55,106-108,121,125]. The common indicators of this regime are an increase of the oxidation rate (often termed breakaway) and the formation of cracks or blisters on the surface. The prevalently proposed mechanism for this behaviour is the formation of cracks in the oxide layer above a certain layer thickness due to compressive stresses that are caused by the higher volume of beryllium oxide compared to beryllium metal (ratio 1,68:1) [9,52,108,125]. These cracks provide increased access of gas to the metal surface, which in turn leads to the acceleration of oxidation, since this process is then progressively repeated. The typical form of a catastrophic weight gain (or reaction product output) curve over heating time starts with a parabolic section, which is followed by an increase in oxidation that can often be described with a linear kinetics model [48,107,108,121]. It was recognized early that this regime is not only a phenomenon of the surface oxide layer, but occurs in combination with an oxidative attack into the bulk of the beryllium samples, mainly along grain boundaries. At its extreme, the disintegration of solid samples into dust was observed [55,107,121].

Most works investigating this effect report that the change from protective to catastrophic oxidation occurs at a temperature around 700°C [9,48,107,108] which depends also on the oxidising atmosphere (humidity) [52,121]. However, there have been indications that instead of a sudden change of behaviour at a discrete temperature, there is a smooth transition from purely protective oxidation to non-protective oxidation over a larger temperature range below 700°C. Ervin *et al.* [55] reported that breakaway occurred at all temperatures in their oxidation experiments (500-900°C), only the time until breakaway increased with decreasing temperature. Furthermore, they found signs of intergranular

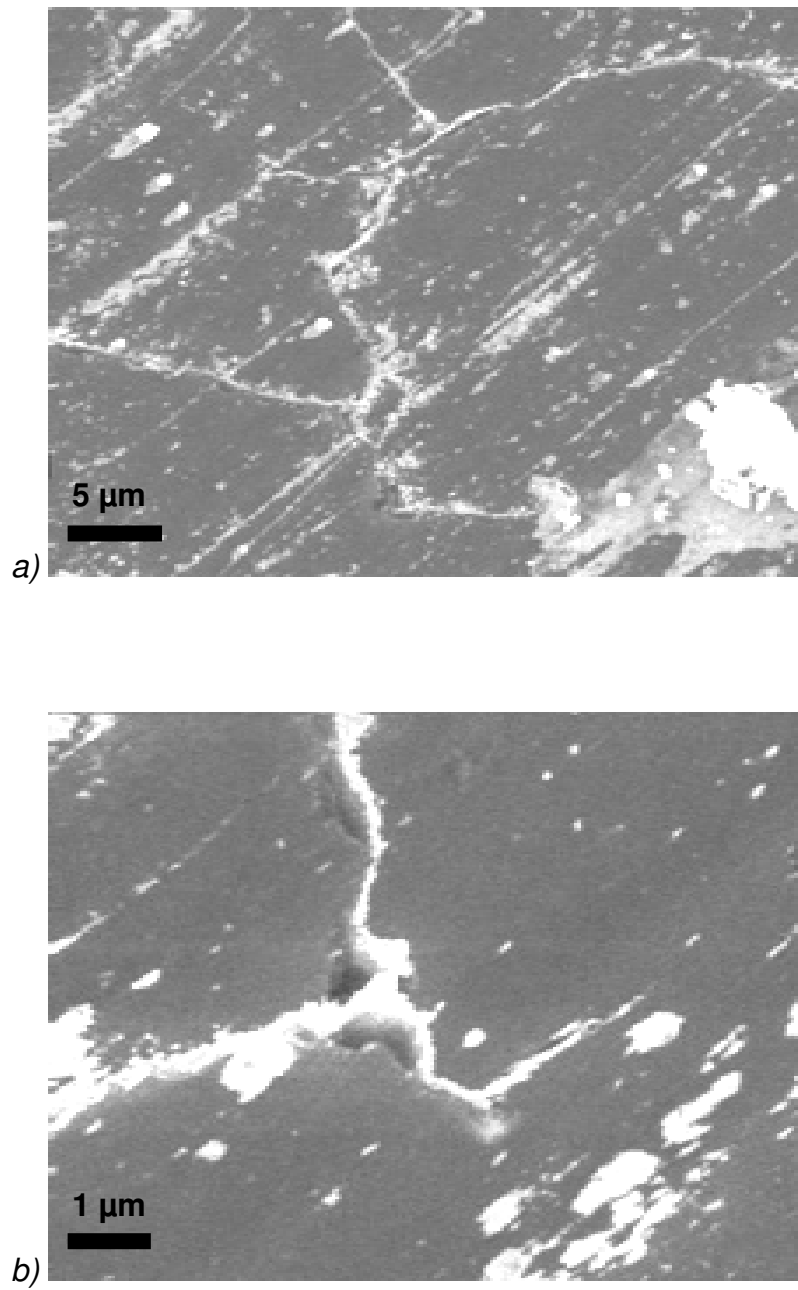


Fig. 12: SEM images of sample surface oxidised 43 h at 500 °C after sputter depth profile. Oxidised grain boundaries are visible. Image sizes: a) 40 x 30 μm, b) 9 x 7 μm

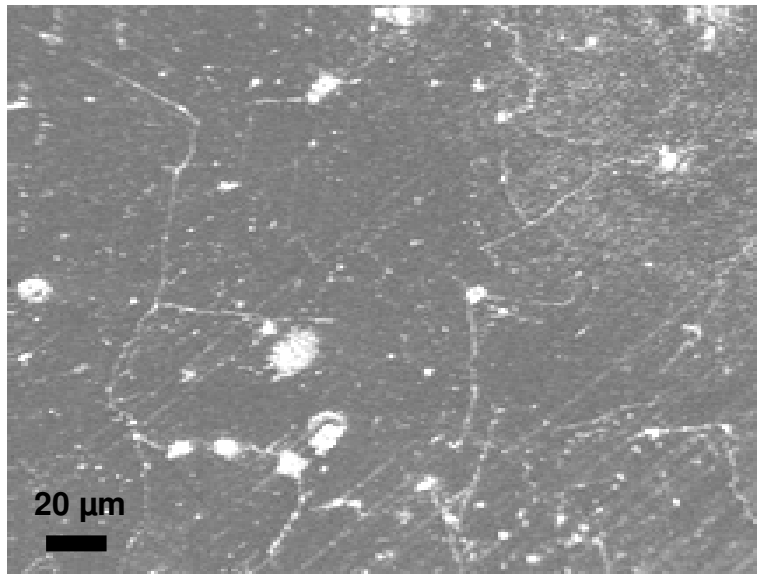
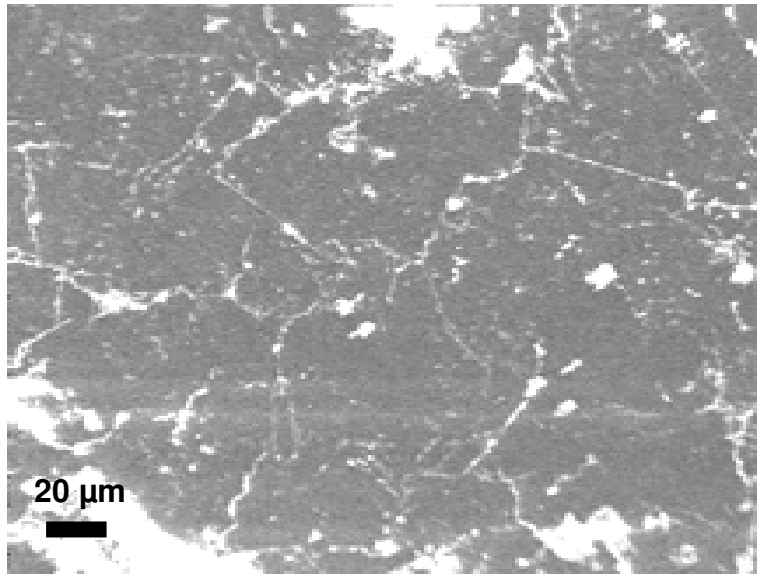


Fig. 13: SEM images of sample surface oxidised 1 h at 600 °C after sputter depth profile. Oxidised grain boundaries are visible. Image size 240 x 180 μm

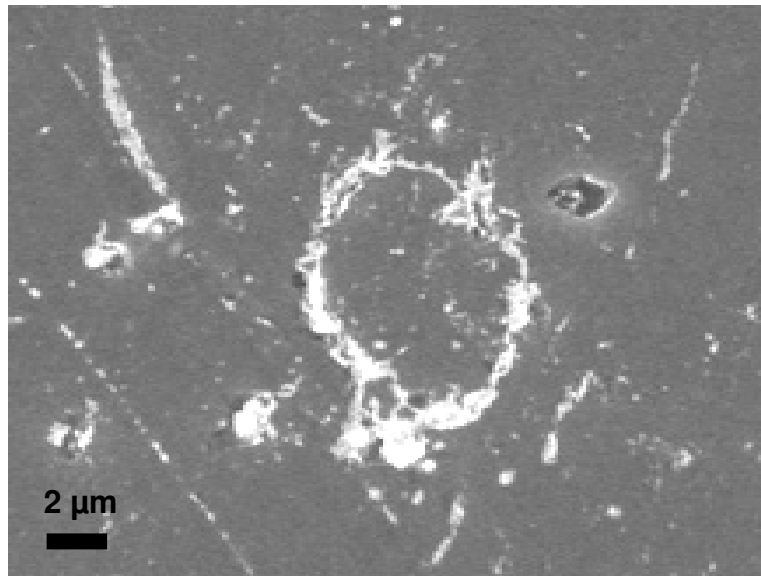
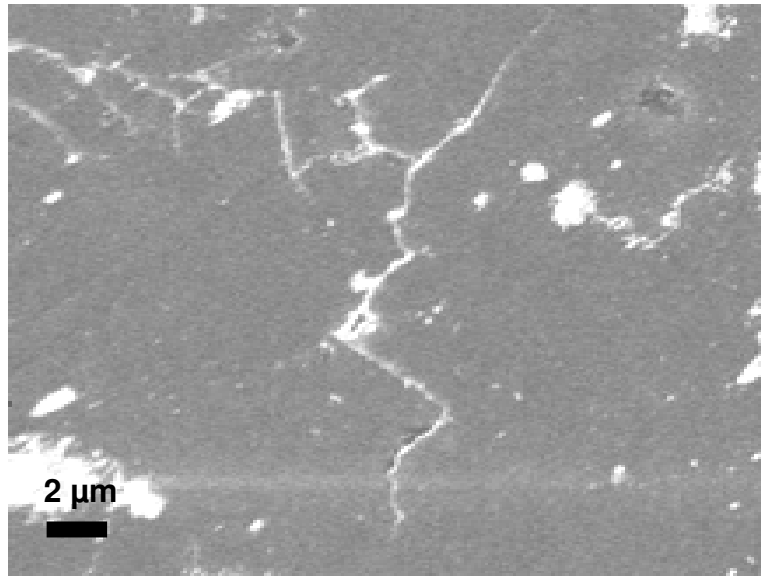


Fig. 14: SEM images of sample surface oxidised 1 h at 600 °C after sputter depth profile. Oxidised grain boundaries are clearly visible. Image size 24 x 18 μm

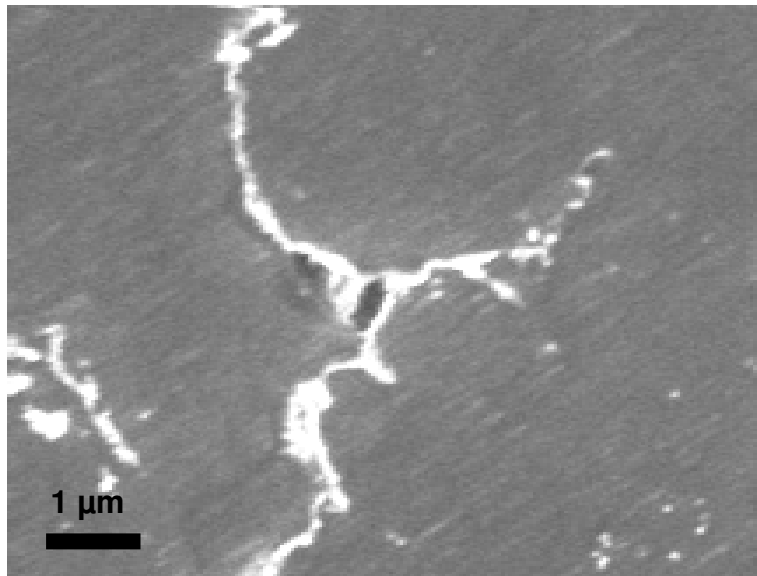
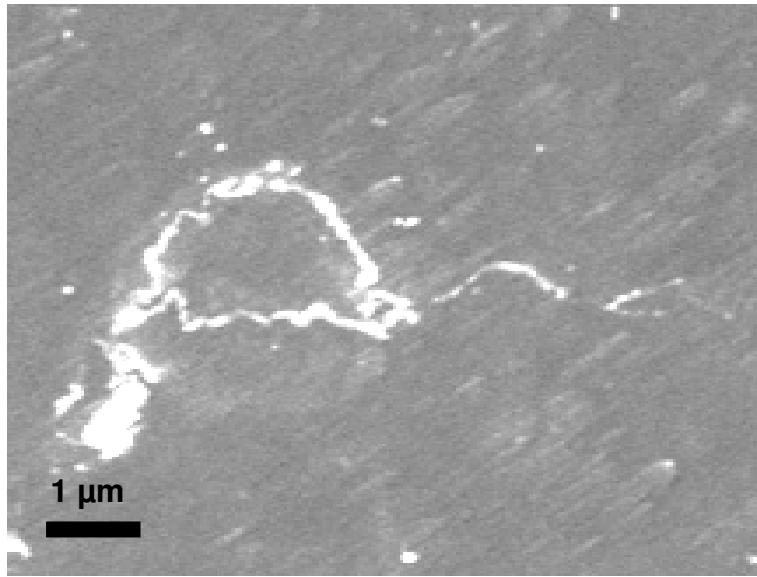


Fig. 15: SEM images of sample surface oxidised 1 h at 600 °C after sputter depth profile. Oxidised grain boundaries are clearly visible. Image size 8 x 6 μm

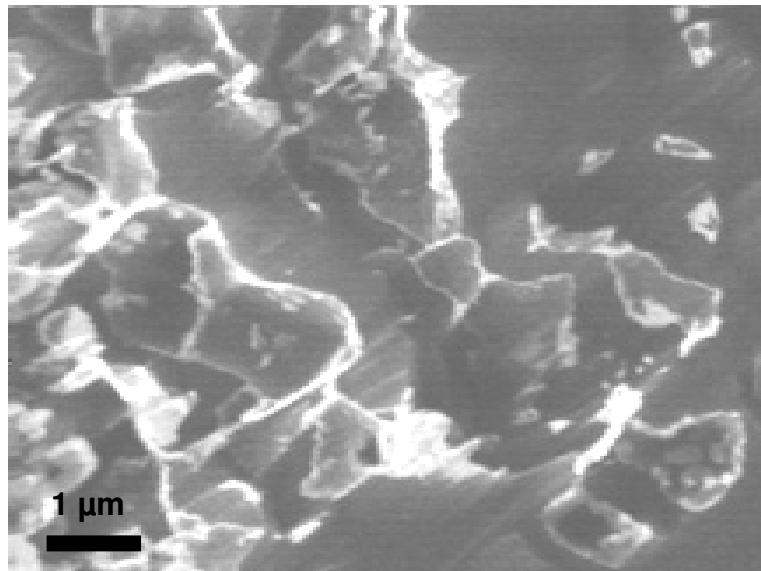
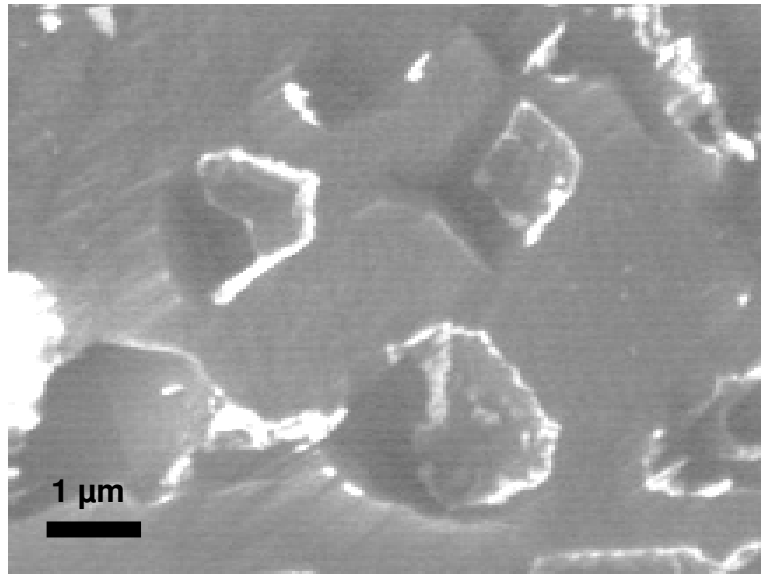


Fig. 16: SEM images of sample surface oxidised 20 h at 600 °C after sputter depth profile. Oxidised grain boundaries and holes from loosened grains are clearly visible. Image size 8 x 6 μm

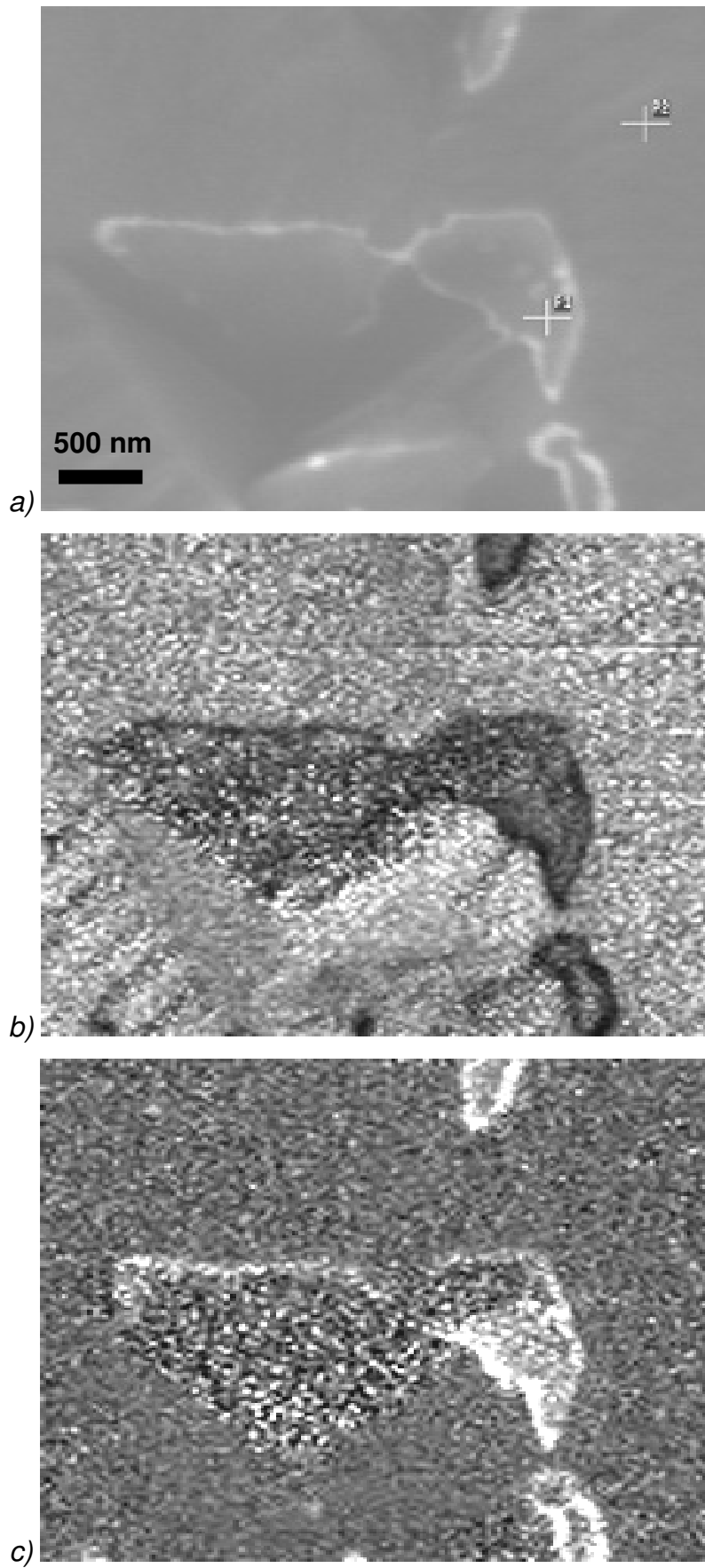


Fig. 17: AES maps of sample surface oxidised 20 h at 600 °C after sputter depth profile. a) SEM image, b) Be map, c) O map. Image size 4 x 3 μm

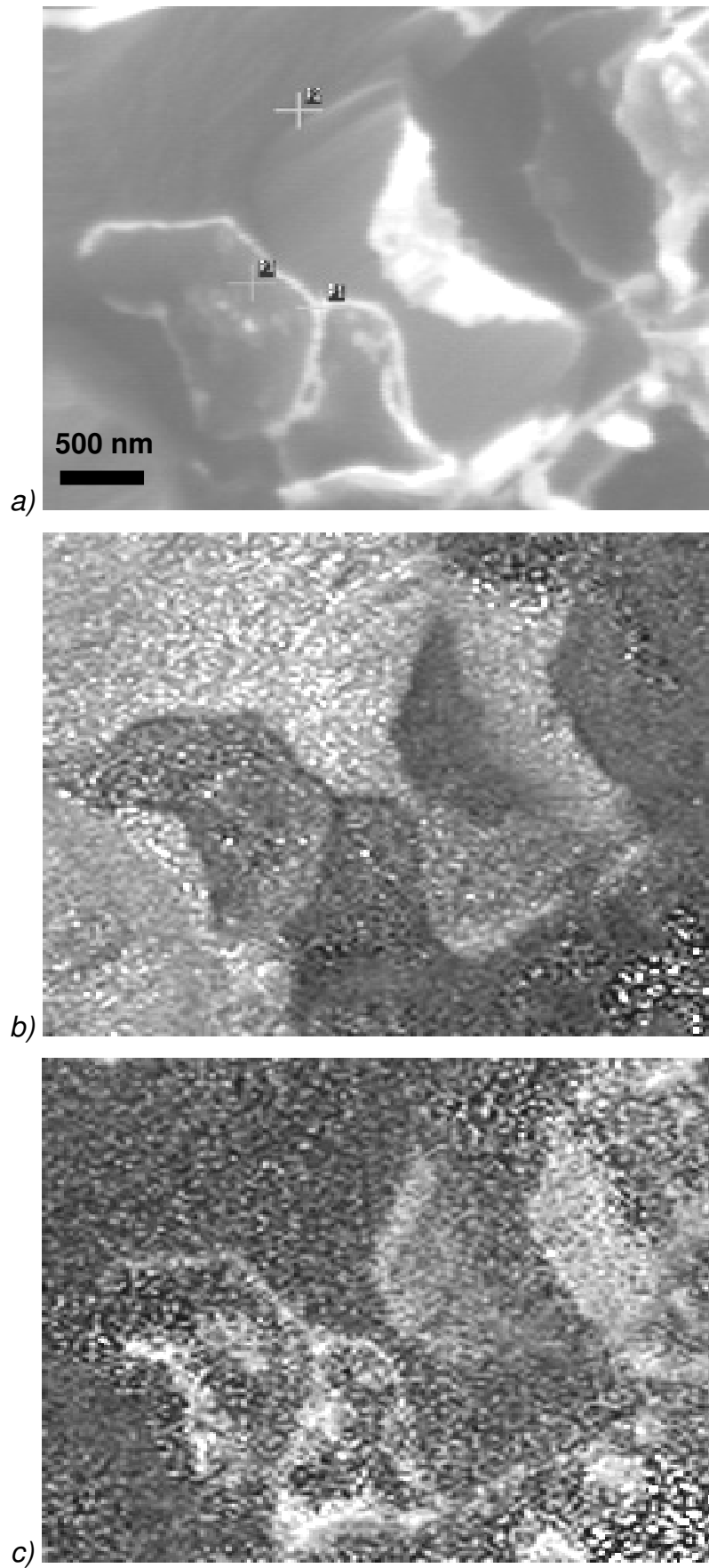


Fig. 18: AES maps of sample surface oxidised 20 h at 600 °C after sputter depth profile.

a) SEM image, b) Be map, c) O map. Image size 4 x 3 μm

oxidation in samples that had been oxidised only within the parabolic regime. Aylmore *et al.* [9,52] reported a transition range for breakaway between 650 and 700°C, but found numerous small discontinuities in the weight gain curves of their oxidation experiments (50-750°C) at all temperatures and in all stages of oxidation. Their interpretation of these discontinuities is that small cracks from compressive stresses appear locally and repeatedly all over the sample surface. The healing up of these cracks causes the observed abrupt weight gains. This phenomenon, termed localised breakaway, is again accompanied by intergranular oxidation in the bulk. Jepson *et al.* [54] likewise observed grain boundary oxidation in experiments at 600°C that remained in the parabolic regime as determined from the weight gain curves. They propose the hypothesis that cracks in the oxide layer form already very early during heating, allowing access of gas to the underlying metal surface. The weight gain curve would therefore be a superposition of the growth of the oxide layer at the surface (outer oxidation) and intergranular oxidation in the bulk (inner oxidation) at all times (above 600°C), without abrupt cracking of the oxide layer at a certain temperature/duration. In this model, the kinetic phenomenon of breakaway would occur when the rate of inner oxidation starts to exceed the rate of outer oxidation.

The oxidation experiments in the present work are not quite suitable to analyse the breakaway behaviour of the beryllium samples. Firstly, the temperatures are too low to determine a transition temperature or range adequately. And secondly, by determining the oxidation curves with a surface analytical method, the contribution of grain boundary oxidation to the overall oxidation kinetics is neglected. However, these results confirm that access of gas to the metal surface - most likely via cracks in the oxide layer - occurs at temperatures as low as 500°C, causing grain boundary oxidation, and that loosening of particles starts already at 600°C. This demonstrates that for mechanical issues, oxidative disintegration has to be taken into account even below the kinetically determined breakaway transition region to catastrophic oxidation around 700°C.

5.2 Interaction of Beryllium Oxide with Hydrogen Plasma

The supply of hydrogen and water vapour to the furnace allowed the examination of the interaction of beryllium oxide with hydrogen plasma of various compositions. The lower limit for oxygen containing impurities, given by dry hydrogen without addition of water vapour, was estimated to be below $3 \cdot 10^{-6}$ mbar partial pressure in the furnace, which corresponds to a fraction of approx. 3 ppm ($3 \cdot 10^{-6}$) (see chapter 4.3). The upper limit was given by saturation of water vapour in hydrogen at 11 °C, which amounts to a partial pressure of 13 mbar in the water chamber. With a supply line pressure of approx. 1300 mbar, this corresponds to a concentration of approx. 1% (10^{-2}). Concentrations in between could be achieved by mixing dry and water saturated hydrogen.

Heating experiments in hydrogen were carried out in nominally dry hydrogen (water vapour fraction lower than $3 \cdot 10^{-6}$). Plasma exposure experiments were carried out with nominally dry hydrogen and at fractions of 10^{-4} , 10^{-3} and 10^{-2} water vapour in hydrogen plasma. Since the results for dry hydrogen are qualitatively different from the results for water vapour concentrations above 10^{-4} , they will be described separately.

5.2.1 Heating and Plasma Exposure in Dry Hydrogen

Heating and plasma exposure experiments in dry hydrogen were carried out at different temperatures and durations, and with various initial oxide thicknesses. Larger initial oxide thicknesses were produced by pre-oxidising samples, based on the oxidation kinetics determined previously. These were used to investigate oxide reducing effects in the experiments. A compilation of the complete measurements is given in the appendix. The results are shown in fig. 19 in the form of oxide thicknesses before and after the experiments.

Heating in hydrogen gas (without plasma excitation) was carried out for comparison, although no oxide reduction was expected under the given conditions, as can be seen from the Richardson-Ellingham diagram (fig. 20). The reaction



does not take place spontaneously in the applied temperature range (390-600 °C).

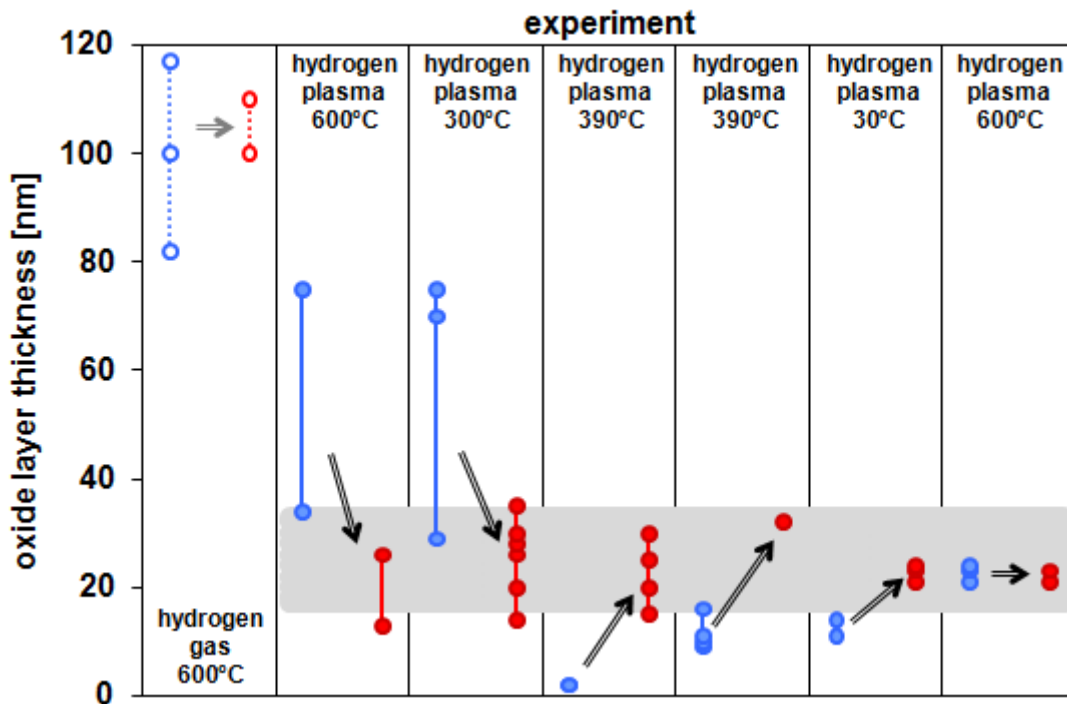


Fig. 19: Oxide layer thicknesses before (light blue symbols) and after (dark red symbols) exposure of the samples to dry hydrogen gas (empty symbols) or plasma (full symbols) at various temperatures. The shaded area indicates the thickness range of the quasi-equilibrium oxide layers.

As can be seen in fig. 19, although some of the resulting oxide thicknesses were below the range of the initial oxide thickness, no consistent oxide-reducing effect was observed. Exposure to hydrogen plasma resulted for each experiment in an oxide thickness within a range of approx. 15-35 nm, independent of temperature, duration and, most importantly, initial oxide thickness (see fig. 19). Initially thinner oxide layers were further oxidised, whereas initially thicker oxide layers were reduced. This indicates the development of a steady state between oxidation and reduction during plasma exposure, with a corresponding final oxide layer thickness.

Reduction of oxides on metal surfaces in hydrogen plasma has been known for many years and applied extensively for removing oxide and contamination layers [e.g. 127-134]. The glow discharges used for this purpose typically have a hydrogen dissociation degree between 1 and 10 %. Since the ionisation degree is much lower than that and ion energies are also low under these conditions, physical sputtering of the surface can be neglected. Hydrogen atoms have therefore been confirmed as the active species responsible for the chemical reduction of the oxide in the plasma. The process is assumed to proceed in two steps: hydroxylation of the metal oxide



and subsequent reduction of the hydroxide



giving the net reduction equation



Phenomena indicative of the competition between reduction and oxidation have been observed before, although they have not been investigated more closely.

During the investigation of glow discharge cleaning of steel surfaces [128,130,131], it was discovered that the oxygen layer could not be removed completely. The reoxidation of the surface was attributed to oxygen from the surrounding oxide and water vapour in the plasma.

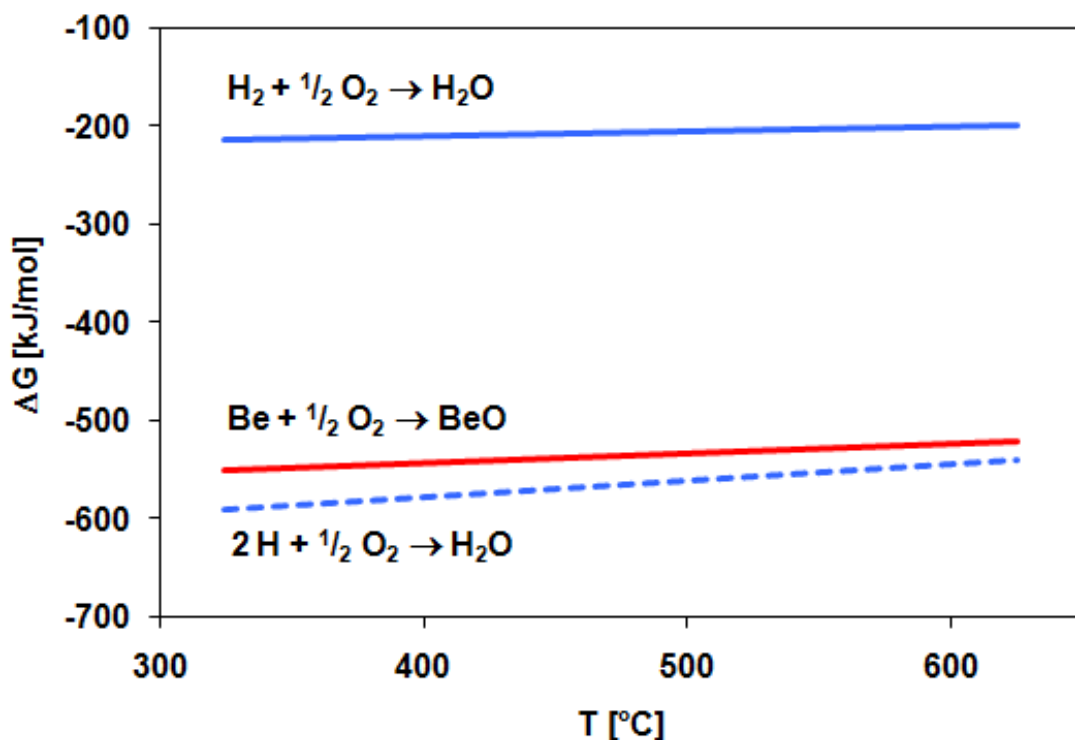


Fig. 20: Richardson-Ellingham diagram for the oxidation reactions of molecular hydrogen (blue solid line), atomic hydrogen (blue dashed line) and beryllium (red line) [126]

Bastasz [66] investigated the bombardment of beryllium samples and thin beryllium oxide layers with hydrogen ions (2 keV H₂⁺). He observed that, depending on the plasma conditions (incident hydrogen flux, residual gas pressure), either a clean metal surface or a stable oxide layer developed.

At the PISCES-B plasma generating facility (San Diego, USA), Conn *et al.* [10] and Won *et al.* [135] found that contamination layers form on beryllium surfaces in deuterium plasma at elevated temperatures (250-720 °C; 100-200 eV ion energy), and remained stable throughout exposure. Surface analysis revealed that they consisted of beryllium, oxygen, carbon and nitrogen, attributed to residual gases in the vessel. The results lead the authors to the conclusion that the formation of this overlayer protects the beryllium bulk from erosion.

Bastasz [66] and Won [135] attribute the increased oxide growth competing with the reduction reaction to radiation-enhanced oxidation. This effect was first described by Langley [65] and explained with increased diffusion of beryllium ions through the oxide layer, caused by the lattice damage and disturbance from the incident hydrogen atoms and ions in the oxide.

In all cases the steady state oxide layer is formed by the stationary competition of reduction with hydrogen atoms



and oxidation with water vapour



However, the simultaneous occurrence of oxidation and reduction at the sample surface alone cannot explain the formation of an oxide layer with a thickness that lies within a specific narrow range. The references ([10,66,135]) point out the increased oxidation necessary for an oxide layer to grow, but give no explanation for the formation of a stable oxide layer (i.e. with a stable thickness).

Indications for other involved mechanisms have been found for other metals. During the investigation of the reduction of oxide layers on steel surfaces with hydrogen plasma [130-132], the activation energies for the rate limiting process were determined by monitoring the water vapour production rate in dependence of the temperature and fitting it with an Arrhenius equation. The resulting energies were consistently below ~ 80 kJ/mol

(~ 20 kcal/mol), which is too low for a purely chemical process and, according to the authors, indicates that a physical process is dominating or at least participating in the reduction. For the reduction on steel, this was assumed to be the diffusion of hydrogen and/or oxygen, although it could be argued that the reduction of metal oxides with atomic hydrogen has a substantially lower activation energy than the reduction with molecular hydrogen, which would likewise account for the observed energy values.

For the present case of beryllium oxide reduction, the development of a certain final steady state thickness is an indicator that diffusion is significantly influencing the overall behaviour. Both the growth of initially thin oxide layers and the diminishing of thick layers require the diffusion of beryllium through the oxide layer, from interface to surface or from surface to interface, respectively. However, the simple linear diffusion model (see chapter 3) used for evaluating the beryllium oxidation kinetics (chapter 5.1) is not able to describe the diffusion processes involved in the observed behaviour and provide a steady state oxide thickness. By assuming that the concentration of metallic beryllium at the surface depends on the prevailing plasma-conditions and that the chemical potential of metallic beryllium at the surface is not different from the beryllium in the bulk, a continuous parabolic oxide growth, possibly slower than in air, would be expected.

Generally, in all cases where an oxide layer is reduced by reactive agents in the gas phase, a process transporting the reduced metal from the surface to the bulk or oxygen to the surface is required. Such a process cannot be explained by simple diffusion theory based on gradients of concentrations. It must be assumed that the diffusing beryllium interacts non-linearly with the chemical species and influences the chemical reactions taking place at the surface. Furthermore, hydrogen can be assumed to diffuse into the oxide layer. On the one hand, it cannot be excluded that the conditions for beryllium diffusion are influenced by it and therefore change with depth. On the other hand, it is possible that the reduction reaction (19) takes place also inside the oxide, further altering the distribution of chemical species.

The described development of a steady state might be expected considering the empirical concept of plasma-chemical quasi-equilibrium introduced by Rutscher and Wagner [136], or the more or less equivalent concept of the thermodynamic effect of plasma chemistry, introduced by Veprek [137,138,139]. According to these concepts, a chemical equilibrium far from the thermodynamic equilibrium state can be established in a plasma, and according to Veprek, the important factor for setting up such a steady state is the inner energy of the plasma that lies mainly in the dissociation of the molecules. The steady state behaviour of such a system is macroscopically similar to a thermodynamic equilibrium and

stable with regard to chemical composition. The difference to a thermodynamic equilibrium is that there is no local (i.e. microscopic) thermodynamic equilibrium (LTE). The deviation from LTE leads to a continuous turnover of energy, e.g. by the dissociation of molecules by energetic electrons causing a continuous supply of radicals. The flow of energy from more to less energetic species also leads to the continuous generation of entropy, making the maintenance of such an equilibrium an irreversible thermodynamic process.

For a simple chemical process this means that the reaction



which in a thermodynamic equilibrium is valid macroscopically and microscopically, is replaced by two unidirectional reactions (22a) and (22b), consuming the dissociated species B and converting it to the molecule B_y , and by the electron impact (22c), dissociating B_y into y B:



⇓



⇓



⇓



Such a quasi-equilibrium seems to develop under the present plasma conditions, within the applied ranges of temperature and pressure. The steady state composition, together with stationary diffusion processes within the oxide layer, would result in an equilibrium value for the oxide layer thickness. Temperature variations do not significantly influence the final oxide thickness, but it could be assumed that it depends to a certain degree on the composition of the gas supply, i.e. the concentration of oxygen-containing impurities in the hydrogen.

A thorough investigation of this phenomenon would have to include an extensive theoretical approach, possibly involving detailed numerical simulations taking into account both chemical reactions and diffusion processes, as well as their interaction with each other. This was not possible within the frame of this work, and further work in this direction is commended to future studies.

As far as the application of beryllium in a hydrogen (isotope) plasma environment is concerned, the observed results confirm that stable oxide layers are formed during exposure already at very low levels of oxygen-containing impurities. A continuing gettering of oxygen during discharges seems unlikely since the described quasi-equilibrium implies a stationary exchange of oxygen with the plasma phase. However, the initial gettering is still considerable, if an oxide layer of approx. 20-30 nm is formed on top of the native surface.

5.2.2 Plasma Exposure in Wet Hydrogen

Only samples with native oxide layers were used for these experiments, assuming that a quasi-equilibrium between oxidation and reduction develops during plasma exposure, and that pre-oxidised beryllium ends up with a final oxide layer thickness in the same range. The experiments were carried out without a closed sample holder, the temperature was therefore restricted to 390°C. Exposure durations were varied between 1 h and 6 h, with no consistent effect of duration on final oxide thickness. The experiments were carried out at concentrations of water vapour in hydrogen of 10^{-4} , 10^{-3} and 10^{-2} , to determine if a dependence of the quasi-equilibrium oxide thickness on the water vapour concentration exists.

The results are shown in fig. 21, including the results for dry hydrogen at a concentration of water vapour of $3 \cdot 10^{-6}$. The range of final oxide thicknesses for wet hydrogen is much higher and reaches much higher values. These values are also higher than the oxide thicknesses determined for oxidation at atmosphere (see chapter 5.1), indicating that other processes besides oxidation and reduction take place. A dependence of oxide thickness on water vapour concentration cannot be determined, although there is a tendency of higher oxide thicknesses for higher water vapour concentrations. The extension of the thickness range to very low values suggests that the layer forming under wet hydrogen plasma conditions is most likely prone to severe flaking.

In addition to the sputter depth profiles, the surfaces were examined by scanning electron microscopy after plasma exposure. Fig. 22-26 show electron micrographs of beryllium surfaces after plasma exposure under various conditions: before exposure (fig. 22), dry plasma at 390°C for 1 h (fig. 23), dry plasma at 390°C for 6 h (fig. 24), 1% water vapour at 390°C for 1 h (fig. 25), and 1% water vapour at 390°C for 6 h (fig. 26). The surface before exposure is quite smooth and uniform, after dry plasma exposure the images show some

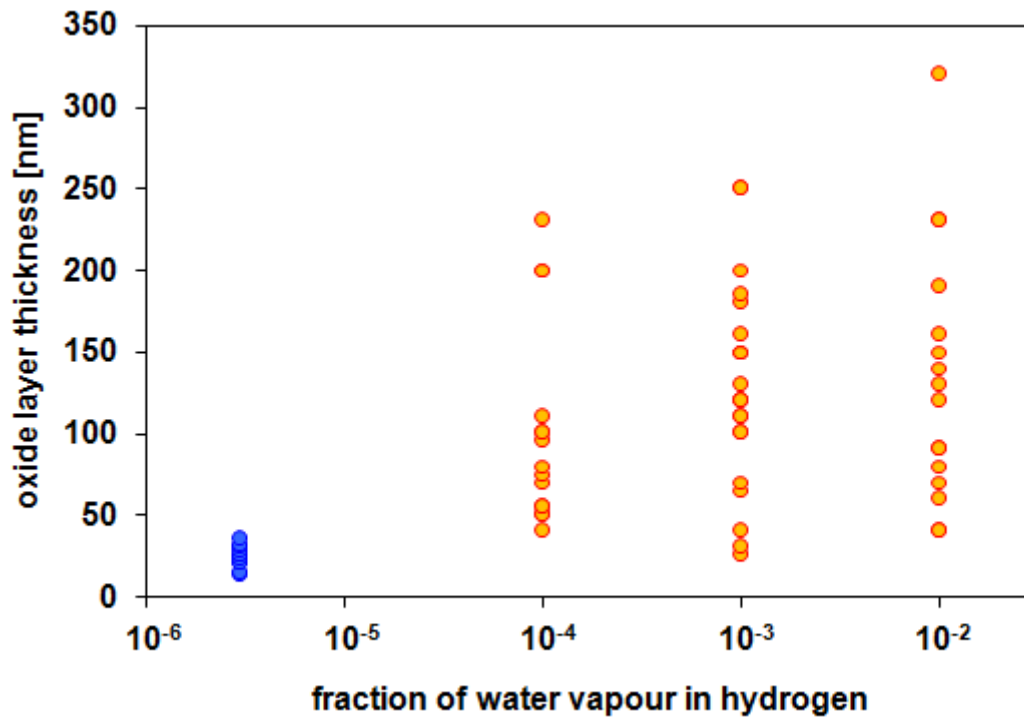
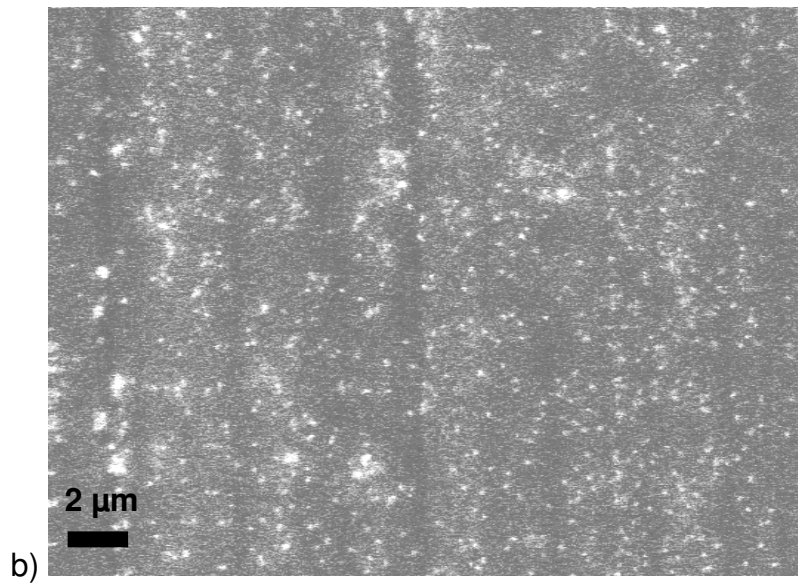
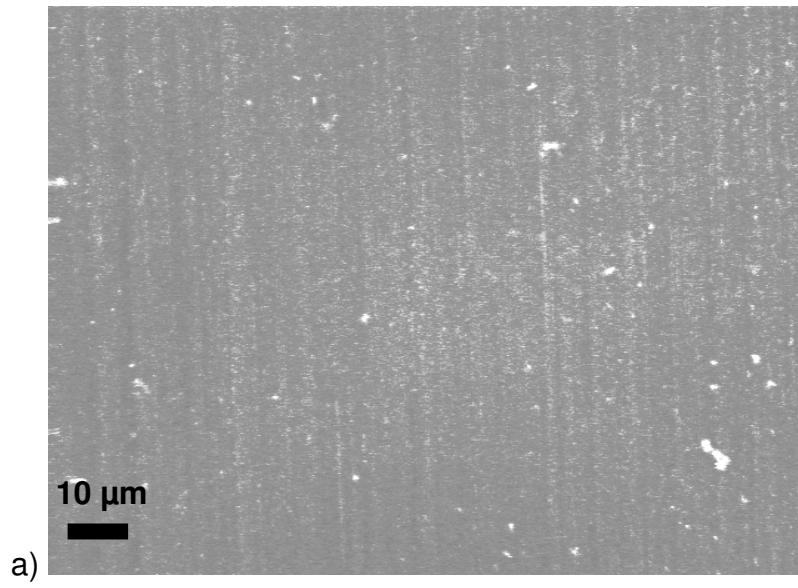


Fig. 21: Oxide layer thicknesses after exposure to hydrogen plasma with various fractions of water vapour added; results for nominally dry hydrogen are shown at a fraction of $3 \cdot 10^{-6}$

sporadic holes at high magnification. After wet plasma exposure, on the other hand, clear signs of a structural change can be seen, as well as loose particles or clusters of particles. Considering the porous structure and rough surface of the samples exposed to wet hydrogen, the thickness results acquired by sputter depth profiling have to be reassessed. Under these conditions a straight conversion from sputtering time to depth with a simple factor is not valid, since ion beam shadowing effects are highly distorting the sputtering depth scale. A reliable evaluation of the depth is therefore not possible anymore. However, the profiles can still be used for comparison, and in this way provide some qualitative information about the samples. Exemplary profiles of oxide layers with comparable thicknesses (approx. 40 nm) from plasma exposure experiments with different fractions of water vapour are shown in fig. 27. The large range of thicknesses down to very low values furthermore indicates that the layer must be prone to local delamination or flaking.

The immediate impression following from the depth profile results and SEM images is that the addition of water vapour qualitatively changes the nature of the interactions occurring during plasma exposure. Indeed, from oxidation experiments it is known that the addition of water vapour dramatically accelerates the oxidation kinetics and promotes breakaway [52,54,101,107,121]. The cause proposed for this phenomenon is the formation of hydrogen in the oxidation reaction



*Fig. 22: SEM images of sample surface before plasma exposure
Image sizes: a) 120 x 90 μm, b) 24 x 18 μm*

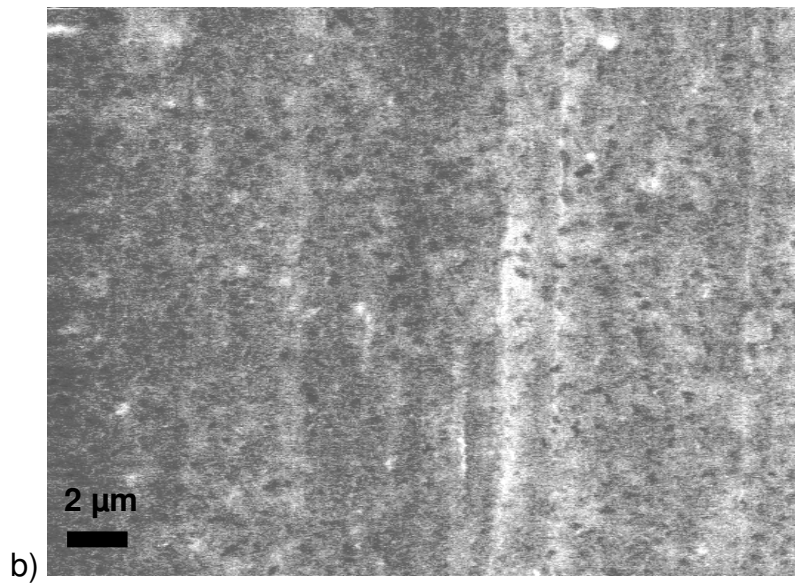
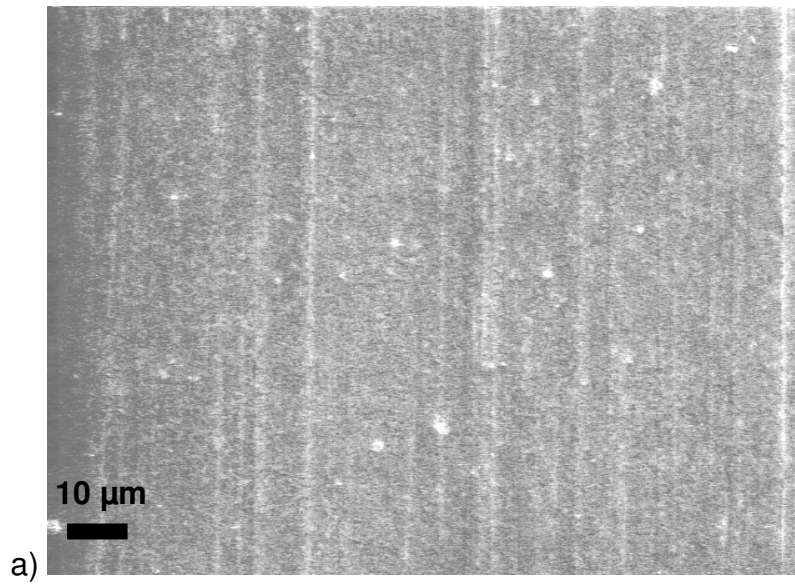


*Fig. 23: SEM images of sample surface after dry plasma exposure (390 °C, 1 h)
Image sizes: a) 120 x 90 μm , b) 24 x 18 μm*

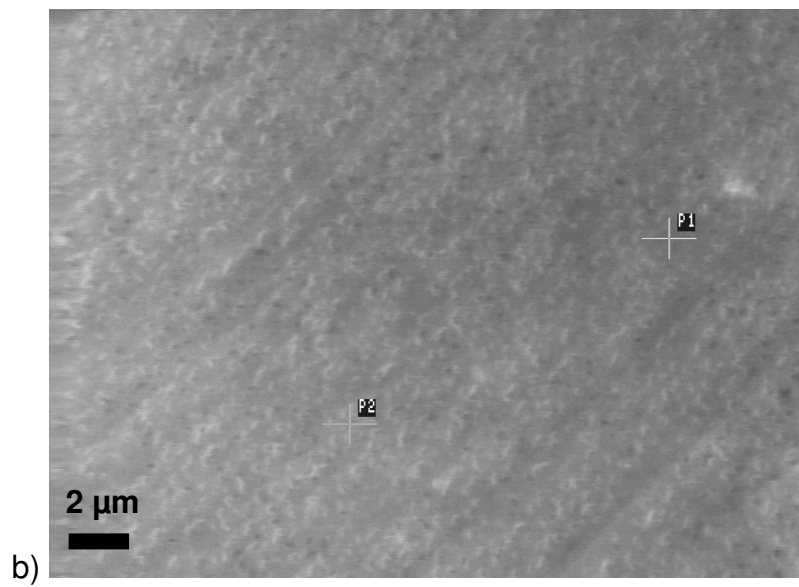
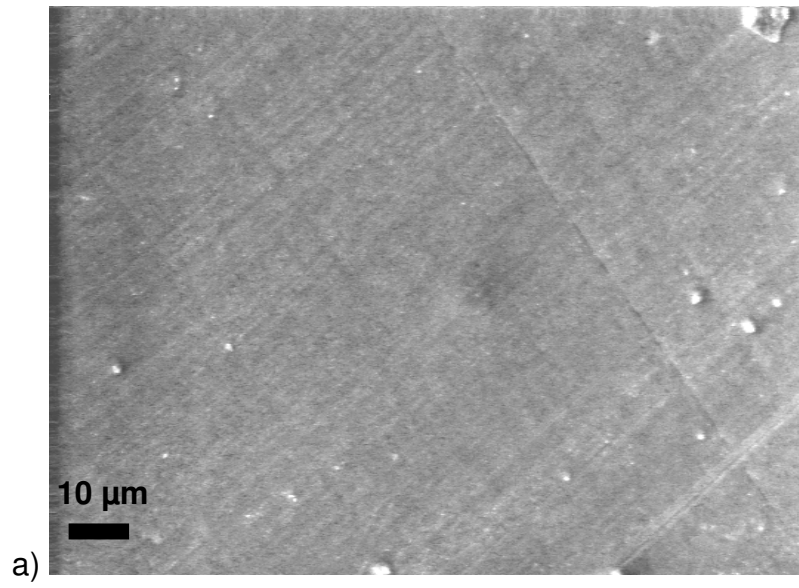


*Fig. 24: SEM images of sample surface after dry plasma exposure (390 °C, 6 h)
Image sizes: a) 120 x 90 μm, b) 24 x 18 μm*

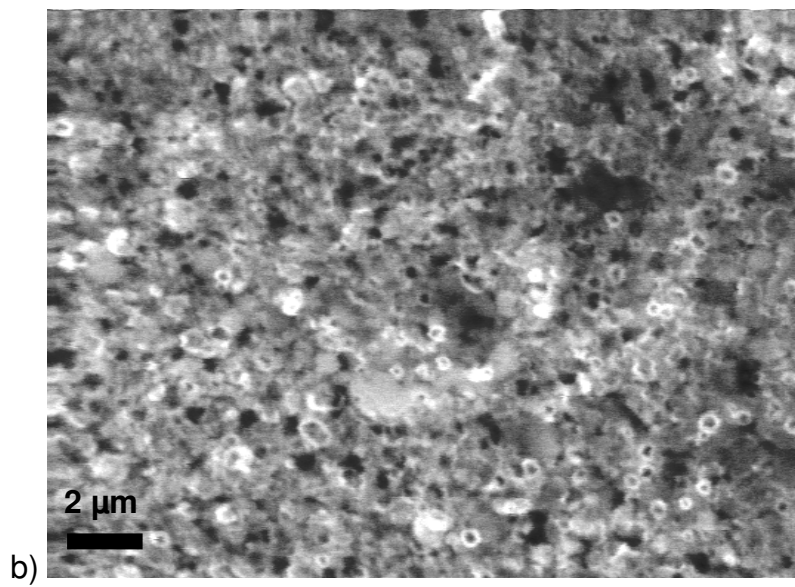
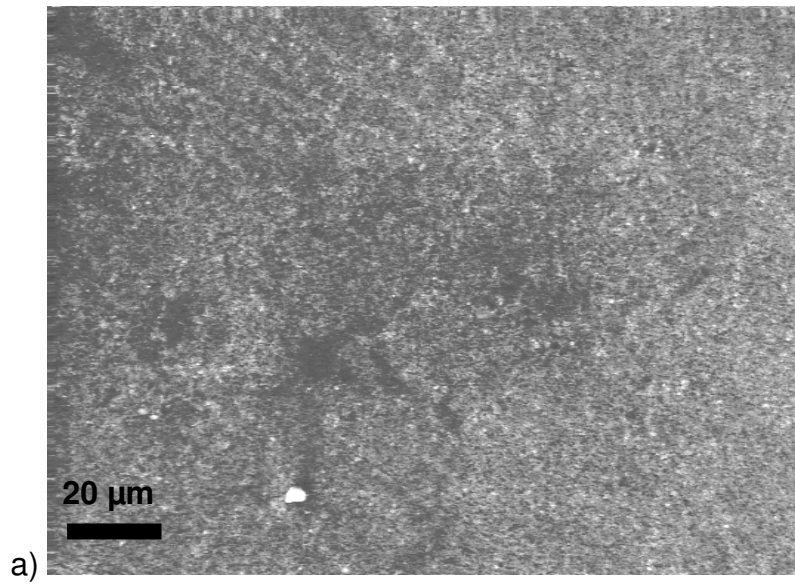


Fig. 25: SEM images of sample surface after wet plasma exposure (390 °C, 1 h, 1% water vapour). Image sizes: a) 160 x 120 μm, b) 20 x 15 μm

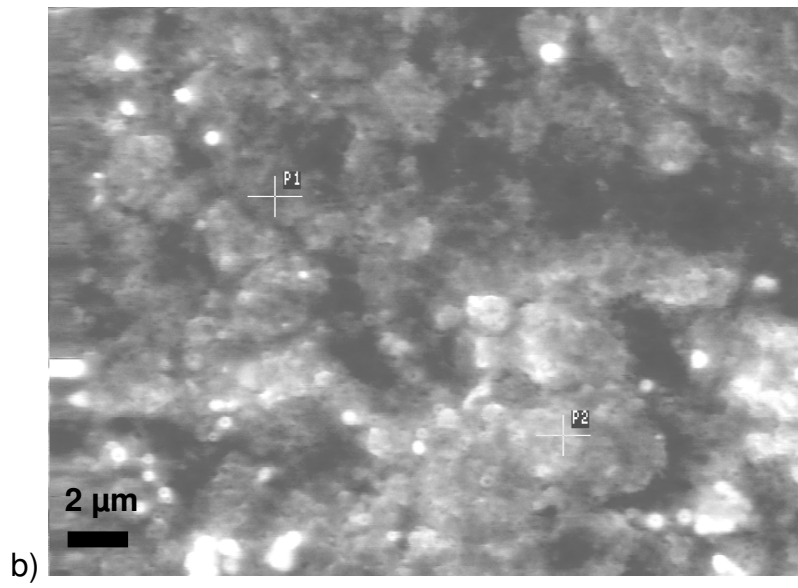
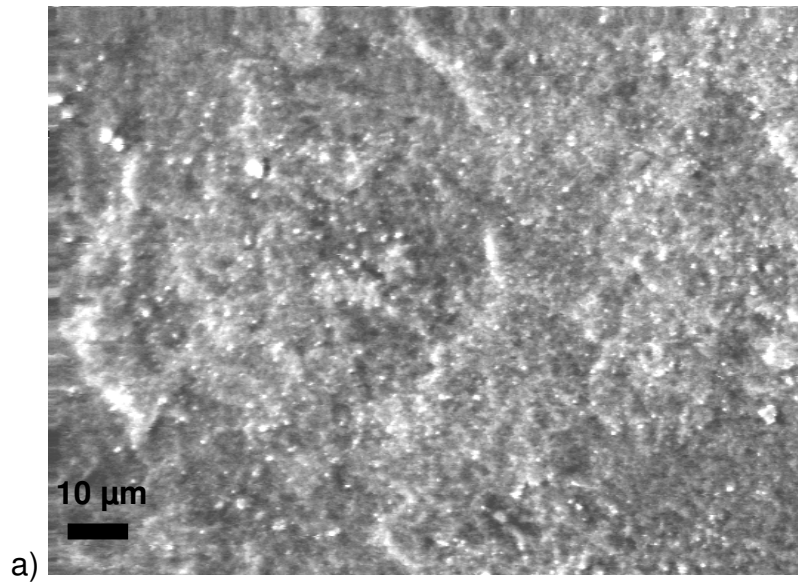


Fig. 26: SEM images of sample surface after wet plasma exposure (390 °C, 6 h, 1% water vapour). Image sizes: a) 120 x 90 μm, b) 24 x 18 μm



The hydrogen gas can subsequently diffuse into the oxide and destabilize it by accumulating into gas bubbles [52] or formation of hydroxide [54]. Moreover, beryllium oxide has been found to be porous to water vapour [52,121], which increases the previous effect as the oxidation reaction occurs also inside the oxide layer. This in turn is aggravated by the formation of hydrogen gas bubbles and the accompanying increase in porosity.

In the present case of hydrogen plasma exposure, the effect of the addition of water vapour cannot be explained in the same line, since hydrogen is already available without the oxidation reaction. Rather, the abundance of a source of oxygen seems to be the key

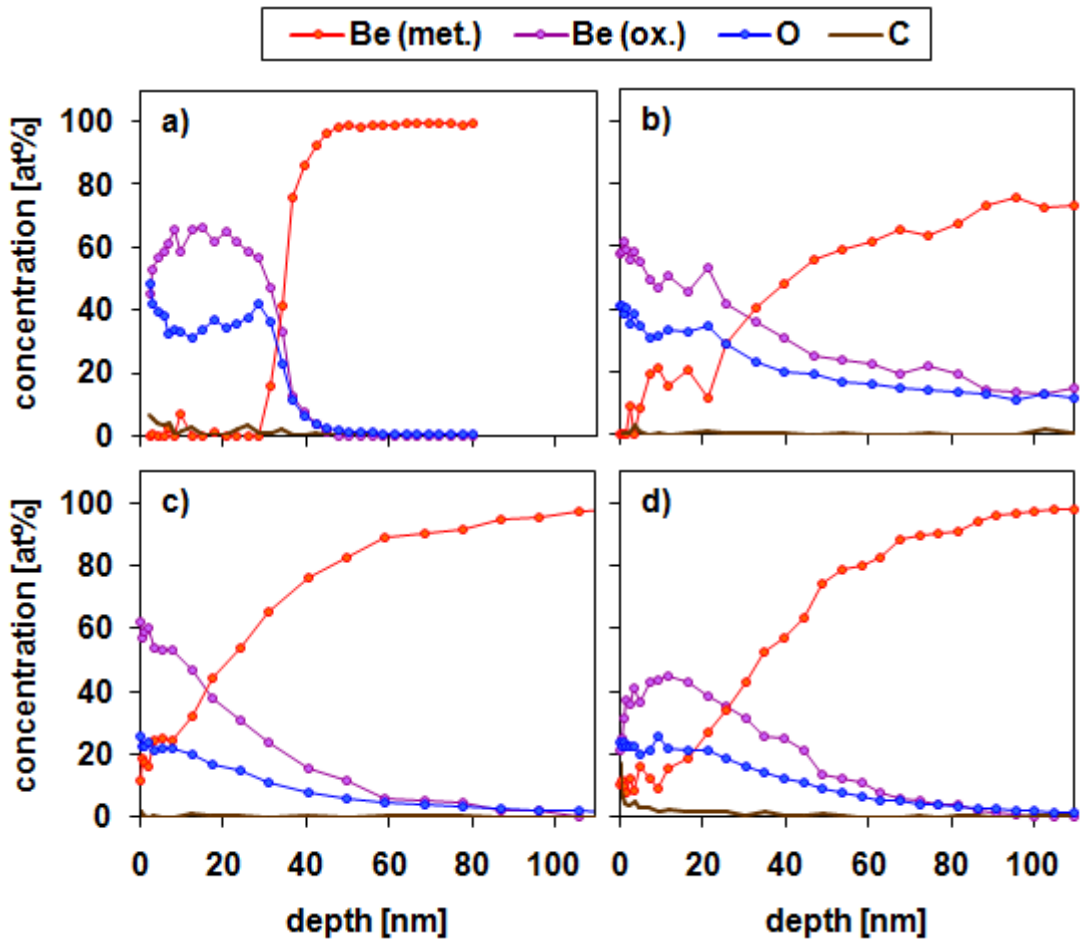


Fig. 27: Depth profiles of oxide layers with comparable thickness (approx. 40 nm) from plasma exposure experiments with different fractions of water vapour: a) dry hydrogen ($3 \cdot 10^{-6}$), b) 10^{-4} , c) 10^{-3} , d) 10^{-2}

factor that determines whether a quasi-equilibrium layer develops or oxidation dominates. From this point of view, in the dry case, there would be just sufficient water molecules to oxidise the free beryllium appearing at the surface, according to reaction (20) [10,39,107,109,135]. In the wet case, on the other hand, the surface would contain only a very small concentration of free beryllium, and the water molecules would be able to react with the oxide to form hydroxide, according to the reaction



The formation of beryllium hydroxide under hydrogen (deuterium) plasma exposure has been reported before.

In [38], deuterium retention in the beryllium oxide layer was studied by exposing beryllium samples to a deuterium plasma at temperatures between room temperature and 470 °C. After exposure, the samples were examined with secondary ion mass spectrometry (SIMS), which revealed that part of the oxide layer had been transformed into hydroxide ($\text{Be}(\text{OD})_2$). The fact that this transformation coincided with the growth of the oxide layer during exposure was explained with the release of beryllium in the hydroxylation reaction



which migrates to the surface where it is oxidised by residual gases. The distribution of hydroxide in the overlayer leads to the conclusion that these processes were not only occurring at the surface, but that deuterium atoms were able to diffuse into the oxide, initiating the hydroxylation throughout the layer. Evidence for deuterium gas bubbles in the oxide/hydroxide layer was detected as well.

In a recent series of papers [42,140,141], the optical properties of beryllium mirrors under bombardment with deuterium ions were investigated. The deuterium ion energies were between 20 and 1350 eV. During exposure the surface reflectance and mass change of the samples were monitored. After the experiments the sample surface was imaged with atomic force microscopy (AFM). The most remarkable feature was that during the first minutes of exposure, the reflectance of the samples dropped significantly. The AFM images showed a smooth, flat surface for the original samples, whereas the surfaces after exposure were considerably rougher. Since no mass loss was detected in the time of the reflectance drop, sputtering was excluded as its cause. The authors interpreted the results as the transformation of the surface oxide layer into hydroxide ($\text{Be}(\text{OD})_2$), which

possesses different optical properties than beryllium oxide, and subsequent growth of this layer.

In both literature works, the authors base the formation of beryllium hydroxide in their experiments on the reaction (25) of beryllium oxide with hydrogen/deuterium atoms or ions. However, considering the observed differences between the results for dry and wet hydrogen in the present work, the reaction (24) of beryllium oxide with water vapour is likely to play an important part in the chemical behaviour. Both literature works specify a base pressure of their respective system of approx. 10^{-4} Pa, and a deuterium working pressure of 0,5 Pa [38] and 0,04 Pa [42,140,141], respectively. Assuming that the content of water vapour in the residual gas is in the order of at least 50 %, this would put the reported conditions around 10^{-4} and 10^{-3} on the fraction scale used in this work, which is well within the range for wet hydrogen as used in the present study and supports the importance of a relatively high concentration of water vapour for the formation of the hydroxide.

Beryllium hydroxide has a distinctly higher ratio of oxygen to beryllium ($O/Be = 2$) than beryllium oxide ($O/Be = 1$), which should make them easy to distinguish in chemical analysis. However, analysing the AES sputter depth profiles of dry and wet plasma exposure experiments, no such difference can be found (as can be seen in the exemplary profiles shown in fig. 27). On the other hand, comparison of the SEM images of the samples (fig. 22 to 26) with the AFM images from [141] clearly show a similarity between the surfaces exposed to wet plasma in this work and the surfaces identified as hydroxide in [141]. A reason for the lack of difference in the AES profiles may be found in the fact that beryllium hydroxide decays slowly at room temperature [38,42]. In the present case, the time between heating experiment and analysis may have been enough to leave only beryllium oxide on the surface. Furthermore, hydroxides are prone to degradation in the electron beam [142,143]. The prolonged exposure to medium energy electrons (10 keV) in the AES analysis, as well as the additional bombardment with 3 keV Ar ions for sputtering, can be assumed to break up the hydroxide, reducing the bulk material to oxide and releasing the hydrogen. Fast sample transfer between experiment and analysis and monitoring the hydrogen partial pressure with a mass spectrometer in future analysis of this kind may be a way to further confirm the presence of hydroxide on the sample surface. Because of the assumed decay of the hydroxide and the roughness of the surface, it was not tried to account for the difference in sputtering rates between oxide and hydroxide, keeping the depth scale used for the oxide experiments.

For the use of beryllium in a hydrogen plasma environment the present experiments

demonstrate a further pathway of erosion besides melting, physical sputtering and oxidation. Hydroxylation is clearly a more severe chemical erosion than oxidation because the surface structure is damaged in the process and disintegration into dust is therefore accelerated, whereas oxidation may even prove beneficial (see chapter 5.2.1). The key parameter that determines if the chemical behaviour will be dominated by oxidation or hydroxylation is the concentration of oxygen-containing molecules (water vapour), and this emphasises the importance of minimising residual gas pressure in the vessel prior to hydrogen plasma experiments.

6. Summary and Conclusion

The research on nuclear fusion for the generation of energy has received much interest in recent years, and the numbers of test reactor experiments and laboratory studies have grown enormously since the beginning of fusion research in the 20th century. For reactor types using magnetic confinement of a deuterium/tritium plasma, beryllium is considered one of the most promising candidates for manufacture of components interacting with the fusion plasma (first wall). Besides its most important advantage of low atomic mass (reducing radiation losses in the fusion plasma by sputtered first wall impurities), it was found that beryllium reduces the concentration of residual oxygen by gettering impurities. In this context, the oxidation behaviour of beryllium is of obvious importance. It has been thoroughly investigated in the 1960's, building the data-base which is still used for reference today. As only few studies have dealt with the oxidation of beryllium since then, this work re-examines the oxidation kinetics and related phenomena with modern surface analytical methods. The results are then applied to selected experiments investigating the interaction of beryllium and beryllium oxide with hydrogen plasma.

Oxidation in air was studied with sintered and plasma-sprayed beryllium samples, which were heated in a tubular furnace for durations between 1 and 43 h at temperatures of 390, 500 and 600 °C. After heating, the sample surfaces were analysed by AES sputter depth profiling. This method is perfectly suited for the problem at hand because metallic and oxidised beryllium can be well distinguished in Auger electron spectra.

Since the as-received samples were too rough for feasible surface analysis, they had to be polished prior to the experiments. For this purpose a glove box with integrated grinding machine and filtered air circulation system was set up, in order to avoid exposure of the laboratory environment to toxic beryllium dust.

For heating durations up to approx. 20 h at 390 °C and 500 °C, and up to 1 h at 600 °C, diffusion-controlled parabolic oxidation behaviour was observed, with oxide layers growing to approx. 15, 40 and 50 nm, respectively. Longer heating resulted in a saturation of the oxide layer thickness, which was tentatively attributed to impurities in the samples. The experimental data were evaluated by fitting them with the simple TPB-model (Tammann, Pilling and Bedworth) for parabolic oxidation. The resulting oxidation rate constants were used in an Arrhenius plot to determine the activation energy for the diffusion process controlling the oxidation rate, with a result of $1,16 \pm 0,2$ eV.

Comparison with earlier measurements in the literature show that this value lies well within a rather extensive range of activation energy results (0,37-2,8 eV). The variety of

conditions and applied analysis techniques makes it difficult to determine the causes for this high spread. However, a frequently reported problem is the low repeatability of the experiments within each study, which is commonly attributed to impurities in the bulk sample material.

The present experiments contribute a set of data to narrow down the range where the oxidation kinetics can be established, and confirm particularly the results previously obtained with surface analytical methods.

After depth profiling, the surfaces were examined with SEM and AES mapping. The images obtained reveal that with increasing temperature and heating duration first grain boundary oxidation of the bulk sets in, which finally causes whole grains to break away. This is an indication of the onset of non-protective or catastrophic oxidation, which is characterised by a dramatic increase in oxidation rate, formation of cracks in the oxide layer, and oxidative attack of the underlying bulk. In contrast to earlier publications, where the transition from protective (parabolic) to catastrophic oxidation was found around 700°C, the present experiments demonstrate that the first signs of the non-protective regime can already appear at temperatures as low as 500°C.

Interaction of beryllium with hydrogen plasma was investigated with the same beryllium samples that were used for the oxidation studies. A roughing pump and a high purity hydrogen supply were attached to the furnace, as well as external electrodes for the excitation of a capacitively coupled r.f. plasma inside the furnace tube. Plasma exposure experiments were carried out at temperatures between room temperature and 600°C, and for durations between 1 and 6 h. To allow for oxide reducing effects, several experiments were done with pre-oxidised samples with an initial oxide layer thickness between 10 and 80 nm.

The results showed that for all temperatures and durations, an oxide layer with a thickness in a range of approx. 15-35 nm was formed on the surface. The development of this quasi-equilibrium oxide thickness can in part be explained by the simultaneous occurrence of the competing processes of reduction by hydrogen atoms and oxidation with residual water vapour. However, the diffusion of beryllium and hydrogen in the oxide layer is assumed to play an essential role that is as yet not clarified.

Since water vapour as the main oxygen-containing residual gas turned out to be a key component for the behaviour of the beryllium-hydrogen system, in a further experimental step the furnace was fitted with an assembly for controlled admixture of minute amounts of water vapour to the hydrogen plasma. Fractions used for the subsequent wet hydrogen plasma exposure experiments were 10^{-4} , 10^{-3} and 10^{-2} water vapour in hydrogen,

whereas residual water vapour in the previous dry hydrogen experiments could be estimated to be below a concentration of $3 \cdot 10^{-6}$ in hydrogen.

The resulting oxide layers were much thicker and more rough than in both the oxidation and dry plasma experiments, as could be discerned from depth profiles and SEM images. Comparison with experiments under similar conditions from literature suggest that the overlayer formed consists mostly of beryllium hydroxide and only in small parts of oxide, although this cannot be verified with AES.

To apply the results described to nuclear fusion research, one has to consider that particle energies are much higher in a fusion plasma reactor than in the laboratory scale furnace, and therefore physical sputtering is a critical issue here. Additionally occurring effects are a high neutron flux to the wall and, in the frame of the current reactor design, material mixing by migration of carbon to beryllium first wall regions. Thermal loads can get high enough to cause melting of beryllium first wall segments in the course of so-called edge-localised modes (ELMs) of the plasma, but in normal operation (steady state without ELMs) typical first wall temperatures lie around $100\text{ }^{\circ}\text{C}$ - $300\text{ }^{\circ}\text{C}$ [24,133], with some smaller components reaching up to approx. $500\text{ }^{\circ}\text{C}$ [24]. Concentrations of oxygen-containing impurities are estimated at 1% or lower [10,144].

The present experiments with dry hydrogen show that even at impurity concentrations as low as $3 \cdot 10^{-6}$, a stable oxide layer forms at the surface. Under the increased sputtering and with lower temperature in reactor operation, an oxide layer with a smaller thickness ($< 10\text{ nm}$) should be expected, although complete removal of the oxide layer may also be possible [66]. Formation of an oxide layer, possibly with admixture of other impurities (carbon), may even prove beneficial by providing a higher resistance against physical sputtering [10]. However, continuous gettering of oxygen does not seem possible in this regime, the observed oxygen reduction [1,18] being an initial one-time effect only.

The results described also present an increased potential for the erosion of beryllium. The non-negligible impurity concentration involves the increased risk of chemical erosion by formation of hydroxide, and for components reaching around $500\text{ }^{\circ}\text{C}$, increased disintegration and dust formation has to be expected due to grain boundary oxidation. This is an additional reason to reduce residual gas pressure prior to plasma excitation as much as possible, and minimise particularly the water vapour concentration in the reactor vessel.

References

- [1] F. Scaffidi-Argentina, G.R. Longhurst, V. Shestakov, H. Kawamura, Beryllium R&D for Fusion Applications, *Fusion Eng. Des.* 51-52 (2000) 23-41
- [2] K.A. Walsh, *Beryllium Chemistry and Processing*, ASM International, USA (2009)
- [3] B. Patel, W. Parsons, Operational Beryllium Handling Experience at JET, *Fusion Eng. Des.* 69 (2003) 689-694
- [4] M.A. Gomez, L.R. Pratt, J.D. Kress, D. Asthagiri, Water Adsorption and Dissociation on BeO(001) and (100) Surfaces, *Surface Science* 601 (2007) 1608-1614
- [5] V.N. Chernikov, V.K. Alimov, A.V. Markin, A.P. Zakharov, Gas Swelling and Related Phenomena in Beryllium Implanted with Deuterium Ions, *J. Nucl. Mat.* 228 (1996) 47-60
- [6] J. Roth, W.R. Wampler, W. Jacob, Release of Deuterium from Carbon-Deuterium Films on Beryllium During Carbide Formation and Oxidation, *J. Nucl. Mat.* 250 (1997) 23-28
- [7] E.A. Gulbransen, K.F. Andrew, The Kinetics of the Reactions of Beryllium with Oxygen and Nitrogen and the Effect of Oxide and Nitride Films on its Vapor Pressure, *J. Electrochem. Soc.* Vol. 97, Iss. 11 (1950) 383-395
- [8] R.O. Adams, J.T. Hurd, The Properties of Beryllium Surfaces and Films, *J. Less-Common Metals* 18 (1969) 399-409
- [9] D.W. Aylmore, S.J. Gregg, W.B. Jepson, The High Temperature Oxidation of Beryllium - Part I, *J. Nucl. Mat.* 2, 2 (1960) 169-175
- [10] R.W. Conn, R.P. Doerner, J. Won, Beryllium as the plasma-facing material in fusion energy systems—experiments, evaluation, and comparison with alternative materials, *Fusion Eng. Des.* 37 (1997) 481-513
- [11] W.M. Stacey, *Fusion Plasma Analysis*, Wiley, New York (1981)
- [12] E. Teller, *Fusion, Part B*, Academic Press, New York (1981)
- [13] G.M. McCracken, P.E. Stott, Plasma-surface interactions in TOKAMAKs, *Nuclear Fusion* 19 (7) (1979) 889-981
- [14] D.M. Meade, Effect of high Z impurities on the ignition and Lawson conditions for a thermonuclear reactor, *Nuclear Fusion* 14 (2) (1974) 289-291
- [15] R.V. Jensen, D.E. Post, W.H. Grasberger, Calculations of impurity radiation and its effect on tokamak experiments, *Nuclear Fusion* 17 (6) (1977) 1187-1196
- [16] R.V. Jensen, D.E. Post, D.L. Jassby, Critical impurity concentrations for power multiplication in beam-heated toroidal fusion reactors, *Nuclear Science and Engineering* 65 (2) (1978) 282-289

- [17] R.W. Conn, Pumped divertors and limiters for tokamaks, *Fusion Engineering and Design* 14 (1-2) (1991) 81-97
- [18] G. Janeschitz, ITER JCT and HTs, Plasma-Wall Interaction Issues in ITER, *J. Nucl. Mat.* 290-293 (2001) 1 - 11
- [19] J. Roth, E. Tsitrone, A. Loarte, T. Loarer, G. Counsell, R. Neu, V. Philipps, S. Brezinsek, M. Lehnen, P. Coad, C. Grisolia, K. Schmid, K. Krieger, A. Kallenbach, B. Lipschultz, R. Doerner, R. Causey, V. Alimov, W. Shu, O. Ogorodnikova, A. Kirschner, G. Federici, A. Kukushkin, EFDA PWI Task Force, ITER PWI Team, Fusion for Energy, ITPA SOL/DIV, Recent Analysis of Key Plasma Wall Interactions Issues for ITER, *J. Nucl. Mat.* 390-391 (2009) 1 - 9
- [20] G.L. Kulcinski, R.W. Conn, G. Lang, Reduction of plasma contamination effects and first-wall erosion in fusion devices, *Nuclear Fusion* 15 (2) (1975) 327-333
- [21] M. Ulrickson, The JET Team, The TFTR Team, A review of carbon blooms on JET and TFTR, *J. Nucl. Mat.* 176-177 (1990) 44-50
- [22] R. Reichle, D.D.R. Summers, M.F. Stamp, Carbon yields and influxes as a function of target temperatures in JET X-point discharges, *J. Nucl. Mat.* 176-177 (1990) 375-380
- [23] J. Roth, E. Vietzke, A.A. Haasz, Erosion of graphite due to particle impact, Atomic and Plasma-Wall Interaction Data for Fusion, IAEA, Vienna (Nuclear Fusion Supplemental) 1 (1991) 63-78
- [24] G. Federici, R.A. Anderl, P. Andrew, J.N. Brooks, R.A. Causey, J.P. Coad, D. Cowgill, R.P. Doerner, A.A. Haasz, G. Janeschitz, W. Jacob, G.R. Longhurst, R. Nygren, A. Peacock, M.A. Pick, V. Philipps, J. Roth, C.H. Skinner, W.R. Wampler, In-vessel Tritium Retention and Removal in ITER, *J. Nucl. Mat.* 266-269 (1999) 14-29
- [25] G. Federici, P. Andrew, P. Barabaschi, J. Brooks, R. Doerner, A. Geier, A. Herrmann, G. Janeschitz, K. Krieger, A. Kukushkin, A. Loarte, R. Neu, G. Saibene, M. Shimada, G. Strohmayer, M. Sugihara, Key ITER Plasma Edge and Plasma–Material Interaction Issues, *J. Nucl. Mat.* 313-316 (2003) 11 - 22
- [26] M. Lipa, J. Linke, G. Martin, E. Wessel, Behaviour of Molten Beryllium with ITER Reference CFC SEPCARB® NB31 Under Moisture, *Fusion Eng. Des.* 82 (2007) 1688–1693
- [27] M.J. Saltmarsh, Review of the ISX-B Experimental Program, *J. Vac. Sci. Technol.* 17 (1) (1980) 260-267
- [28] R. Flohr, C. Gillet, J. Hackmann, G. Reinhold, G. Ritter, J. Uhlenbusch, S. Zakaria, The Tokamak Experiment "UNITOR" - A Device for Plasma-Wall Interaction Research, *Physica B+C* 104 (3) (1981) 423-433
- [29] K.J. Dietz and the JET team, Effect of Beryllium on Plasma Performance in JET, *Plasma Physics and Controlled Fusion* Vol. 32, No. 11 (1990) 837-852

- [30] K.L. Wilson, R.A. Causey, W.L. Hsu, B.E. Mills, M.F. Smith, J.B. Whitley, Beryllium - a Better Tokamak Plasma-Facing Material?, *J. Vac. Sci. Technol. A* 8 (3) (1990) 1750
- [31] J. Roth, Erosion and Impurity Production of C and Be: a Comparison, *J. Nucl. Mat.* 145-147 (1987) 87-95
- [32] R. Behrisch, A.P. Martinelli, S. Grigull, R. Grötzschel, U. Kreissig, D. Hildebrandt, W. Schneider, Surface layer composition of the JET vessel walls, *J. Nucl. Mat.* 220-222 (1995) 590-594
- [33] S. Zalkind, M. Polak, N. Shamir, Adsorption of Hydrogen on Clean and Oxidized Beryllium Studied by Direct Recoil Spectrometry, *Applied Surface Science* 115 (1997) 273-278
- [37] R.A. Causey, D.S. Walsh, Codeposition of Deuterium with Beryllium, *J. Nucl. Mat.* 254 (1998) 84-86
- [38] V.M. Sharapov, V.K. Alimov, L.E. Gavrilov, Deuterium Accumulation in Beryllium Oxide Layer Exposed to Deuterium Atoms, *J. Nucl. Mat.* 258-263 (1998) 803-807
- [39] R.A. Anderl, K.A. McCarthy, M.A. Oates, D.A. Petti, R.J. Pawelko, G.R. Smolik, Steam-chemical Reactivity for Irradiated Beryllium, *J. Nucl. Mat.* 258-263 (1998) 750-756
- [40] O.V. Ogorodnikova, Comparison of Hydrogen Gas-, Atom- and Ion-Metal Interactions, *J. Nucl. Mat.* 277 (2000) 130-142
- [41] A.V. Markin, V.P. Dubkov, A.E. Gorodetsky, M.A. Negodaev, N.V. Rozhanskii, F. Scaffidi-Argentina, H. Werle, C.H. Wu, R.K. Zalavutdinov, A.P. Zakharov, Codeposition of Deuterium Ions with Beryllium Oxide at Elevated Temperatures, *J. Nucl. Mat.* 283-287 (2000) 1094-1099
- [42] A.F. Bardamid, A.I. Belyayeva, V.N. Bondarenko, A.A. Galuza, V.V. Gann, L. Jacobson, V.G. Konovalov, D.V. Orlinskij, I.I. Papirov, I.V. Ryzhkov, A.N. Shapoval, A.F. Shtan, S.I. Solodovchenko, A.A. Vasilev, V.S. Voitsenya, Some Peculiarities in the Behavior of Be Surfaces Under Bombardment by Ions from a Deuterium Plasma, *J. Nucl. Mat.* 313-316 (2003) 112-115
- [43] M.J. Baldwin, K. Schmid, R.P. Doerner, A. Wiltner, R. Seraydarian, C. Linsmeier, Composition and Hydrogen Isotope Retention Analysis of Co-deposited C/Be Layers, *J. Nucl. Mat.* 337-339 (2005) 590-594
- [44] J. Roth, E. Tsitrone, A. Loarte, Plasma–Wall Interaction: Important Ion Induced Surface Processes and Strategy of the EU Task Force, *Nuclear Instruments and Methods in Physics Research B* 258 (2007) 253-263
- [45] R.P. Doerner, The Implications of Mixed-Material Plasma-Facing Surfaces in ITER, *J. Nucl. Mat.* 363-365 (2007) 32-40
- [46] D. Nishijima, R.P. Doerner, M.J. Baldwin, G. De Temmerman, Erosion Yields of Deposited Beryllium Layers, *J. Nucl. Mat.* 390-391 (2009) 132-135

- [47] R.P. Doerner, M.J. Baldwin, D. Buchenauer, G. De Temmerman, D. Nishijima, The Role of Beryllium Deuteride in Plasma-Beryllium Interactions, *J. Nucl. Mat.* 390-391 (2009) 681-684
- [48] F. Druyts, J. Fays, P. Van Iseghem, F. Scaffidi-Argentina, Chemical Reactivity of Beryllium Pebbles in Air, *Fusion Eng. Des.* 58-59 (2001) 695-700
- [49] S. Zalkind, M. Polak, N. Shamir, Oxidation of Ion-Bombarded vs. Annealed Beryllium, *Surface Science* 513 (2002) 501-510
- [50] F. Druyts, J. Fays, C.H. Wu, Interaction of Plasma-Facing Materials with Air and Steam, *Fusion Eng. Des.* 63-64 (2002) 319-325
- [51] S. Zalkind, M. Polak, N. Shamir, The Initial Interactions of Beryllium with O₂ and H₂O Vapor at Elevated Temperatures, *Surface Science* 601 (2007) 1326-1332
- [52] D.W. Aylmore, S.J. Gregg, W.B. Jepson, The High Temperature Oxidation of Beryllium - Part IV, *J. Nucl. Mat.* 3, 2 (1961) 190-200
- [53] W.B. Jepson, J.B. Warburton, , B.L. Myatt, The High Temperature Oxidation of Beryllium and the Fate of Beryllium Carbide Inclusions, *J. Nucl. Mat.* 10, 2 (1963) 127-133
- [54] W.B. Jepson, B.L. Myatt, J.B. Warburton, J.E. Antill, Some Topographical Observations on the Oxidation of Beryllium, *J. Nucl. Mat.* 10, 3 (1963) 224-232
- [55] G. Ervin, Jr., T.L. Mackay, Catastrophic Oxidation of Beryllium Metal, *J. Nucl. Mat.* 12, 1 (1964) 30-39
- [56] L. Hackspill, A.P. Kieffer, Contribution to the study of hydroxides and mineral salts, *Annales de Chimie France* 14 (1930) 227-282
- [57] H. Terem, , *Rev. Faculte Sci. Univ. Istanbul* 8A (1943) 9
- [58] C.A. Hutchison, jr., J.G. Malm, The Volatilization of Beryllium Oxide in the Presence of Water, *J. Amer. Chem. Soc.* 71 (4) (1949) 1338-1339
- [59] D. Cubicciotti, The Oxidation of Beryllium at High Temperatures, *J. Amer. Chem. Soc.* 72 (1950) 2084-2086
- [60] R.J. Fortner, R.G. Musket, Chemical Effects in the Auger Electron Spectra of Beryllium, *Surface Science* 28 (1) (1971) 339-343
- [61] E.J. Lejeune, Jr., R.D. Dixon, Interpretation of the Auger Electron Spectrum from Oxidized Beryllium, *J. Appl. Phys.* Vol. 43, No. 4 (1972) 1998
- [62] D.E. Fowler, J.M. Blakely, An Auger Electron Spectroscopy (AES) Study of the Initial Stages of Oxidation of the Single Crystal Be (0001) Surface, *J. Vac. Sci. Technol.* 20 (4) (1982) 930
- [63] D.E. Fowler, J.M. Blakely, The Initial Oxidation of the Beryllium (0001) Surface, *Surface Science* 148 (1984) 265-282

- [64] D.E. Fowler, J.M. Blakely, Surface Reconstruction of BeO (0001) During Be Oxidation, *Surface Science* 148 (1984) 283-291
- [65] R.A. Langley, Interaction of Implanted Deuterium and Helium with Beryllium: Radiation Enhanced Oxidation, *J. Nucl. Mat.* 85 & 86 (1979) 1123-1126
- [66] R. Bastasz, Hydrogen Bombardment of the Oxide Layer on Beryllium, *Thin Solid Films* 121 (1984) 127-133
- [67] R.C. Isler, K. Behringer, E. Kallne, P.D. Morgan, N.J. Peacock, P.H. Edmonds, P.K. Mioduszewski, Impurity Fluxes and Concentrations in the ISX-B Beryllium Limiter Experiment, *Nuclear Fusion* 25 (1985) 1635-1655
- [68] J. Hackmann, J. Uhlenbusch, Test of a Beryllium Limiter in the Tokamak Uinitor, *J. Nucl. Mat.* 128-129 (1984) 418-421
- [69] D.M. Goebel, Y. Hirooka, R.W. Conn, W.K. Leung, G.A. Campbell, J. Bohdanský, K.L. Wilson, W. Bauer, R.A. Causey, A.E. Pontau, A.R. Krauss, D.M. Gruen, M.H. Mendelsohn, Erosion and Redeposition Experiments in the Pisces Facility, *J. Nucl. Mat.* 145-147 (1987) 61-70
- [70] A.P. Martinelli, R. Behrisch, H. Hammer, J. Hackmann, Surface composition of the Be limiters and the stainless steel torus wall after operation in UNITOR, *J. Nucl. Mat.* 145-147 (1987) 755-760
- [71] M. Bessenrodt-Weberpals, J. Hackmann, C. Nieswand, J. Uhlenbusch, Distribution of Beryllium Concentrations and Fluxes in the Tokamak UNITOR, *Plasma Physics and Controlled Fusion* 30 (4) (1988) 407-413
- [72] C. Nieswand, M. Born, J. Hackmann, Release of Beryllium from Poloidal Limiters in UNITOR, *Plasma Physics and Controlled Fusion* 32 (3) (1990) 197-202
- [73] M. Born, H.-D. Dicken, J. Hackmann, J. Uhlenbusch, Local Ion Temperature Measurements in the Tokamak UNITOR by Collective Thomson Scattering, *Plasma Physics and Controlled Fusion* 34 (1993) 391-396
- [74] A.T. Peacock, J.P. Coad, F. Lama, Impurity coverage and deuterium inventory of beryllium and carbon first wall components after beryllium operation in JET, *J. Nucl. Mat.* 176-177 (1990) 326-331
- [75] H. Bergsaker, J.P. Coad, R. Behrisch, Deposition of carbon and beryllium and retention of deuterium on probes in the scrape-off layer of JET, *J. Nucl. Mat.* 176-177 (1990) 941-946
- [76] S. Zalkind, M. Polak, N. Shamir, The Adsorption of H₂O vs O₂ on Beryllium, *Surface Science* 385 (1997) 318-327
- [77] S. Zalkind, M. Polak, N. Shamir, Temperature Dependent Interactions of Water Vapor with a Beryllium Surface, *Surface Science* 529 (2003) 189-196
- [78] S. Zalkind, M. Polak, N. Shamir, Effects of Preadsorbed Hydrogen on the Adsorption of O₂, CO and H₂O on Beryllium, *Surface Science* 539 (2003) 81-90

- [79] Ishitsuka et al, Surface Characterization of Hot-Pressed Beryllium with X-ray Photoelectron Spectroscopy, *J. Nucl. Mat.* 191-194 (1992) 183-185
- [80] E.B. Deksnis, A.T. Peacock, H. Altmann, C. Ibbot, H.D. Falter, Beryllium Plasma-facing Components: JET Experience, *Fusion Eng. Des.* 37 (1997) 515-530
- [81] R.G. Castro, P.W. Stanek, K.E. Elliott, D.L. Youchison, R.D. Watson, D.S. Walsh, Plasma-Sprayed Beryllium for ITER, *Fusion Engineering, SOFE'95, 16th IEEE/NPSS Symposium, Champaign, IL, USA 1* (1995) 381-384
- [82] R.G. Castro, P.W. Stanek, K.E. Elliott, J.D. Cotton, R.D. Watson, Optimizing the Thermal Conductivity of Vacuum Plasma-Sprayed Beryllium for Fusion Applications, *J. Nucl. Mat.* 226 (1995) 170-177
- [83] D.J. Varacalle, Jr., R.G. Castro, Analysis of the Plasma-Particle Interaction During the Plasma Spraying of Beryllium, *J. Nucl. Mat.* 230 (1996) 242-246
- [84] R.G. Castro, P.W. Stanek, K.E. Elliott, The Structure, Properties and Performance of Plasma-Sprayed Beryllium for Fusion Applications, *Physica Scripta T64* (1996) 77-83
- [85] R.G. Castro, A.H. Bartlett, K.J. Hollis, R.D. Fields, The Effect of Substrate Temperature on the Thermal Diffusivity and Bonding Characteristics of Plasma Sprayed Beryllium, *Fusion Eng. Des.* 37 (1997) 243-252
- [86] R.G. Castro, K.E. Elliot, R.D. Watson, D.L. Youchison, K.T. Slattery, Fabrication and High Heat Flux Testing of Plasma Sprayed Beryllium ITER First Wall Mock-ups, *J. Nucl. Mat.* 258-263 (1998) 252-257
- [87] I.S. Landman, B.N. Bazylev, I.E. Garkusha, A. Loarte, S.E. Pestchanyi, V.M. Safronov, Simulation of Tokamak Armour Erosion and Plasma Contamination at Intense Transient Heat Fluxes in ITER, *J. Nucl. Mat.* 337-339 (2005) 761-765
- [88] K. Schmid, M. Baldwin, R. Doerner, Modelling of Thermally Enhanced Erosion of Beryllium, *J. Nucl. Mat.* 348 (2006) 294-301
- [89] B. Bazylev, G. Janeschitz, I. Landman, S. Pestchanyi, A. Loarte, Erosion Simulation of First Wall Beryllium Armour Under ITER Transient Heat Loads, *J. Nucl. Mat.* 386-388 (2009) 919-921
- [90] R.P. Doerner, M.J. Baldwin, S.I. Krasheninnikov, K. Schmid, High Temperature Erosion of Beryllium, *J. Nucl. Mat.* 337-339 (2005) 877-881
- [91] A. Loarte, G. Saibene, R. Sartori, D.J. Campbell, P.J. Lomas, G.F. Matthews, EFDA-JET workprogramme collaborators, A New Look at JET Operation with Be as Plasma Facing Material, *J. Nucl. Mat.* 337-339 (2005) 816-820
- [92] K. Krieger, S. Brezinsek, S. Jachmich, S. Lisgo, M. Stamp, H.G. Esser, A. Kreter, S. Menmuir, P. Mertens, V. Philipps, P. Sundelin, JET EFDA contributors, Be Wall Sources and Migration in L-mode Discharges after Be Evaporation in the JET Tokamak, *J. Nucl. Mat.* 390-391 (2009) 110-114

- [93] M. Rödiger, R. Conrad, H. Derz, R. Duwe, J. Linke, A. Lodato, M. Merola, G. Pott, G. Vieider, B. Wiechers, Neutron-Irradiation Effects on High Heat Flux Components - Examination of Plasma-Facing Materials and Their Joints, *J. Nucl. Mat.* 283-287 (2000) 1161-1165
- [94] M.I. Guseva, V.M. Gureev, L.S. Danelyan, B.N. Kolbasov, S.N. Korshunov, I.D. Skorlupkin, V.G. Stolyarova, V.I. Vasilev, V.M. Strunnikov, V.V. Zatyokin, V.S. Kulikauskas, Study of Hydrogen Isotope Interaction with Beryllium and Carbon Surfaces under their Simultaneous Exposure to Stationary and Powerful Pulsed Plasma, *J. Nucl. Mat.* 329-333 (2004) 825-829
- [95] A.T. Peacock, W.J. Haws, M.A. Pick, Development of Beryllium-Carbide Fibre Reinforced Beryllium for Fusion Applications, Fusion Engineering, 15th IEEE/NPSS Symposium, Hyannis, MA, USA n.a. (1993) 50-53
- [96] K. Munakata, H. Kawamura, M. Uchida, Reaction of Titanium Beryllide with Water Vapor, *Fusion Eng. Des.* 75-79 (2005) 997-1002
- [97] K. Munakata, H. Kawamura, M. Uchida, Kinetics of Reaction with Water Vapor and Ab Initio Study of Titanium Beryllide, *J. Nucl. Mat.* 367-370 (2007) 1057-1062
- [98] P.-H. Rebut, From JET to the Reactor, *Plasma Physics and Controlled Fusion* 48 (2006) B1-B13
- [99] G. Kalinin, V. Barabash, A. Cardella, J. Dietz, K. Ioki, R. Matera, R.T. Santoro, R. Tivey, The ITER Home Teams, Assessment and Selection of Materials for ITER In-Vessel Components, *J. Nucl. Mat.* 283-287 (2000) 10 - 19
- [100] M. Shimada, A.E. Costley, G. Federici, K. Ioki, A.S. Kukushkin, V. Mukhovatov, A. Polevoi, M. Sugihara, Overview of Goals and Performance of ITER and Strategy for Plasma-Wall Interaction Investigation, *J. Nucl. Mat.* 337-339 (2005) 808-815
- [101] I. Ovchinnikov, A. Komarov, V. Kuznetsov, V. Titov, Real-Time Measurement of Hydrogen Generation Level During Beryllium Dust Oxidation by Steam Depending on the Dust Arrangement Geometry, *Fusion Eng. Des.* 81 (2006) 2073-2084
- [102] K.A. McCarthy, D.A. Petti, W.J. Carmack, G.R. Smolik, The Safety Implications of Tokamak Dust Size and Surface Area, *Fusion Eng. Des.* 42 (1998) 45-52
- [103] R.A. Anderl, F. Scaffidi-Argentina, D. Davydov, R.J. Pawelko, G.R. Smolik, Steam Chemical Reactivity of Be Pebbles and Be Powder, *J. Nucl. Mat.* 283-287 (2000) 1463-1467
- [104] V. Chuyanov, L. Topilski, Prevention of Hydrogen and Dust Explosion in ITER, *Fusion Eng. Des.* 81 (2006) 1313-1319
- [105] S. Rosanvallon, C. Grisolia, P. Andrew, S. Ciattaglia, P. Delaporte, D. Douai, D. Garnier, E. Gauthier, W. Gulden, S.H. Hong, S. Pitcher, L. Rodriguez, N. Taylor, A. Tesini, S. Vartanian, A. Vetry, M. Wykes, Dust Limit Management Strategy in Tokamaks, *J. Nucl. Mat.* 390-391 (2009) 57-60

- [106] B.J. Merrill, R.L. Moore, J.P. Sharpe, A Preliminary Assessment of Beryllium Dust Oxidation During a Wet Bypass Accident in a Fusion Reactor, *Fusion Eng. Des.* 84 (2009) 1285-1288
- [107] F. Druyts, P. Van Iseghem, Thermogravimetric Analysis of the Beryllium-Steam Reaction, *Fusion Eng. Des.* 51-52 (2000) 499-503
- [108] D.A. Petti, G.R. Smolik, R.A. Anderl, On the Mechanisms Associated with the Chemical Reactivity of Be in Steam, *J. Nucl. Mat.* 283-287 (2000) 1390-1395
- [109] F. Druyts, E.C. Alves, C.H. Wu, Methods for the Mitigation of the Chemical Reactivity of Beryllium in Steam, *J. Nucl. Mat.* 329-333 (2004) 1353-1356
- [110] T. Ihli, T.K. Basu, L.M. Giancarli, S. Konishi, S. Malang, F. Najmabadi, S. Nishio, A.R. Raffray, C.V.S. Rao, A. Sagara, Y. Wu, Review of Blanket Designs for Advanced Fusion Reactors, *Fusion Eng. Des.* 83 (2008) 912-919
- [111] A.T. Fromhold, *Theory of Metal Oxidation*, North Holland Publishing Company, Amsterdam (1976)
- [112] G. Tammann, The Heat Tinting of Metals, *Journal of Inorganic and General Chemistry* 111 (1) (1920) 78-89
- [113] N.B. Pilling, R.E. Bedworth, The Oxidation of Metals at High Temperatures, *Journal of the Institute of Metals* 29 (1923) 529-582
- [114] S. Elliott, *The Physics and Chemistry of Solids*, John Wiley & Sons, Chichester, England (1998)
- [115] R. Dobrozemsky, G. Tirlir, W. Grum, J. Neuwirth, Thermal desorption measurements on first wall protection materials: plasma-sprayed beryllium, Contract V66-1999-018 of the Association Euratom-OeAW (final report, OeAW, Vienna, April 2000) (2000)
- [116] R. Dobrozemsky, G. Tirlir, J. Neuwirth, Gas reactions on hot Be surfaces: Thermal desorption measurements on plasma-sprayed and sintered Be, Contract T438-2000-033 of the Association Euratom-OeAW (intermediate report, OeAW, Vienna, September 2000)
- [117] L. Meitner, Concerning the beta-ray spectra and their connection to the gamma rays, *Zeitschrift für Physik* 11 (1) (1922) 35-54
- [118] P. Auger, Secondary beta rays produced in gas by X-rays, *Comptes rendus hebdomadaires des Seances de l'Academie* 177 (1925) 169-171
- [119] M. Suleman, E.B. Pattinson, Interpretation of the Auger Spectrum of Clean and Oxidized Be, *J. Phys. F: Metal Phys.* 3 (1973) 497
- [120] D.A. Shirley, High Resolution X-ray Photoemission Spectrum of the Valence Bands of Gold, *Phys. Rev. B* Vol. 5, No. 12 (1972) 4709-4714
- [121] G.R. Smolik, B.J. Merrill, R.S. Wallace, Implications of Beryllium: Steam Interactions in Fusion Reactors, *J. Nucl. Mat.* 191-194 (1992) 153-157

- [122] B.A. Pint, Experimental Observations in Support of the Dynamic-Segregation Theory to Explain the Reactive-Element Effect, *Oxidation of Metals* 45 (1-2) (1996) 1-37
- [123] T. Do, N.S. McIntyre, Oxidation Kinetics of Mg-, Si, and Fe-Implanted Aluminum by Using X-ray Photoelectron Spectroscopy, *J. Phys. Chem. B* 103 (1999) 2402-2407
- [124] M. Suleman, E.B. Pattinson, The SEE Yield Changes in Slowly Oxidised Be with Surface Characterisation by AES, *J. Phys. D: Appl. Phys.* 13 (1980) 693-700
- [125] V.K. Alimov, R.K. Zalavutdinov, A.E. Gorodetsky, A.P. Zakharov, Penetration of Oxygen into Beryllium Irradiated with Deuterium and Helium Ions, *J. Nucl. Mat.* 220-222 (1995) 947-951
- [126] JANAF Thermochemical Tables of the National Institute of Standards and Technology (USA), accessed at <http://kinetics.nist.gov/janaf/> (July 2012)
- [127] L. Oren, R.J. Taylor, Trapping and Removal of Oxygen in Tokamaks, *Nuclear Fusion* 17 (6) (1977) 1143-1151
- [128] H.F. Dylla, A Review of the Wall Problem and Conditioning Techniques for Tokamaks, *J. Nucl. Mat.* 93/94 (1980) 61-74
- [129] J. Winter, F. Waelbroeck, B. Brandt, On the Cleaning of 1st Wall Materials by Glow-Discharges in Hydrogen, *J. Nucl. Mat.* 93/94 (1980) 812-819
- [130] F. Waelbroeck, J. Winter, P. Wienhold, Cleaning and Conditioning of the Walls of Plasma-Devices by Glow-Discharges in Hydrogen, *J. Vac. Sci. Technol. A* 2 (4) (1984) 1521-1536
- [131] H.F. Dylla, Glow-Discharge Techniques for Conditioning High-Vacuum Systems, *J. Vac. Sci. Technol. A* 6 (3) (1988) 1276-1287
- [132] K. Dimoff, C. Boucher, K.J. Parbhakar, Modeling of Impurity Release Rates during Wall Conditioning of a Vacuum Vessel by Electric Discharge, *J. Vac. Sci. Technol. A* 6 (5) (1988) 2876-2882
- [133] M. Shimada, R.A. Pitts, Wall Conditioning on ITER, *J. Nucl. Mat.* 415 (2011) 1013-1016
- [134] D. Douai, A. Lyssoivan, V. Philipps, V. Rohde, T. Wauters, T. Blackman, V. Bobkov, S. Bremond, S. Brezinsek, F. Clairet, E. de la Cal, T. Coyne, E. Gauthier, T. Gerbaud, M. Graham, S. Jachmich, E. Joffrin, R. Koch, A. Kreter, R. Laengner, P.U. Lamalle, E. Lerche, G. Lombard, M. Maslov, M.-L. Mayoral, A. Miller, I. Monakhov, J.-M. Noterdaeme, J. Ongena, M.K. Paul, B. Pegourie, R.A. Pitts, V. Plyusnin, F.C. Schüller, G. Sergienko, M. Shimada, A. Sirinelli, W. Suttrop, C. Sozzi, M. Tsalas, E. Tsitrone, B. Unterberg, D. Van Eester, the TORE SUPRA Team, the TEXTOR Team, the ASDEX Upgrade Team, JET EFDA Contributors, Recent Results on Ion Cyclotron Wall Conditioning in Mid and Large Size Tokamaks, *J. Nucl. Mat.* 415 (2011) 1021-1028

- [135] J. Won, F.E. Spada, R. Boivin, R. Doerner, S. Luckhardt, F.C. Sze, R.W. Conn, Erosion Behavior and Surface Characterization of Beryllium under High-Flux Deuterium Plasma Bombardment, *J. Nucl. Mat.* 241-243 (1997) 1110-1116
- [136] A. Rutscher, H.E. Wagner, Chemical Quasi-Equilibria: A New Concept in the Description of Reactive Plasmas, *Plasma Sources Sci. Technol.* 2 (4) (1993) 279-288
- [137] S. Veprek, Statistical Model of Chemical Reactions in Nonisothermal Low Pressure Plasma, *J. Chem. Phys.* 57, (1972) 952-959
- [138] S. Veprek, Thermodynamic and Kinetic Aspects of Heterogeneous Reactions in a Nonisothermal Low Pressure Plasma, *IEEE Transactions on Plasma Science* 2 (1) (1974) 25-33
- [139] S. Veprek, Highlights of Preparative Solid State Chemistry in Low Pressure Plasmas, *Pure and Appl. Chem.* 54 (6) (1982) 1197-1220
- [140] V.S. Voitsenya, A.F. Bardamid, V.N. Bondarenko, V.G. Konovalov, D.V. Orlinskij, I.V. Ryzhkov, A.N. Shapoval, A.F. Shtan', S.I. Solodovchenko, K.Y. Vukolov, Modification of Optical Properties of Be Mirrors under Bombardment by Deuterium Ions, *J. Nucl. Mat.* 329-333 (2004) 1476-1480
- [141] A.F. Bardamid, V.N. Bondarenko, J.W. Davis, V.G. Konovalov, O. Litvin, I.V. Ryzhkov, A.N. Shapoval, A.F. Shtan', S.I. Solodovchenko, V.S. Voitsenya, Changes to the Reflectance of Be Mirrors due to Deuterium Plasmas Contaminated with Oxygen, *J. Nucl. Mat.* 405 (2010) 109-117
- [142] I. Yaacob, S. Bhandarkar, A. Bose, Synthesis of Aluminum Hydroxide Nanoparticles in Spontaneously Generated Vesicles, *Journal of Materials Research* 8 (3) (1993) 573-577
- [143] S. Chen, A. Gloter, A. Zobelli, L. Wang, C.-H. Chen, C. Colliex, Electron Energy Loss Spectroscopy and ab initio Investigation of Iron Oxide Nanomaterials Grown by a Hydrothermal Process, *Phys. Rev. B* 79 (2009) 104103
- [144] J.S. Hu, J.G. Li, Y.P. Zhao, Oxygen Removal with D2-ICR Cleanings after Oxidation Experiment in HT-7, *Fusion Engineering and Design* 82 (2007) 133-139

Appendix: Compilation of Measurement Results

Table 5 shows an overview of the profiles that are compiled on the following pages.

Gas / Treatment	Temp. (°C)	Time (h)	Pressure (mbar)	H ₂ O conc.	number of profiles
-----------------	------------	----------	-----------------	------------------------	--------------------

Native oxide and heating in air

none	RT	0	atm.	atm.	12
air	390	1	atm.	atm.	5
air	390	4,5	atm.	atm.	2
air	390	17	atm.	atm.	4
air	390	43	atm.	atm.	5
air	500	1	atm.	atm.	5
air	500	17	atm.	atm.	2
air	500	43	atm.	atm.	3
air	600	1	atm.	atm.	3
air	600	20	atm.	atm.	4
air	600	41	atm.	atm.	4

Dry plasma

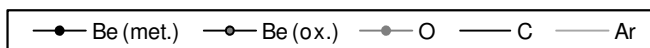
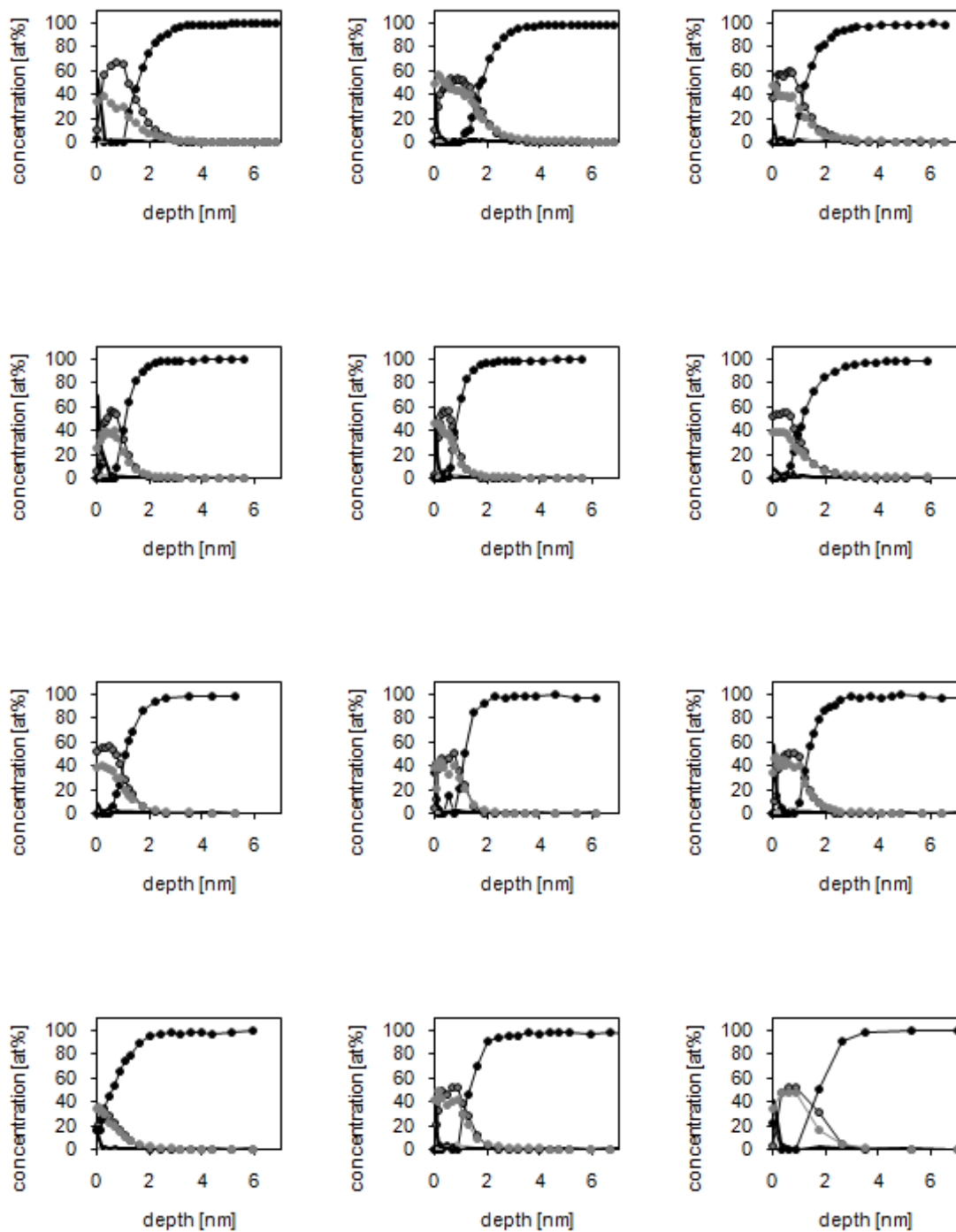
hydrogen	600	4	10	$< 3 \cdot 10^{-6}$	3
hydrogen plasma	30	4	10	$< 3 \cdot 10^{-6}$	3
hydrogen plasma	300	1	10	$< 3 \cdot 10^{-6}$	3
hydrogen plasma	300	5	14	$< 3 \cdot 10^{-6}$	3
hydrogen plasma	390	6	5,5	$< 3 \cdot 10^{-6}$	7
hydrogen plasma	600	6	10	$< 3 \cdot 10^{-6}$	2

Wet plasma

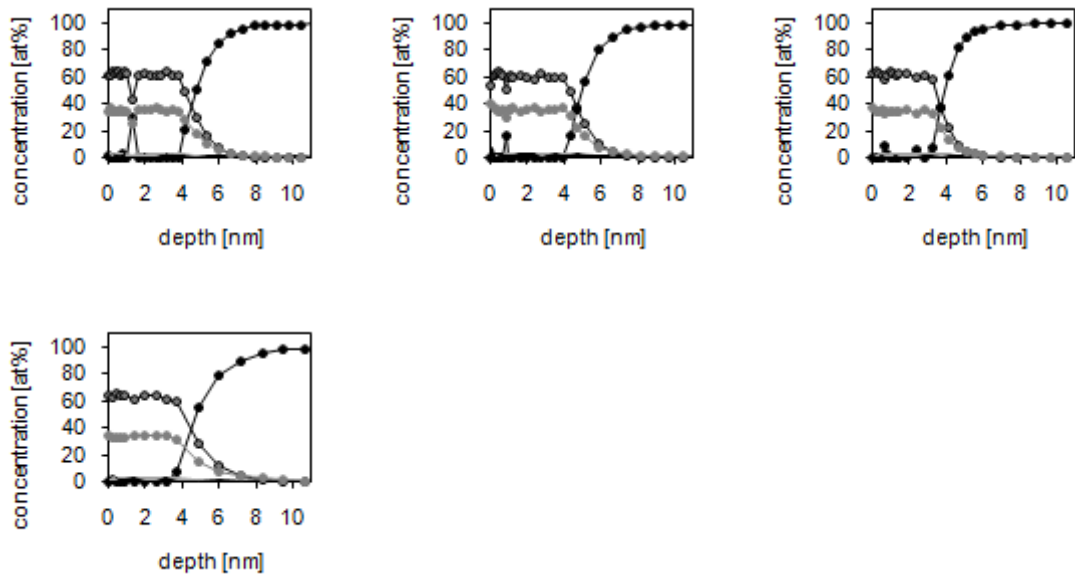
hydrogen plasma	390	6	5,4	$1 \cdot 10^{-4}$	15
hydrogen plasma	390	6	4,7	$1 \cdot 10^{-3}$	3
hydrogen plasma	390	6	5,2	$1 \cdot 10^{-3}$	9
hydrogen plasma	390	6	5,4	$1 \cdot 10^{-3}$	9
hydrogen plasma	390	1	6	$1 \cdot 10^{-2}$	4
hydrogen plasma	390	6	5	$1 \cdot 10^{-2}$	6
hydrogen plasma	390	6	6	$1 \cdot 10^{-2}$	6

Table 5: Overview of measured AES sputter depth profiles

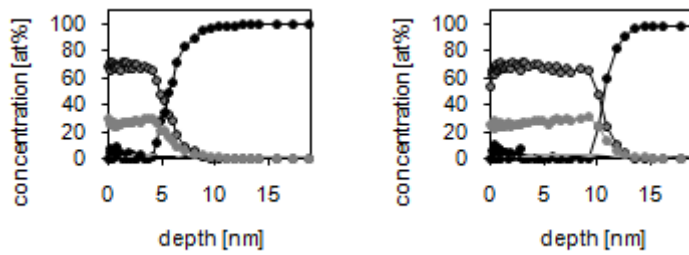
No treatment / native oxide



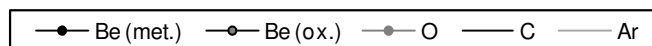
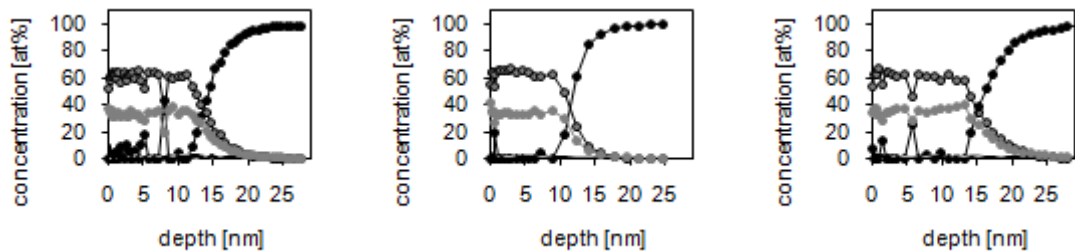
Heating in air, 390 °C / 1 h



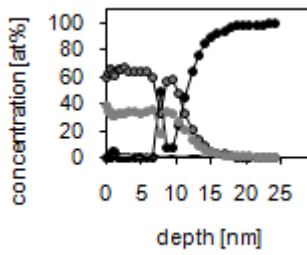
Heating in air, 390 °C / 4,5 h



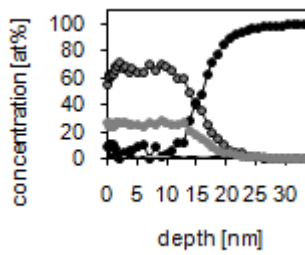
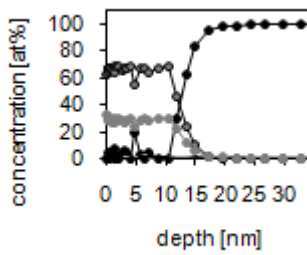
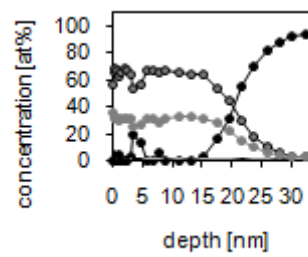
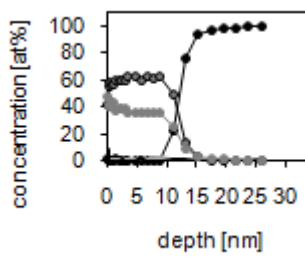
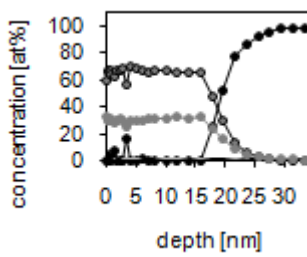
Heating in air, 390 °C / 17 h



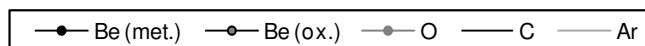
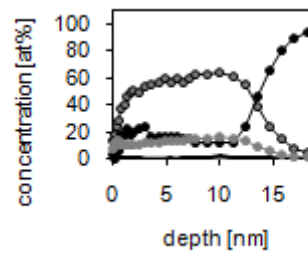
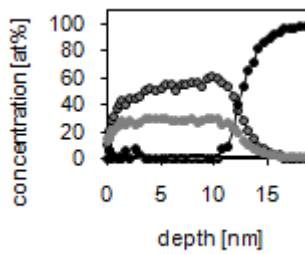
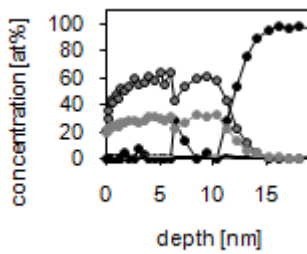
Heating in air, 390 °C / 17 h (continued)



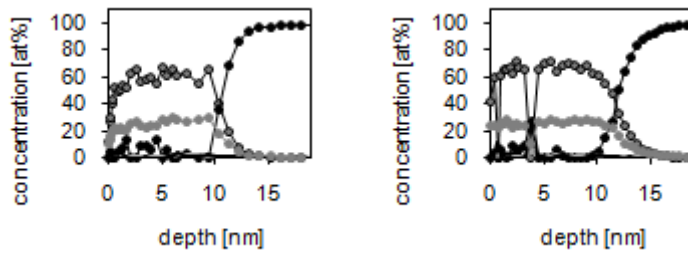
Heating in air, 390 °C / 43 h



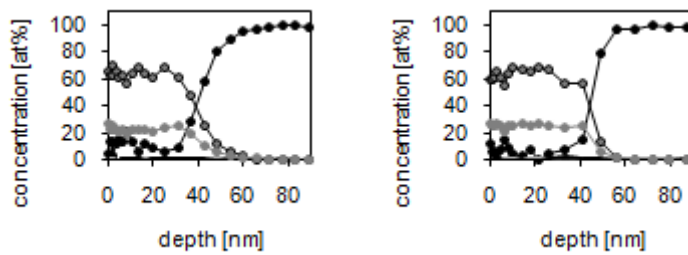
Heating in air, 500 °C / 1 h



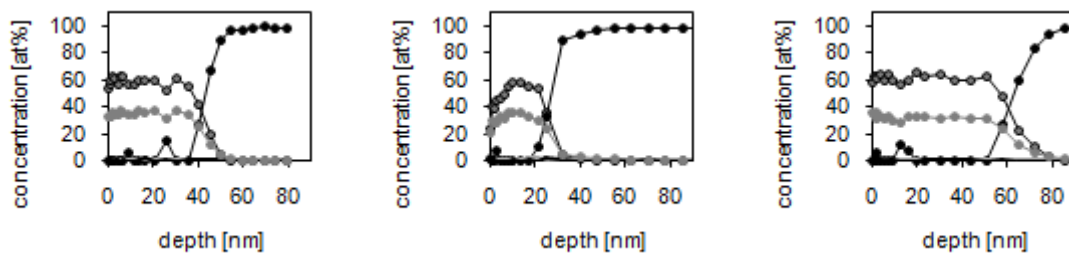
Heating in air, 500 °C / 1 h (continued)



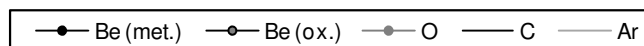
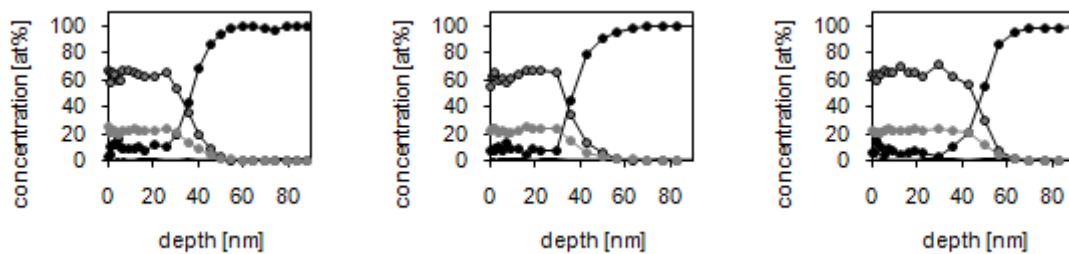
Heating in air, 500 °C / 17 h



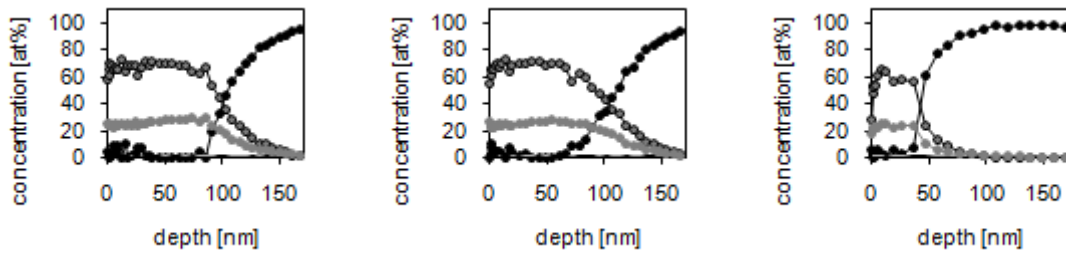
Heating in air, 500 °C / 43 h



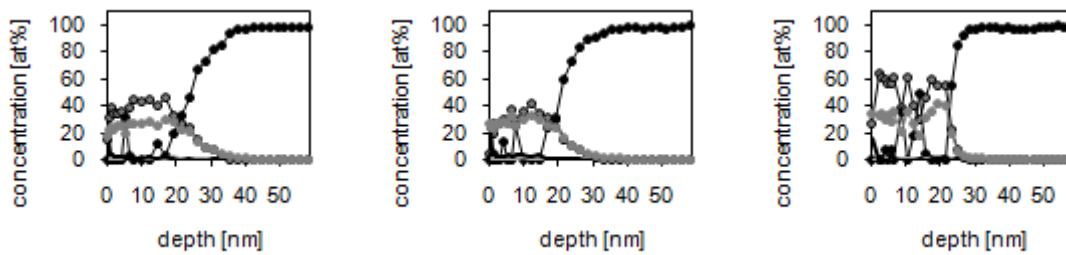
Heating in air, 600 °C / 1 h



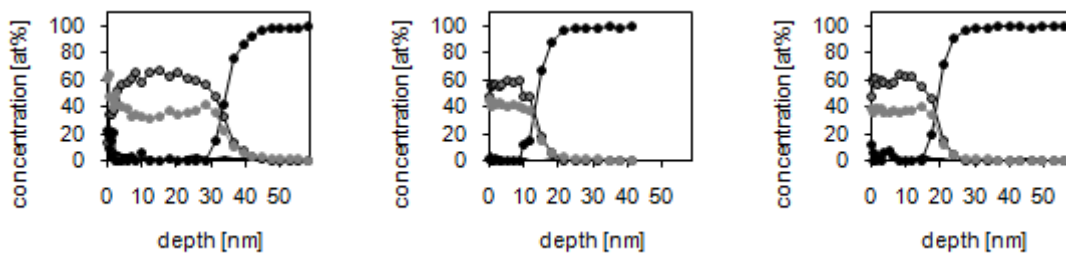
Heating in hydrogen, 600°C / 4 h / 10 mbar



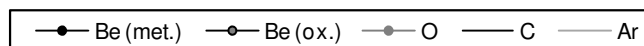
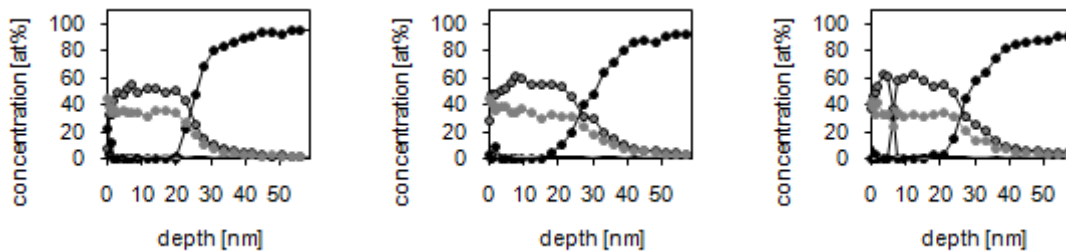
Dry H-plasma, 30°C / 4 h / 10 mbar / $O < 3 \cdot 10^{-6}$



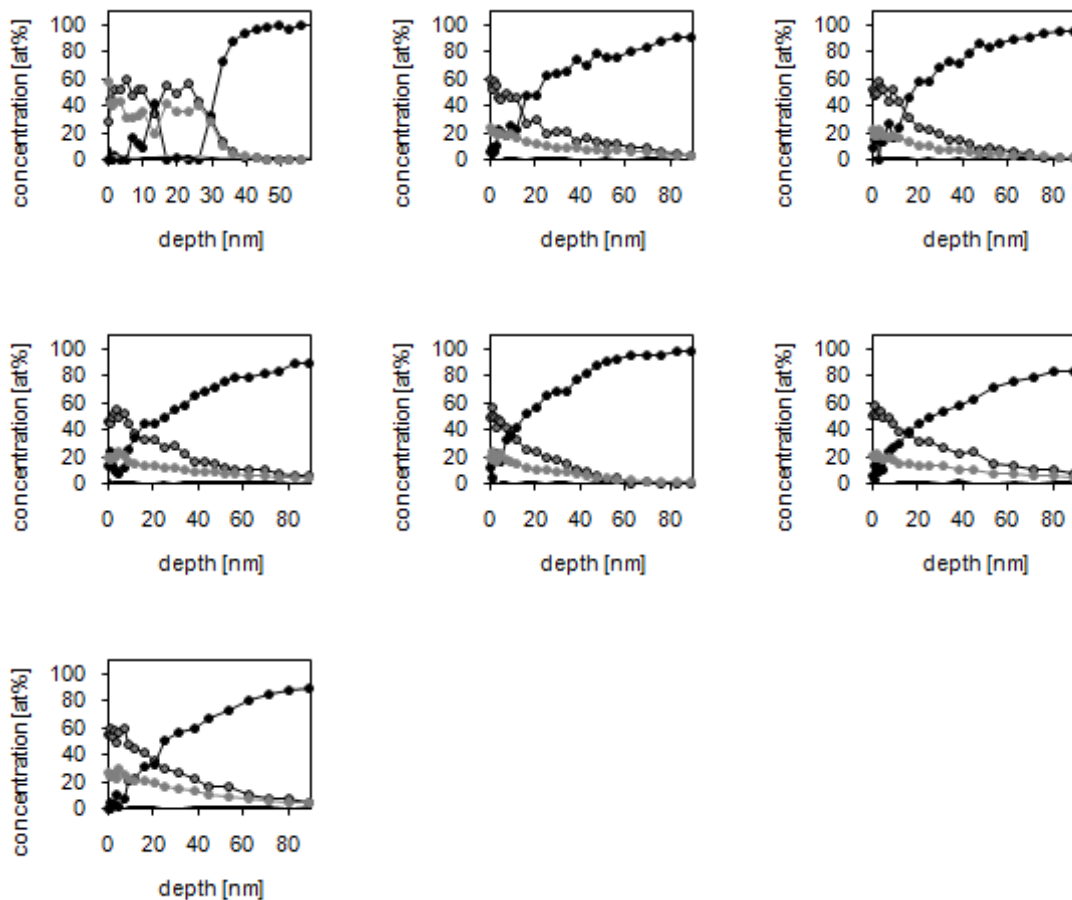
Dry H-plasma, 300°C / 1 h / 10 mbar / $O < 3 \cdot 10^{-6}$



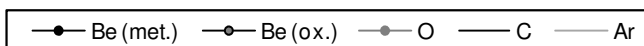
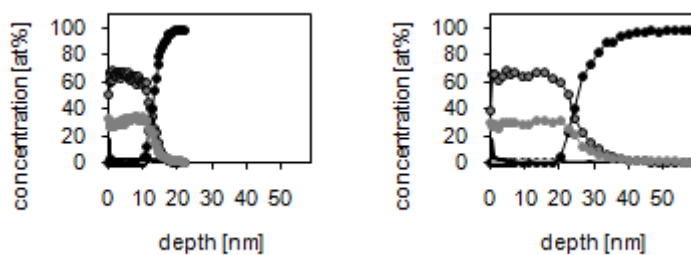
Dry H-plasma, 300°C / 5 h / 14 mbar / $O < 3 \cdot 10^{-6}$



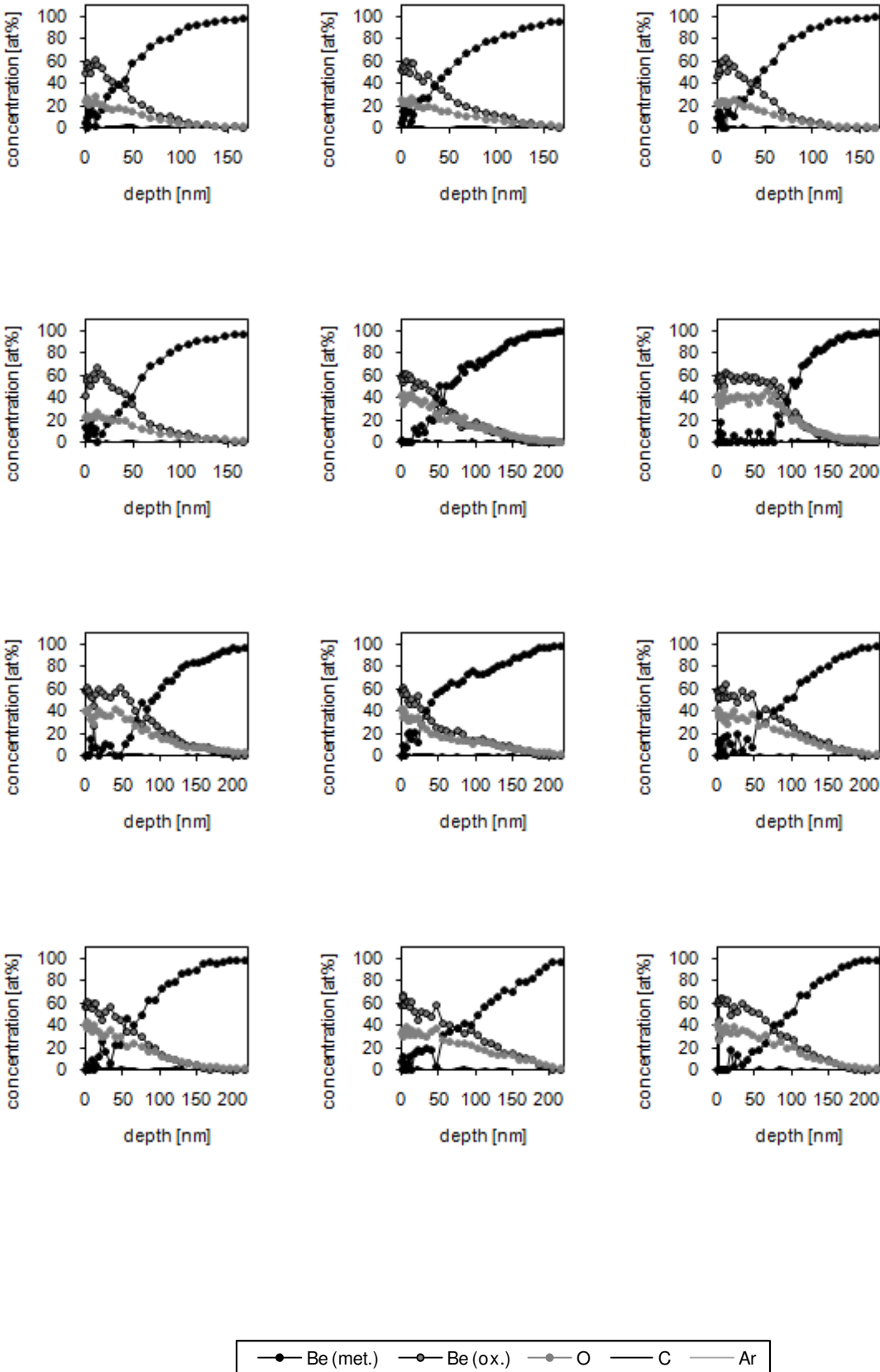
Dry H-plasma, 390°C / 6 h / 5,5 mbar / $O < 3 \cdot 10^{-6}$



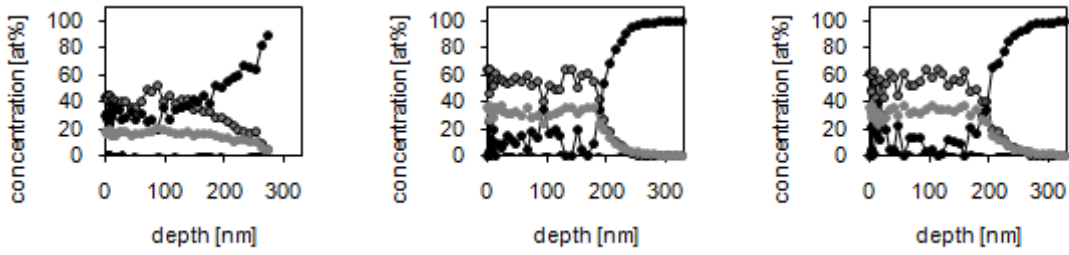
Dry H-plasma, 600°C / 6 h / 10 mbar / $O < 3 \cdot 10^{-6}$



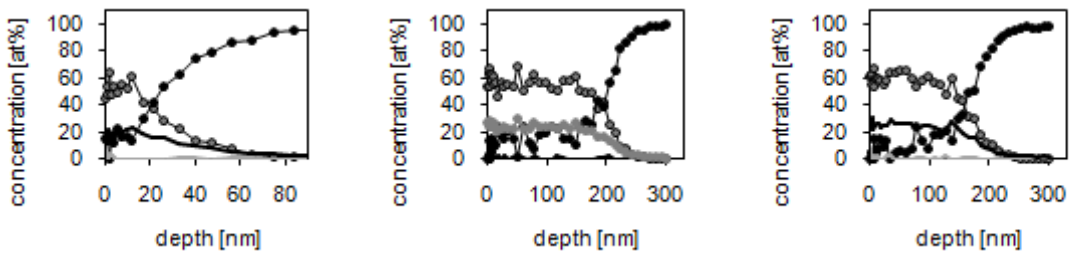
Wet H-plasma, 390 °C / 6 h / 5,4 mbar / O = 1·10⁻⁴



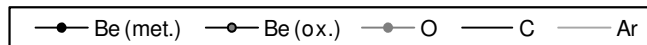
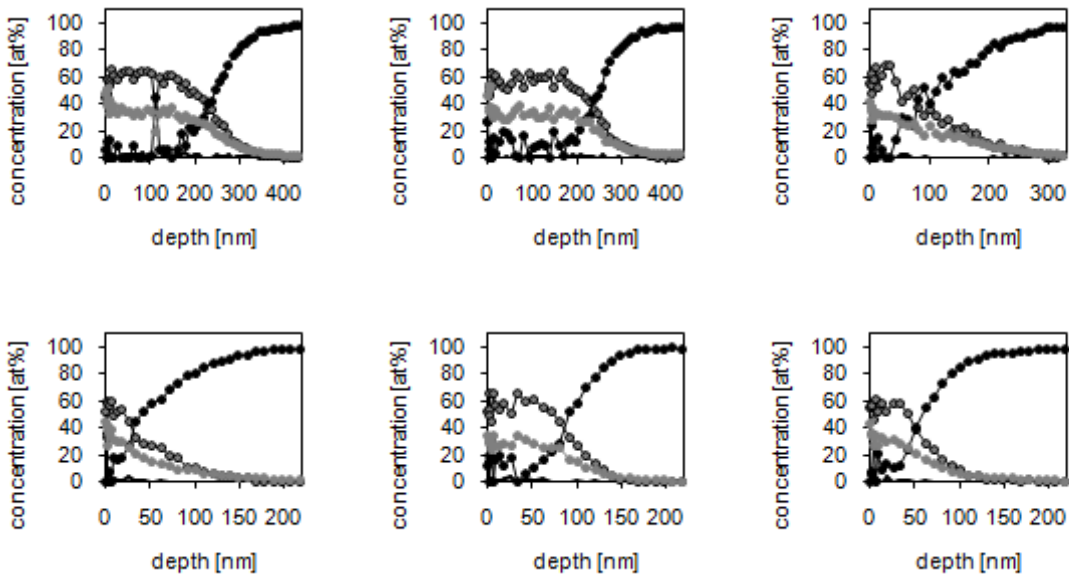
Wet H-plasma, 390 °C / 6 h / 5,4 mbar / O = 1·10⁻⁴ (continued)



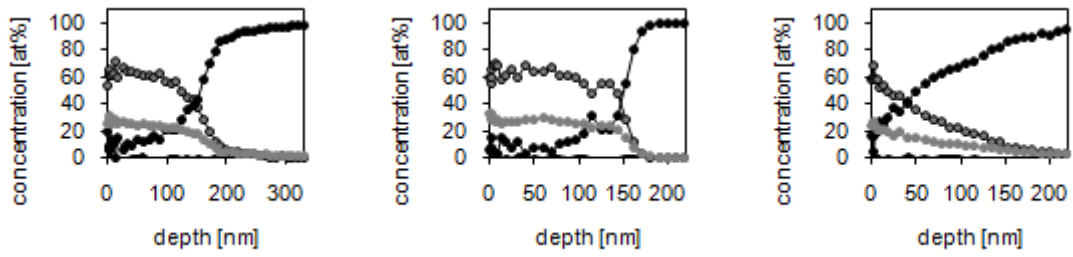
Wet H-plasma, 390 °C / 6 h / 4,7 mbar / O = 1·10⁻³



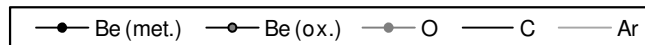
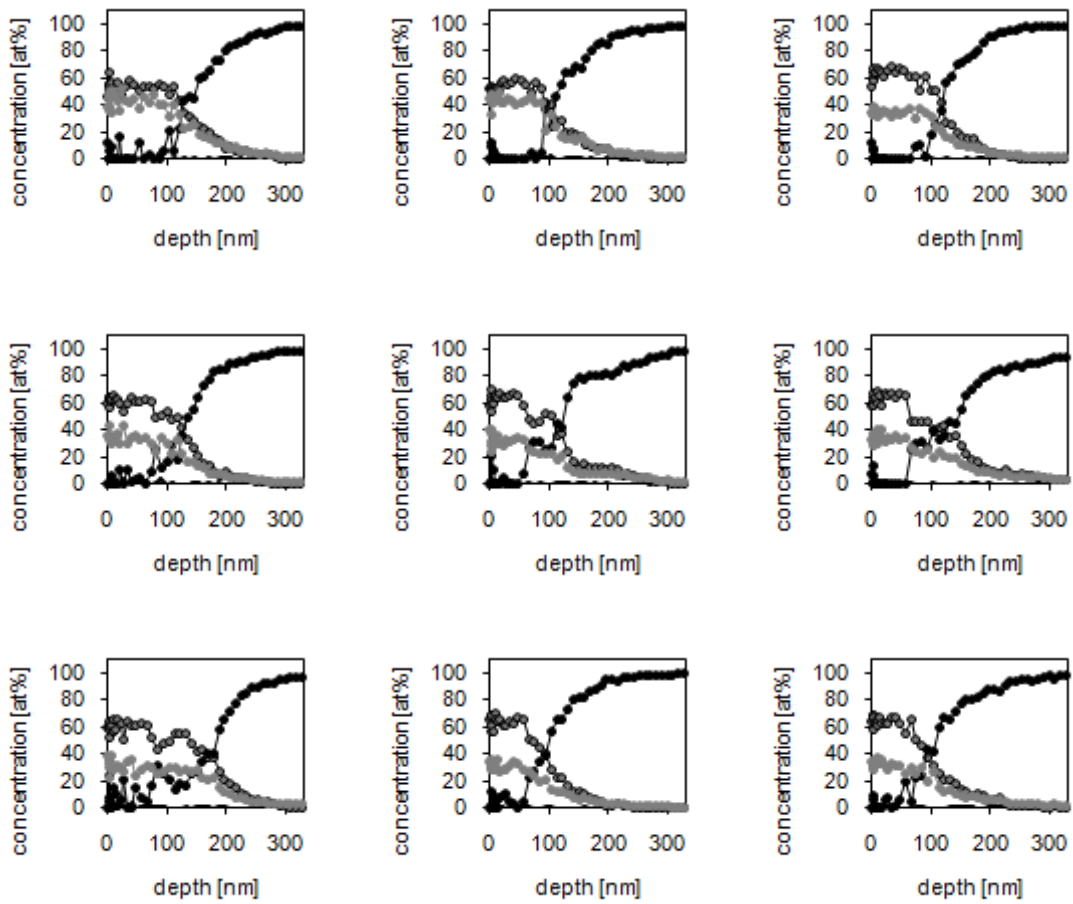
Wet H-plasma, 390 °C / 6 h / 5,2 mbar / O = 1·10⁻³



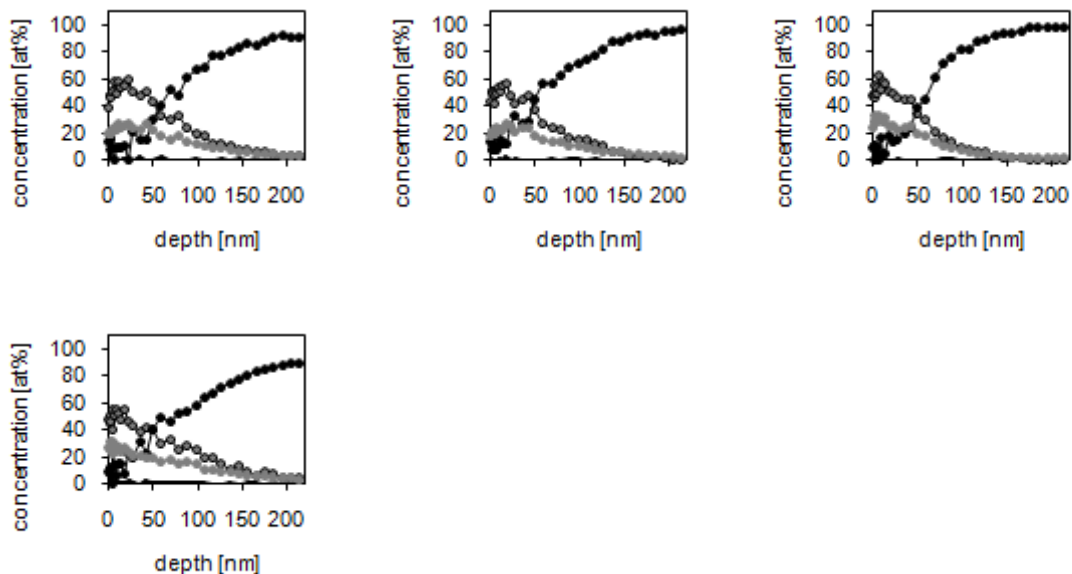
Wet H-plasma, 390 °C / 6 h / 5,2 mbar / O = 1·10⁻³ (continued)



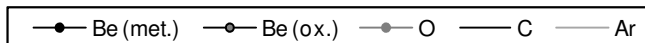
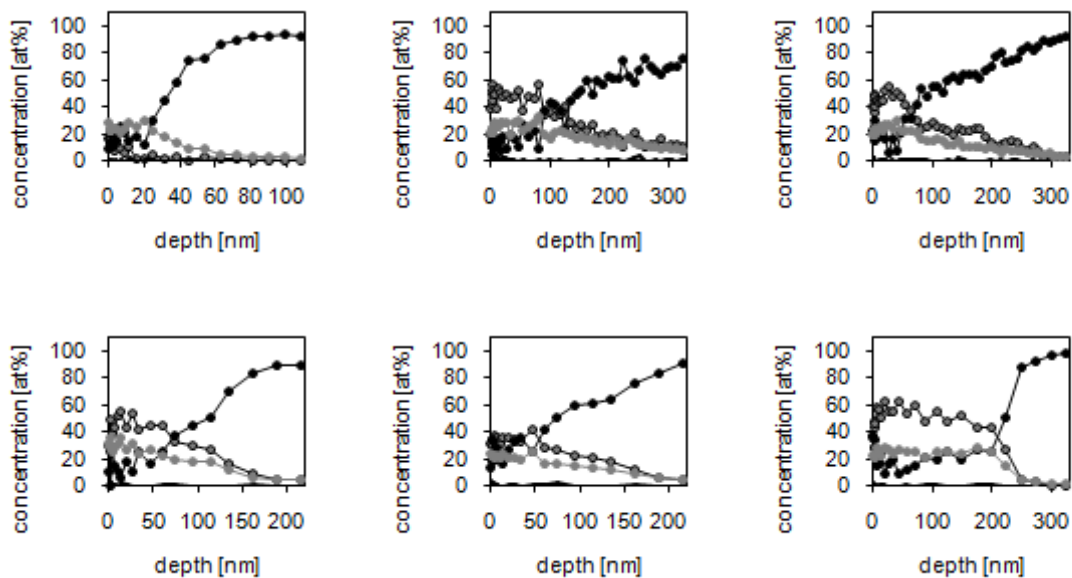
Wet H-plasma, 390 °C / 6 h / 5,2 mbar / O = 1·10⁻³



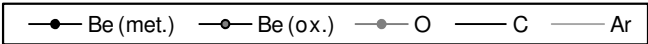
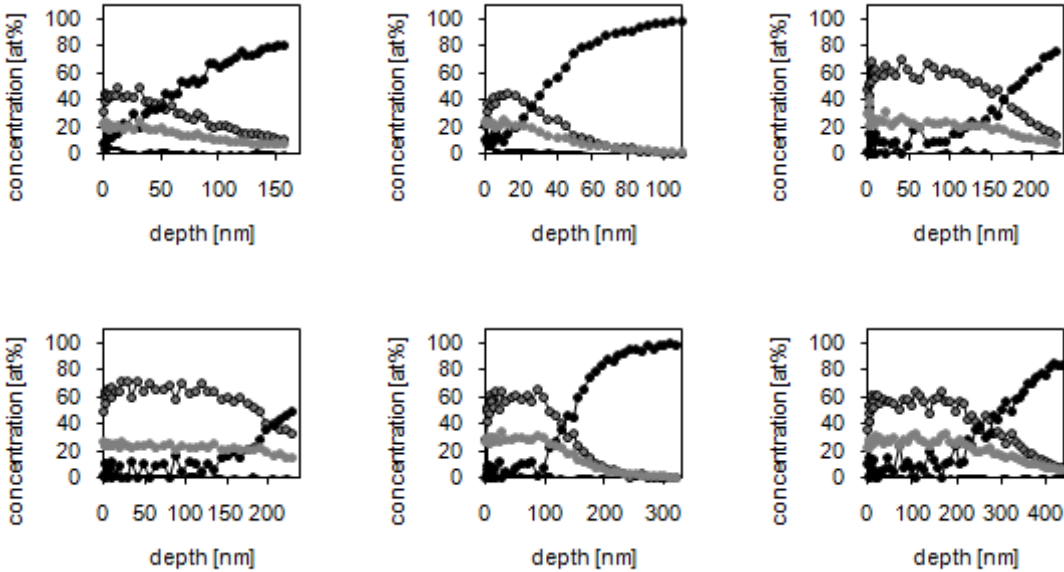
Wet H-plasma, 390 °C / 1 h / 6 mbar / O = 1·10⁻²



Wet H-plasma, 390 °C / 6 h / 5 mbar / O = 1·10⁻²



Wet H-plasma, 390°C / 6 h / 6 mbar / O = 1·10⁻²



List of Figures

Fig. 1	Glove box for sample polishing	14
Fig. 2	Tubular furnace setup	16
Fig. 3	Furnace setup for plasma exposure	18
Fig. 4	Optical emission spectra in the furnace for various plasma compositions	20
Fig. 5	Calibration of the quadrupole mass analyser	22
Fig. 6	Schematics of the Auger spectrometer	25
Fig. 7	SEM image of sputter depth profiling area with marked analysis spots	26
Fig. 8	Auger spectra of beryllium in various states of oxidation	27
Fig. 9	Sputter depth profiles of native oxide and after heating for 43 h at 390 °C in air	28
Fig. 10	Growth of the oxide thickness over time for heating at 390 °C, 500 °C and 600 °C	30
Fig. 11	Arrhenius plot of the oxidation rate constants obtained from the parabolic oxidation fits	32
Fig. 12	SEM images of sample surface oxidised 43 h at 500 °C after sputter depth profile. Image sizes: a) 40 x 30 µm, b) 9 x 7 µm	37
Fig. 13	SEM images of sample surface oxidised 1 h at 600 °C after sputter depth profile. Image size 240 x 180 µm	38
Fig. 14	SEM images of sample surface oxidised 1 h at 600 °C after sputter depth profile. Image size 24 x 18 µm	39
Fig. 15	SEM images of sample surface oxidised 1 h at 600 °C after sputter depth profile. Image size 8 x 6 µm	40
Fig. 16	SEM images of sample surface oxidised 20 h at 600 °C after sputter depth profile. Image size 8 x 6 µm	41
Fig. 17	AES maps of sample surface oxidised 20 h at 600 °C after sputter depth profile. Image size 4 x 3 µm	42
Fig. 18	AES maps of sample surface oxidised 20 h at 600 °C after sputter depth profile. Image size 4 x 3 µm	43

Fig. 19	Oxide layer thicknesses before and after exposure of the samples to dry hydrogen gas or plasma at various temperatures	46
Fig. 20	Richardson-Ellingham diagram for the oxidation reactions of molecular hydrogen, atomic hydrogen and beryllium	47
Fig. 21	Oxide layer thicknesses after exposure to hydrogen plasma with various fractions of water vapour added	52
Fig. 22	SEM images of sample surface before plasma exposure. Image sizes: a) 120 x 90 μm , b) 24 x 18 μm	53
Fig. 23	SEM images of sample surface after dry plasma exposure (390°C, 1 h). Image sizes: a) 120 x 90 μm , b) 24 x 18 μm	54
Fig. 24	SEM images of sample surface after dry plasma exposure (390°C, 6 h). Image sizes: a) 120 x 90 μm , b) 24 x 18 μm	55
Fig. 25	SEM images of sample surface after wet plasma exposure (390°C, 1 h, 1% water vapour). Image sizes: a) 160 x 120 μm , b) 20 x 15 μm ...	56
Fig. 26	SEM images of sample surface after wet plasma exposure (390°C, 6 h, 1% water vapour). Image sizes: a) 120 x 90 μm , b) 24 x 18 μm	57
Fig. 27	Depth profiles of oxide layers with comparable thickness (approx. 40 nm) from plasma exposure experiments with different fractions of water vapour: a) dry hydrogen ($3 \cdot 10^{-6}$), b) 10^{-4} , c) 10^{-3} , d) 10^{-2}	58

List of Tables

Table 1	Mechanical properties of beryllium (hot isostatic pressed grade I220H and vacuum hot pressed grade S65C) and the respective ranges for various steels for comparison	1
Table 2	Composition of the two sets of beryllium samples (S65C grade vacuum hot pressed from Brush Wellman and plasma-sprayed from Los Alamos National Laboratory)	13
Table 3	Oxide thicknesses after heating at various temperatures for different durations	29
Table 4	Experimental parameters and activation energies for diffusion-controlled oxidation from this work and various references	33
Table 5	Overview of measured AES sputter depth profiles	75

Curriculum Vitae

Christian Tomastik

Born: 21.7.1971 in Vienna, Austria
Address: Wehlistrassen 45/1/4, 1200 Vienna, Austria
Phone: +43 664 4633389
E-mail: christian.tomastik@chello.at

Education

2004 Technical Physics Degree
Diploma Program (Dipl.-Ing.), The Faculty of Technology and Natural Sciences, Vienna University of Technology, Austria
Diploma Thesis: Determination of the Inelastic Mean Free Path of Medium Energy Electrons in 24 Elemental Solids by Means of Elastic Peak Electron Spectroscopy

1989 High School Diploma
BRG X, Ettenreichgasse 41-43, 1100 Vienna, Austria

Professional experience

2007 - present Scientist, AC²T research GmbH
Viktor-Kaplan-Straße 2, 2700 Wr. Neustadt, Austria

1999 - 2007 Member of research staff, Institute of Applied Physics
Vienna University of Technology
Wiedner Hauptstrasse 8-10, 1040 Vienna, Austria

List of Publications

Papers in Reviewed Journals

A. Zikin, I. Hussainova, C. Katsich, E. Badisch, C. Tomastik, Advanced chromium carbide-based hardfacings, *Surface and Coatings Technology* 206 (19-20) (2012) 4270-4278

G. Tasneem, C. Tomastik, S. Gerhold, W. S. M. Werner, W. Smekal and C. J. Powell, Photoelectron angular distributions of Cu, Ag, Pt and Au samples: experiments and simulations, *Surface and Interface Analysis* 43 (6) (2011) 934-939

M. Roy, S. Ghodbane, T. Koch, A. Pauschitz, D. Steinmüller-Nethl, A. Tomala, C. Tomastik, F. Franek, Tribological investigation of nanocrystalline diamond films at low load under different tribosystems, *Diamond and Related Materials* 20 (4) (2011) 573-583

C. Gabler, C. Tomastik, J. Brenner, L. Pisarova, N. Doerr, G. Allmaier, Corrosion properties of ammonium based ionic liquids evaluated by SEM-EDX, XPS and ICP-OES, *Green Chemistry* 13 (10) (2011) 2869-2877

A. Schneider, J. Brenner, C. Tomastik, F. Franek, Capacity of selected ionic liquids as alternative EP/AW additive, *Lubrication Science* 22 (6-7) (2010) 215-223

C. Tomastik, M. Jech, T. Wopelka, F. Franek, Surface analysis of cylinder liners from tribological model experiments and internal combustion engines, *Surface and Interface Analysis* 42 (6-7) (2010) 1357-1360

M. Vlad, M.M. Szczerek, R. Michalczewski, C. Kajdas, C. Tomastik, E. Osuch-Slomka, The influence of antiwear additive concentration on the tribological behaviour of a-C:H:W/steel tribosystem, *Journal of Engineering Tribology* 224 (J10) (2010) 1079-1089

W. Vollnhofer, C. Eisenmenger-Sittner, J. Hell, M. Kiniger, B. Schwarz, H. Steiner, C. Tomastik, The influence of temperature treatment and carbon addition on the surface morphology and the surface energy of molybdenum layers on carbon substrates, *Surface and Interface Analysis* 40 (3-4) (2008) 526-528

A. Lugstein, C. Schoendorfer, M. Weil, C. Tomastik, A. Jauss, E. Bertagnolli, Study of focused ion beam response of GaSb, *Nuclear Instruments and Methods in Physics Research B - Beam Interactions with Materials and Atoms* 255 (2) (2007) 309-313

B. Schwarz, C. Eisenmenger-Sittner, E. Klein, C. Tomastik, K. Mayerhofer, P.B. Barna, A. Kovacs, Passivation of Al surfaces against oxidation by monoatomic Sn wetting layers, *Surface and Coatings Technology* 200 (22-23) (2006) 6484-6489

C. Eisenmenger-Sittner, B. Schwarz, C. Tomastik, P.B. Barna, A. Kovacs, Experimental studies of solid state surface wetting of tin (Sn) on aluminium (Al), *Applied Surface Science* 252 (15) (2006) 5466-5469

A. Lugstein, J. Bernardi, C. Tomastik, E. Bertagnolli, Synthesis of nanowires in room temperature ambient: A focused ion beam approach, *Applied Physics Letters* 88 (16) (2006) 163114

E. Klein, B. Schwarz, C. Eisenmenger-Sittner, C. Tomastik, P.B. Barna, A. Kovacs, The initial states of wetting and spreading of Sn on Al surfaces, Vacuum 80 (1-3) (2005) 74-80

C. Tomastik, W.S.M. Werner, H. Stoeri, Oxidation of Beryllium - a Scanning Auger Investigation, Nuclear Fusion 45 (9) (2005) 1061-1065

A. Lugstein, M. Weil, B. Basnar, C. Tomastik, E. Bertagnolli, A novel fabrication technique for crystallite growth on a (100) InAs surface utilizing focused ion beams, Nuclear Instruments and Methods in Physics Research B - Beam Interactions with Materials and Atoms 222 (1-2) (2004) 91-95

G. Erdelyi, G. Langer, J. Nyeki, L. Köver, C. Tomastik, W.S.M. Werner, A. Csik, H. Stoeri, D.L. Beke, Investigation of Ta grain boundary diffusion in copper by means of Auger electron spectroscopy, Thin Solid Films 459 (1-2) (2004) 303-307

B.X. Mayer-Helm, W. Rauter, G. Rauchbauer, C. Tomastik, H. Bangert, Approaches for the coating of capillary columns with highly phenylated stationary phases for high-temperature GC, Journal of Separation Science 27 (4) (2004) 335-342

C. Eisenmenger-Sittner, E. Neubauer, C. Schrank, J. Brenner, C. Tomastik, Solid state de-wetting of vapor deposited films on planar and fiber-shaped carbon substrates, Surface and Coatings Technology 180 (2004) 413-420

C. Eisenmenger-Sittner, H. Bangert, C. Tomastik, P.B. Barna, A. Kovacs, F. Misiak, Solid state diffusion of Sn in polycrystalline Al films, Thin Solid Films 433 (1-2) (2003) 97-102

W.S.M. Werner, W. Smekal, C. Tomastik, H. Störi, Surface excitation probability of medium energy electrons in metals and semiconductors, Surface Science 486 (3) (2001) L461-L466

W.S.M. Werner, C. Tomastik, T. Cabela, G. Richter, H. Störi, Elastic electron reflection for determination of the inelastic mean free path of medium energy electrons in 24 elemental solids for energies between 50 and 3400 eV, Journal of Electron Spectroscopy and Related Phenomena 113 (2-3) (2001) 127-135

W.S.M. Werner, C. Tomastik, T. Cabela, G. Richter, H. Störi, Electron inelastic mean free path measured by elastic peak electron spectroscopy for 24 solids between 50 and 3400 eV, Surface Science 470 (1-2) (2000) L123-L128

Conference Contributions

C. Tomastik, H. Störi, Diffusion of Oxygen in Beryllium, ECASIA'03 - 10th European Conference on Applications of Surface and Interface Analysis, 5.-10. October 2003, Berlin, Germany

C. Tomastik, H. Störi, Oxidation of Beryllium - a Scanning Auger Investigation, FEC2004 - 20th IAEA Fusion Energy Conference, 1.-6. November 2004, Villamoura, Portugal

C. Tomastik, W.S.M. Werner, H. Störi, Interaction of Beryllium Oxide with Hydrogen Plasma, FEC2006 - 21st IAEA Fusion Energy Conference, 16.-21. October 2006, Chengdu, China

C. Tomastik, M. Jech, T. Wopelka, Comparative Nanoindentation Analysis of Cylinder Liners from Tribological Model Experiments and from Internal Combustion Engines, VIENNANO'09 - 3rd Vienna International Conference on Nano-Technology, 18.-20. March 2009, Vienna, Austria

C. Tomastik, M. Jech, F. Franek, Surface Analysis of Cylinder Liners from Tribometers and from Internal Combustion Engines, ECASIA'09 - 13th European Conference on Applications of Surface and Interface Analysis, 18.-23. October 2009, Antalya, Turkey

C. Tomastik, C. Lenauer, C. Besser, T. Wopelka, M. Jech, Nanoscopic Analysis of Cylinder Liner Surfaces Tribomutated under the Influence of Ethanol Bio-Fuel, VIENNANO'11 - 4th Vienna International Conference on Nano-Technology, 7.-9. June 2011, Vienna, Austria